SYNTHESIS, STRUCTURE AND REACTIVITY STUDIES OF DINUCLEAR GROUP 11 N-HETEROCYCLIC CARBENE COMPLEXES

A Dissertation
Presented to
The Academic Faculty

by

Chelsea Marie Wyss

In Partial Fulfillment
of the Requirements for the Degree
Doctor of Philosophy in the
School of Chemistry and Biochemistry

Georgia Institute of Technology
December 2015

SYNTHESIS, STRUCTURE AND REACTIVITY STUDIES OF DINUCLEAR GROUP 11 N-HETEROCYCLIC CARBENE COMPLEXES

Approved by:

Dr. Joseph P. Sadighi, Advisor
School of Chemistry and Biochemistry
Georgia Institute of Technology

Dr. Jake D. Soper
School of Chemistry and Biochemistry
Georgia Institute of Technology

Dr. Christopher W. Jones
School of Chemical and Biomolecular Engineering
Georgia Institute of Technology

Dr. Angus P. Wilkinson
School of Chemistry and Biochemistry
Georgia Institute of Technology

Dr. Seth R. Marder
School of Chemistry and Biochemistry
Georgia Institute of Technology

Dr. Z. John Zhang
School of Chemistry and Biochemisty
Georgia Institute of Technology

Date Approved: July 31, 2015

ACKNOWLEDGEMENTS

The list is long of who I give thanks and acknowledgements to throughout this journey. I would first like to thank my advisor Dr. Joseph Sadighi for your advice, guidance and support. I am a better chemist because of you. I would also like to thank all of the Sadighi lab members past and present. In particular, I want to thank Brandon Tate. You have been a pleasure to work with, and I will miss our lengthy conversations on chemistry and life. Your friendship has meant a lot throughout this experience. I owe much gratitude to Aubrey Smith Shahriari and Michel Bayless. You not only gave me much needed advice and a synthetic foundation that aided me for the rest of my graduate career, but you welcomed me as one of your own. To my friends that I have collected along the way, especially the ones made here in Atlanta, thank you for the love, support, and laughs. It is rare to find friends that become family, and I am lucky to call you family. To my family, all of you, you have each aided in making me the woman I am. I am eternally grateful for your unconditional love. We are the lucky ones. I would especially like to thank my parents Russell and Sheila Wyss: thank you, thank you, thank you. There are no words. And finally to my husband, Justin Bordley, I like you and I love you.

TABLE OF CONTENTS

LIST OF TABLES

LIST OF FIGURES

LIST OF SCHEMES

LIST OF SYMBOLS AND ABBREVIATIONS

NHC	N-heterocyclic carbene
IDipp	1,3-bis(2,6-diisopropylphenyl)imidazol-2-ylidene
IMe	1,3-bis(methyl)imidazole-2-ylidene
L	ligand
Å	angstrom
DFT	density functional theory
SIDipp	1,3-bis(2,6-diisopropylphenyl)-4,5-dihydroimidazol-2-ylidene
NMR	nuclear magnetic resonance
FT-IR	fourier transform infrared spectroscopy
Me	methyl
Et	ethyl
iPr	isopropyl
tBu	tertbutyl
THF	tetrahydrofuran
Ph	phenyl
ºC	degrees Celcius
ppm	parts per million
λ	wavelength
MHz	megahertz
δ	chemical shift
MO	molecular orbital
HOMO	highest occupied molecular orbital
LUMO	lowest unoccupied molecular orbital

eV	electron volt
pin	pinacolate
cat	catecholate
atm	atmosphere
ORTEP	Oak Ridge thermal ellipsoid plot
OTf^-	trifluoromethanesulfonate
°	degree
ν	wavenumber
σ	sigma
π	pi
μ	mu
η	eta
κ	kappa
g	gram
mL	milliliter
cm	centimeter

SUMMARY

This thesis describes the synthesis, structure and reactivity of singly bridged dinuclear Group 11 metal complexes, supported by N-heterocyclic carbene (NHC) ligands. These complexes include dinuclear copper(I) complexes that demonstrate three-center, two-electron bonding with short intermetallic distances. In the first part of this study, I isolated a hydride-bridged dicopper cation, $\{[(IDipp)Cu]_2(\mu\text{-}H)\}^+ BF_4^-$, which adopts a bent arrangement about the hydride. It undergoes facile methanolysis, readily reacts with carbon dioxide to afford a (κ^2-formate)-bridged dicopper species, and coordinates carbon monoxide reversibly to form a carbonyl adduct. The $[(LCu)_2H]^+$ cation also inserts phenylacetylene to afford a *gem*-dicopper vinyl cation, a rare example of the insertion of carbon–carbon multiple bonds into a copper hydride.

In the second part of this thesis, I describe the synthesis and structural characterization of the first boryl-bridged dicopper cation $\{[(SIDipp)Cu]_2(\mu\text{-}BO_2C_6H_4)\}^+ BF_4^-$. The solid-state structure shows a bent arrangement about the boryl with a short intermetallic distance of 2.4082(2) Å. The boryl-bridged dicopper cation deprotonates phenylacetylene to form a phenylacetylide dicopper complex. It also readily reacts with methanol to form the hydride-bridged dicopper cation. Density functional theory (DFT) calculations were applied to give further insight into the nature of the metal–boron bonds in comparison to the mononuclear analogue. The two electrons contributed by the bridging boryl are shared between the boron and the two copper centers in the $[(LCu)_2B]^+$ core. This three-center, two-electron bonding orbital is lower-lying in energy in

comparison to the Cu–B σ-bonding molecular orbital in the mononuclear analogue, consistent with a less nucleophilic Cu–B bond.

The NHC ligand also stabilizes an isoleptic series of dinuclear μ-fluoro cations of copper(I), silver(I), and gold(I). In these complexes, a single fluoride acts as the sole bridging ligand between the two group 11 metal centers of the form $[(LM)_2(\mu\text{-}F)]^+$. All three cations are highly sensitive to adventitious moisture, readily forming the hydroxide-bridged dinuclear cations. The gold(I) complex is the most reactive. It activates the C–Cl bonds of CD_2Cl_2 and adds rapidly across an allene C=C bond to form an allylic C–F bond, and a vinyl anion bound asymmetrically to the two gold(I) centers.

CHAPTER 1

Introduction

This thesis focuses mainly on the synthesis and reaction chemistry of a series of anion-bridged dicopper(I) cations. Some of these feature remarkably short copper–copper interactions, whereas others do not. An overview of the nature of such interactions follows.

1.1. Copper(I) Complexes With Short M–M Contacts

Copper(I) has been shown to form complexes with short distances between formally closed shell d^{10} metal centers.[1] While there are numerous copper(I) complexes with short intermetallic distances, there has been much controversy on why such close interactions of closed shell metal centers would arise.[2] Theoretical investigations have since been carried out to gain further insight into copper–copper distances that are shorter then twice the van der Waals radius of copper.[3] Some have ascribed these close copper contacts to geometric constraints imposed by a bridging ligand, some to net attractive interactions between d^{10} metal centers, and others to three-center, two-electron bonding.

1.2. Geometric Constraints

Bridging ligands have been used to promote short copper–copper contacts. These ligand architectures can enforce such contacts, but raise the question of whether these interactions are examples of direct metal–metal bonding or not. Copper(I) complexes supported by azenide ligands[4] (Figure 1.1)

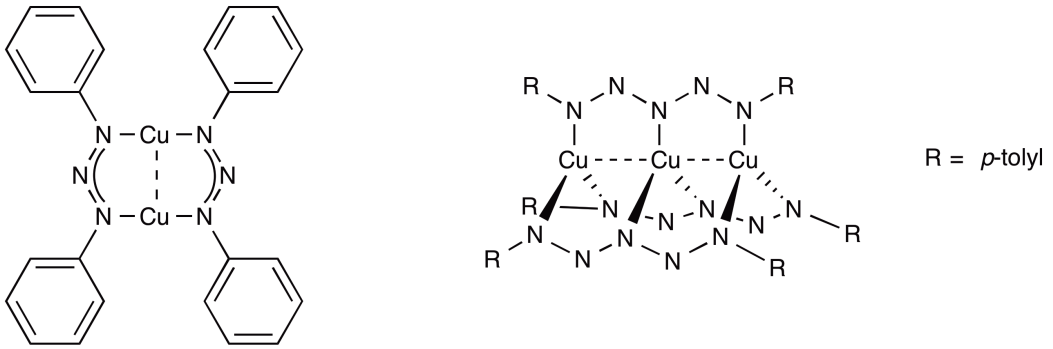

A B

Figure 1.1. Examples of copper(I) complexes supported by azenide ligands: (**A**) Cu–Cu 2.451 Å;[4a] (**B**) Cu–Cu 2.348(2)-2.358(2) Å.[4c]

and copper-containing organometallic compounds of the type Cu_nR_n (n = 3–5)[5] (Figure 1.2) are examples of such complexes and have been heavily investigated theoretically.

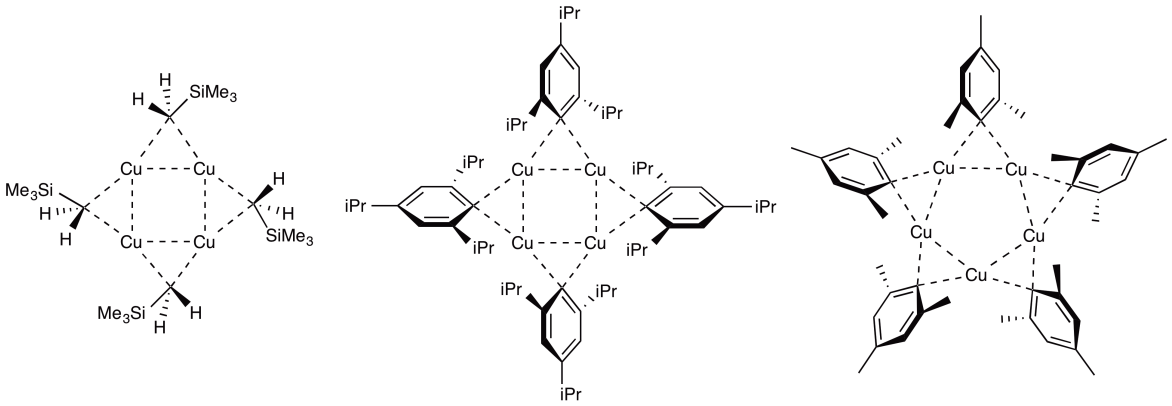

A B C

Figure 1.2. Organocopper compounds with short Cu–Cu distances: (**A**): Cu–Cu 2.417 Å;[5a] (**B**): Cu–Cu 2.445 Å;[5d] (**C**): Cu–Cu 2.44-2.50 Å.[5c]

Cotton and coworkers examined the model azenide complexes, $[(form)Cu]_2$ (form = *p*-$CH_3C_6H_4NCHNC_6H_4$-*p*-CH_3), $[(hpp)_2Cu_2]$ ($hpp^- = C_7N_3H_{12}$) and $[Cu(HN_5H)]_3$, using density-functional theory.[6] The study showed that the short distances between the metal centers are determined by the geometric constraints of the bridging ligands and to the

strong Cu–N bonds. They concluded that there is no net Cu–Cu bond formation between two d^{10} Cu(I) atoms. Kölmel and Ahlrichs also examined $[Cu(HN_5H)]_3$ and $[Cu(RN_3R)]_2$ (R = H and C_6H_5) using coupled pair functional calculations.[7] They too attribute the short intermetallic distances principally to the strong covalent copper–ligand bonding, which tends to fix the positions of the copper atoms. Another study, done by Hoffmann and coworkers on the effects of bridging ligands,[8] was carried out by means of extended Hückel calculations. They used model dimers with phosphonium ylide bridges, tetramers with alkyl bridges, and the trinuclear Cu(I) complex $[Cu(tolylN_5tolyl)]_3$. The calculations determined that the incorporation of bridging ligands brings the copper atoms together as a result of their stereochemical requirements. Other studies support such findings and prefer the term nonbonding close Cu(I)–Cu(I) contacts.[2a,6,9]

1.3. Attractive Interactions

Hoffmann and coworkers furthered their study on Cu(I)–Cu(I) interactions by applying extended Hückel calculations to $[Cu_2]^{2+}$, $[Cu_3]^{3+}$, and $[Cu_4]^{4+}$.[8a] When only looking at 3d orbitals on Cu, they found the expected closed-shell repulsion between the d^{10} metal centers: The antibonding molecular orbitals are more destabilized than the bonding molecular orbitals are stabilized. However, when the symmetry allowed mixing of metal 4s and 4p orbitals was included, an attractive interaction between two Cu^+ centers was evident. The mixing of the 4s and 4p orbitals into the occupied 3d combinations causes the antibonding orbitals to become less destabilized and the bonding orbitals to be more stabilized, resulting in the conversion of repulsive d^{10}–d^{10} interactions into partial bonding. It was concluded in this study that the direct interactions and stereochemical requirements of the ligand set bring the copper atoms together, but that it

would be difficult to distinguish between the two effects.[8b] In agreement, Schwerdtfeger *et al* found attractive intermetallic interactions, and not just ring constraints, the cause of short Cu–Cu distances and C–Cu–C bending in isolated solid-state structures resembling the model species $[(H_3C)Cu]_4$.[10] Other studies have supported the presence of such Cu(I)–Cu(I) attractive interactions.[2c,8,11]

1.4. Cu(I)–Cu(I) Interactions of Model Dimers

Schwerdtfeger *et al* continued their studies on Cu(I)–Cu(I) interactions by investigating model dimers of the form $[(H_3C)CuL]_2$ (L = OH_2, NH_3, SH_2, PH_3, N_2, CO, CS, CNH, CNLi).[10] They again found that Cu(I)–Cu(I) interactions are attractive, and do not result solely from ligand requirements. In general, the weak closed-shell interactions were found to be attractive up to 12 kJ mol^{-1}. However, the strength of the interactions are dependent on the nature of L, increasing with increasing σ-donor and π-acceptor ligands.

Other theoretical studies support these findings in investigations on $Cu_2(\mu\text{-}H)_2$, $Cu_2(\mu\text{-}F)_2$, and $Cu_2(\mu\text{-}Cl)_2$ dimers.[7] σ-Donors such as hydrides donate electron density into the empty σ and π Cu–Cu bonding orbitals (combinations of the empty metal s and p_π orbitals). The Cu–Cu interaction, induced by the bridging hydrides, is then increased. Halide bridges, which contain σ-donor and π-donor capabilities, change the bonding network in comparison to the hydride bridges. In addition to σ-donating electron density into the empty Cu–Cu bonding orbitals, the halides π-donate into the σ* and π* combinations. This causes the M–M bond to vanish.[12]

Even though bridging halides decrease Cu intermetallic interactions, the Cu–Cu distances calculated for $Cu_2(\mu\text{-}F)_2$, and $Cu_2(\mu\text{-}Cl)_2$ dimers are shorter than the distance in copper metal.[7] The computed Cu–Cu distance in the $Cu_2(\mu\text{-}H)_2$ molecule is the shortest at 2.155 Å; this is shorter than the equilibrium distance in gaseous Cu_2 (2.22 Å). It is concluded that the Cu–Cu interaction found in $Cu_2(\mu\text{-}H)_2$ is induced by the bridging hydrides through strong three-center, two electron interactions.[13]

1.5. Cu(I)–Cu(I) Interactions in Three-Center, Two-Electron Bonding

The first dinuclear hydride-bridged copper(I) complex to be structurally characterized was the (κ^2-trisphosphine)copper μ-hydride dimer (Figure 1.3).[14]

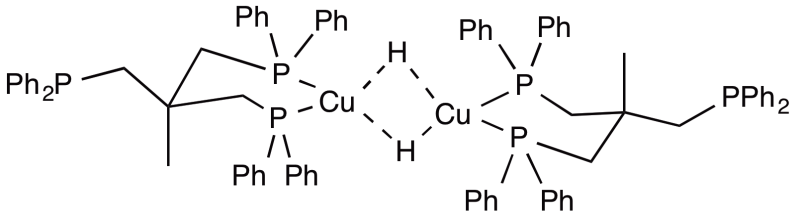

Figure 1.3. (κ^2-trisphosphine)copper μ-hydride dimer, $H_2Cu_2[CH_3C(CH_2PPh_2)_3]_2$; Cu–Cu distance of 2.371(2) Å.[14]

Since then, two three-coordinate hydride-bridged copper(I) complexes have also been identified.[15] The shortest copper–copper distance to date is 2.295(1) Å, found in the solid-state structure of an N-heterocyclic carbene (NHC) supported copper(I) hydride dimer (Figure 1.4).[15a]

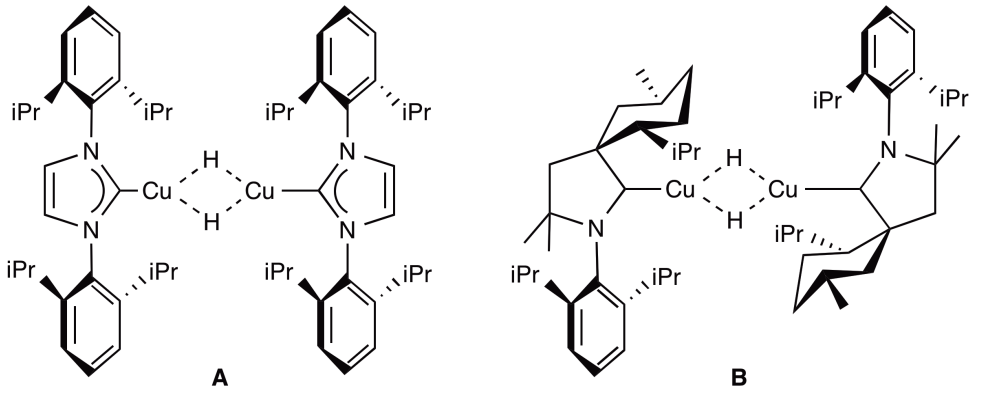

Figure 1.4. Crystallographically characterized dimeric copper(I) hyrdides; (**A**): Cu–Cu average distance 2.30 Å but as low as 2.295(1);[15a] (**B**): Cu–Cu 2.3058(5) Å.[15b]

Calhorda and coworkers predicted a species of the type $LCu(\mu\text{-}H)_2CuL$ would have a Cu–Cu separation of 2.29 Å.[12] Calculations show that the σ hybrid of LCu has more s character and lies lower in energy than that of L_2Cu. This leads to a better interaction between the in-phase combinations of H_{1s} orbitals and the Cu–Cu σ bonding combination. As a result, the Cu–Cu bond is strengthened by the increased electron density in the M–M bonding orbitals.

Three-center, two electron bonding gives rise to many short Cu–Cu intermetallic distances in copper(I) complexes. Examples of such bonding can be seen in oligiomeric copper(I) complexes bridged by carbanions (Figure 1.2); these complexes feature Cu–Cu interactions of 2.4 Å and shorter.[5,16] Another example was reported by Gischig and Togni who synthesized a dinuclear complex bridged by iodide and by an NHC acting as a bridging σ-donor. The rare bridging mode of the NHC carbene carbon between the two copper(I) centers leads to a copper–copper distance of 2.3561(13) Å.[17] In comparison, the more electrophilic carbene, diphenylmethylene, bridges two *β*-diketiminate supported copper(I) centers.[18] Despite the π-back-bonding interaction from the two Cu(I) centers to

the π-accepting carbene, the copper–copper distance of 2.4635(7) Å is longer then the intermetallic distance of the NHC bridged copper dimer.[18a] This supports the idea that better σ-donors as bridging ligands between Cu(I) centers leads to stronger Cu–Cu interactions.

Davenport and Tilley recently reported a series of dicopper(I) complexes bridged by both a naphthyridine scaffold and by single σ-donor ligands.[19] Among these complexes was an acetonitrile-bridged dicopper complex that exhibits a three-center, two-electron bonding interaction. The solid-state structure revealed a Cu–Cu contact of 2.4457(4) Å (Figure 1.5).

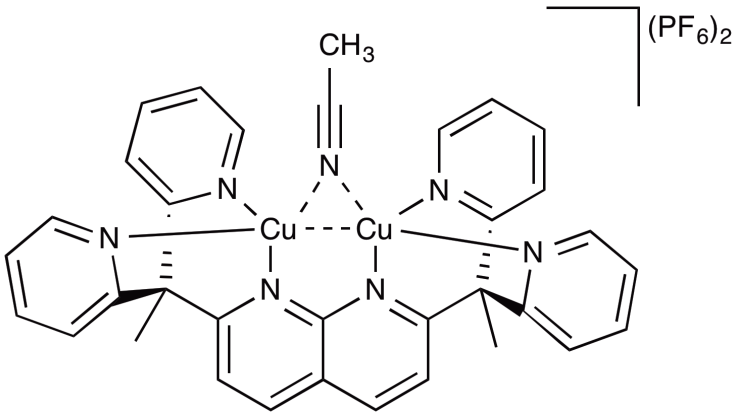

Figure 1.5. Acetonitrile-bridged (naphthyridine)dicopper(I) complex containing bond critical point; Cu–Cu 2.4457(4) Å.[19]

Even though there are geometric constraints imposed by the ligand structure, density functional theory calculations suggest the acetonitrile ligand is necessary for maintaining the close Cu–Cu contact. The Cu–Cu interaction was further investigated by the quantum theory of atoms in molecules.[20] A bond critical point, consistent with an attractive closed-shell interaction, between the two copper metal centers was determined. The

authors concluded that the small Cu–Cu distance is attributed to a cuprophilic interaction. Other Cu–Cu interactions have since been investigated by the quantum theory of atoms in molecules. Bond critical points were found between two Cu atoms in most complexes that were examined. These include Cu_2H_2, Cu_2Cl_2, and unsupported symmetrical [(X–Cu–L)$_2$] dimers (X = F or Cl, L = NH_3).[21]

There is still great variability in descriptions of closed shell d^{10} Cu–Cu interactions. While the short copper–copper contacts can be ascribed to net attractive interactions between d^{10} metal centers, to three-center, two-electron bonding, or to geometric constraints imposed by a bridging ligand, they may often result from a combination of these causes, and differentiating between them can be difficult. The different bonding descriptions necessitates a better experimental understanding of more Cu(I)–Cu(I) complexes and their bonding and reactivity.

1.6. Project Aim

The work discussed within this thesis originates from an interest in synthesizing multinuclear metal complexes for cooperative substrate activations in catalytic cycles. In light of previous studies that demonstrated the ability of N-heterocyclic carbene ligands to stabilize reactive copper(I) complexes,[22] I aimed to synthesize multinuclear (NHC)copper(I) complexes with interesting reactivity. This endeavor led to the synthesis of singly bridged dinuclear group 11 complexes with low coordination numbers. Some of the Cu complexes display bent arrangements around the bridging ligands with short Cu–Cu intermetallic distances. This raised interesting questions about the type of bonding within these Cu(I) complexes. The synthesis, bonding and reactivity of a bridged dinuclear copper(I) hydride, vinyl, boryl, and fluoride were carried out to form a basis for

the development of new catalytic reactions and to get a better understanding of the bonding motif found in such complexes.

1.7. References

1. For a review see: P. Pykkö, Chem. Rev. 97 (1997) 597.

2. a) J.-M. Poblet, M. Bénard, Chem. Commun. (1998) 1179; b) E. O'Grady, N. Kaltsoyannis, Phys. Chem. Chem. Phys. 6 (2004) 680; c) J.-P. Zhang, Y.-B. Wang, X.-C. Huang, Y.-Y. Lin, X.-M. Chen, Chem. Eur. J. 11 (2005) 552; d) X.-Y. Liu, F. Mota, P. Alemany, J.J. Novoa, S. Alvarez, Chem. Commun. (1998) 1149.

3. A. Bondi, J. Phys. Chem. 68 (1964) 441.

4. a) I.D. Brown, J.D. Dunitz, Acta. Cryst. 14 (1961) 480; b) A.L. Johnson, A.M. Willcocks, S.P. Richards, Inorg. Chem. 48 (2009) 8613; c) J. Beck, J. Strähle, Angew. Chem. Int. Ed. Engl. 24 (1985) 409.

5. a) J.A.J. Jarvis, B.T. Kilbourn, R. Pearce, M.F. Lappert, J. Chem. Soc., Chem. Commun. (1973) 475; b) J.M. Guss, R. Mason, I. Søtofte, G. van Koten, J.G. Noltes, J. Chem. Soc., Chem. Commun. (1972) 446; c) E.M. Meyer, S. Gambarotta, C. Floriani, A. Chiesi-Villa, C. Guastini, Organometallics 8 (1989) 1067; d) D. Nobel, G. van Koten, A.L. Spek, Angew. Chem. Int. Ed. Engl. 28 (1989) 208; e) For a review see: G. van Koten, J. Organomet. Chem. 400 (1990) 283.

6. a) F.A. Cotton, X. Feng, M. Matusz, R. Poli, J. Am. Chem. Soc. 110 (1988) 7077; b) F.A. Cotton, X. Feng, D.J. Timmons, Inorg. Chem. 37 (1998) 4066.

7. C. Kölmel, R. Ahlrichs, J. Phys. Chem. 94 (1990) 5536.

8. a) P.K. Mehrotra, R. Hoffmann, Inorg. Chem. 17 (1978) 2187; b) K.M. Merz, Jr., R. Hoffmann, Inorg. Chem. 27 (1988) 2120.

9. A. Avdeef, J.P. Fackler, Jr., Inorg. Chem. 17 (1978) 2182.

10. H.L. Hermann, G. Boche, P. Schwerdtfeger, Chem. Eur. J. 7 (2001) 5333.

11. F.J. Hollander, D. Coucouvanis, J. Am. Chem. Soc. 96 (1974) 5646.

12. C. Mealli, S.S.M.C. Godinho, M.J. Calhorda, Organometallics 20 (2001) 1734.

13. For a review see: G. Parkin, Struct. Bond. 136 (2010) 113.

14. G.V. Goeden, J.C. Huffman, K.G. Caulton, Inorg. Chem. 25 (1986) 2484.

15. a) N.P. Mankad, D.S. Laitar, J.P. Sadghi, Organometallics 23 (2004) 3369; b) G.D. Frey, B. Donnadieu, M. Soleilhavoup, G. Bertrand, Chem. Asian. J. 6 (2011) 402.

16. a) M. Stollenz, F. Meyer, Organometallics 31 (2012) 7708; b) X. He, M.M. Olmstead, P.P. Power, J. Am. Chem. Soc. 114 (1992) 9668; c) M. Håkansson, H. Eriksson, S. Jagner, Inorg. Chim. Acta 359 (2006) 2519; d) M. Niemeyer, Organometallics 17 (1998) 4649.

17. S. Gischig, A. Togni, Organometallics 24 (2005) 203.

18. a) X. Dai, T.H. Warren, J. Am. Chem. Soc. 126 (2004) 10085; b) Y.M. Badiei, T.H. Warren, J. Organomet. Chem. 690 (2005) 5989.

19. T.C. Davenport, T.D. Tilley, Angew. Chem. Int. Ed. 50 (2011) 12205.

20. R.F.W. Bader, Atoms in Molecules: A Quantum Theory, Oxford University Press, Oxford (1990).

21. S. Dinda, A.G. Samuelson, Chem. Eur. J. 18 (2012) 3032.

22. For a review see: a) J.C.Y. Lin, R.T.W. Huang, C.S. Lee, A. Bhattacharyya, W.S. Hwang, I.J.B. Lin, Chem. Rev. 109 (2009) 3561; b) S. Díez-González, N. Marion, S.P. Nolan, Chem. Rev. 109 (2009) 3612.

CHAPTER 2

Bonding and Reactivity of a μ-Hydrido Dicopper Cation

Part of this thesis chapter has been adapted with permission from an article co-written by the author:

C.M. Wyss, B.K. Tate, J. Bacsa, T.G. Gray, J.P. Sadighi, "Bonding and Reactivity of a μ-Hydrido Dicopper Cation." *Angew. Chem. Int. Ed.* **2013**, *52*, 12920-12923.

2.1. Introduction

Copper hydride complexes are versatile reagents, with new applications appearing rapidly.[1] Copper hydride was first prepared in the mid-19th century,[2] but its structure remained unknown for more than 80 years.[3] The characterization[4] of $[\{(Ph_3P)CuH\}_6]$ sparked interest in the structure and bonding of well-defined copper hydride clusters,[5] and the use of copper in the industrial reduction of CO to methanol inspired the synthesis of copper hydride clusters through hydrogenolysis.[6] Following the development of mild and selective reductions using $[\{(Ph_3P)CuH\}_6]$,[7,8] numerous methods were developed for the copper-catalyzed hydrosilylation[8,9] and hydrogenation[10] of organic substrates. Recently, Liu et al. reported a Cu_{20} cluster containing $[Cu_2H_5]^{3-}$ moiety, which releases dihydrogen upon irradiation with sunlight.[11]

Copper hydrides with fewer than six metal centers are rare.[5a,6a,12,13] N-Heterocyclic carbene (NHC)[14,15] and especially cyclic alkylaminocarbene (CAAC)[16] ligands stabilize a $[Cu_2(\mu\text{-}H)_2]$ core. The NHC ligand also supports the hydride-bridged dinuclear species $[(LAu)_2(\mu\text{-}H)]^+$[17] and $[(LAg)_2(\mu\text{-}H)]^+$.[18] These cations adopt bent structures with very short intermetallic distances, and there are indications of direct

metal–metal bonding. Interactions between d^{10} centers, however, are generally weaker for copper than for silver and gold.[19] We sought to explore the structure and reactivity of a hydrido-bridged dicopper cation.

For a number of oligocopper(I) complexes, short copper–copper contacts have been ascribed to net attractive interaction between d^{10} metal centers,[20,21] to three-center, two-electron bonding,[22] or to geometric constraints imposed by a bridging ligand.[23] In the desired species $[(LCu)_2(\mu\text{-}H)]^+$, the presence of a single, spherical bridging ligand minimizes such constraints, permitting but not requiring a direct metal–metal interaction.[24-26] Theoretical studies of $[Cu_2H]^+$ have variously predicted a linear geometry[27] or a bent geometry[28] with a short copper–copper distance.[29]

This thesis chapter describes the isolation of a hydride-bridged dicopper cation, $\{[(IDipp)Cu]_2(\mu\text{-}H)\}^+$, as its BF_4^- salt. The cation adopts a bent arrangement about the hydride with a short intermetallic distance. Density functional theory (DFT) calculations suggest that the copper–copper interaction is mediated primarily by the bridging hydride. Despite its overall positive charge, this complex displays hydridic reactivity. It undergoes facile methanolysis, and undergoes carboxylation to afford a (κ^2-formate)-bridged dicopper species. This complex also coordinates carbon monoxide reversibly to form a labile carbonyl adduct, and insertion of phenylacetylene affords a *gem*-dicopper vinyl cation.

2.2. Results and Discussion

2.2.1. Synthesis of $\{[(IDipp)Cu]_2(\mu\text{-}H)\}^+ BF_4^-$

The desired hydride complex was prepared by reaction of a heteratom-bridged dicopper cation with a main group hydride (Scheme 2.1). Anion exchange between sodium trimethylsilanolate and (IDipp)CuCl[30] affords the useful precursor (IDipp)Cu($OSiMe_3$) in good yield. Treatment of this complex with one-half equivalent of Ph_3C^+ BF_4^- results in siloxide abstraction, with formation of the siloxide-bridged $\{[(IDipp)Cu]_2(\mu\text{-}OSiMe_3)\}^+$ BF_4^-. The reaction between the siloxide-bridged dicopper cation and pinacolborane [4,4,5,5-tetramethyl-1,3,2-dioxaborolane; HB(pin)] leads to hydride exchange, forming $\{[(IDipp)Cu]_2(\mu\text{-}H)\}^+$ BF_4^- (**1**) and the hydrocarbon-soluble byproduct $Me_3SiOB(pin)$.

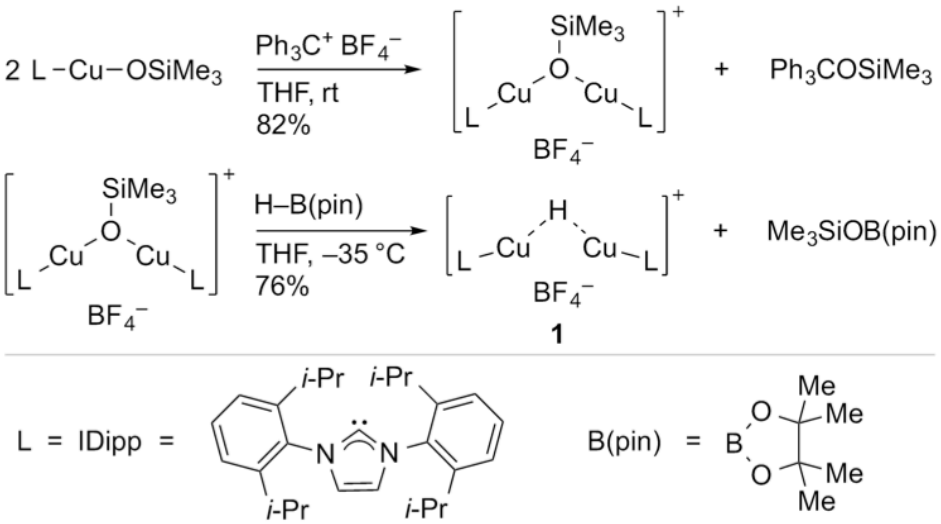

Scheme 2.1. Synthesis of hydride-bridged dicopper complex **1**.

The ^1H NMR spectrum of **1** in THF-d_8 solution displays a single set of resonances arising from the two IDipp ligands, and a singlet resonance at $\delta = -4.13$ ppm assigned to the hydride. Reaction of the siloxide-bridged precursor with $PhSiD_3$ likewise affords deuteride-bridged **1**-*d*. The ^1H NMR spectrum of **1**-*d* is identical to that of **1** except for

the absence of the hydride resonance, and the ^{2}H NMR spectrum shows a singlet resonance at $\delta = -4.13$ ppm.

2.2.2. Structural aspects

Slow diffusion of hexanes into a THF solution of **1** afforded colorless crystals suitable for X-ray diffraction (Figure 2.1).[31] Two crystallographically distinct cations, with similar bond lengths and angles, are present in the asymmetric unit. The BF_4^- anions are located well outside the copper coordination spheres. The C–Cu–Cu angles, ranging from 156.1(3)° to 163.2(3)°, are consistent with the presence of a triangular $[Cu_2H]$ core. The Cu–Cu distances, 2.5331(15) Å and 2.5354(15) Å, are considerably less than twice the van der Waals radius of copper.[32] The positions of the bridging hydrides could be refined; the L–Cu–H angles range from 165(2)° to 175(2)°, and the Cu–H–Cu angles are 121(3)° and 122(3)°.[33]

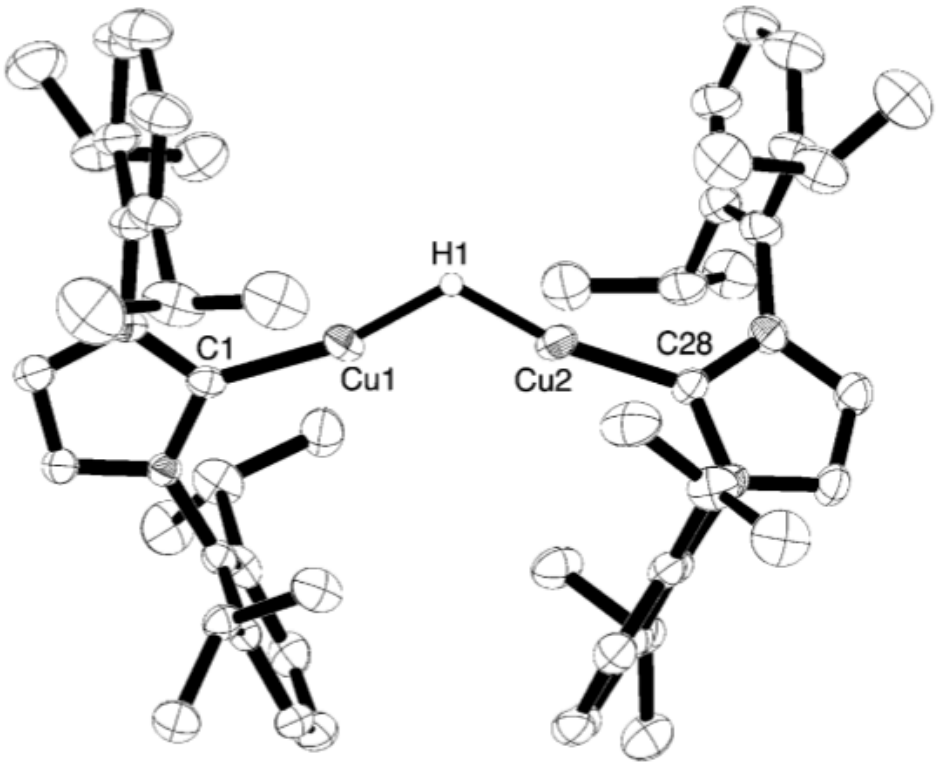

Figure 2.1. ORTEP view of **1**. Ellipsoids are set at 50% probability; the BF_4^- anion and hydrogen atoms except the μ-hydride are omitted for clarity. Only one cation of two in the asymmetric unit is shown. Selected bond lengths [Å] and angles [°]: Cu1–Cu2 2.5331(15), C1–Cu1 1.873(9), Cu1–H1 1.45(2), H1–Cu2 1.45(2), Cu2–C28 1.908(8); C1–Cu1–H1 167.4(16), Cu1–H1–Cu2 122(3), H1–Cu2–C28 174.4(16), C1–Cu1–Cu2 163.2(3), Cu1–Cu2–C28 156.1(3).

2.2.3. Density functional theory calculations

Density functional theory (DFT) calculations were applied to **1′**, a model compound in which the ligand (IMe) bears *N*-methyl rather than *N*-(2,6-diisopropylphenyl) groups, to elucidate the copper–copper and copper–hydrogen interactions. Geometry optimization of **1′** converged on a potential energy minimum with rough C_2 symmetry. The copper–copper distance was calculated at 2.509 Å, which is close to the experimentally determined values.

The highest occupied Kohn–Sham orbital (HOMO) of **1′**, which is largely copper-derived (84% Cu, 16% NHC), is copper–copper antibonding in character (Figure 2.2).

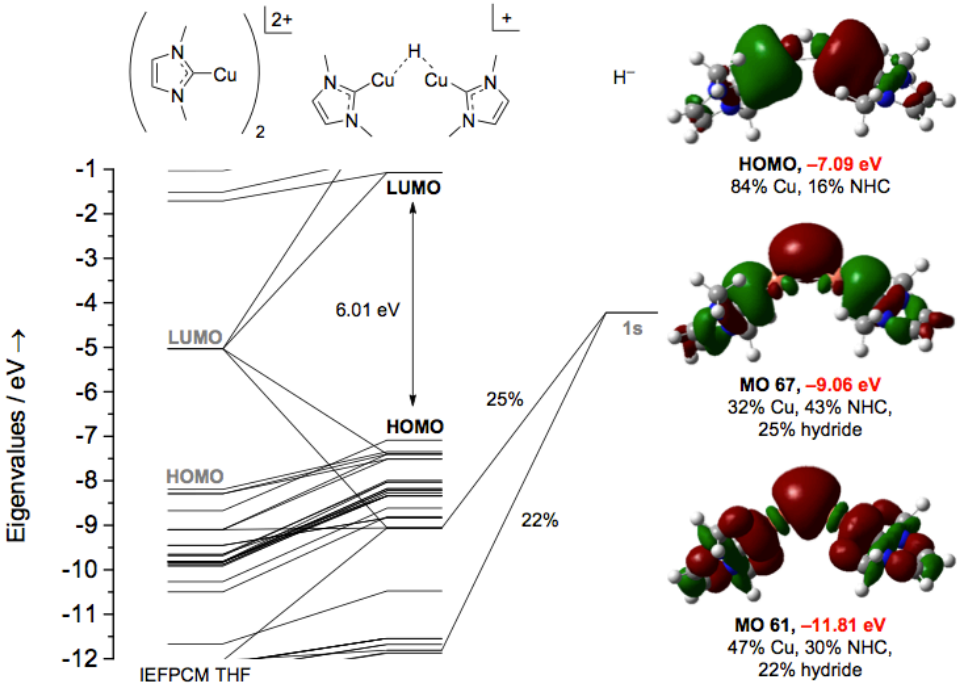

Figure 2.2. Partial Kohn–Sham orbital energy diagram **1′**. Plots of selected orbitals, with eigenvalues and percentage compositions in terms of fragments, appear at the right. Implicit THF solvation is included; see the experimental for details.

Descriptions of three-center, two-electron bonding in $[M_2H]$ complexes depict a similar orbital as the lowest-energy unoccupied level in a three-orbital scheme.[24c-e] This apparent discrepancy is resolved by considering the symmetry-allowed mixing of filled copper 3d orbital combinations with the corresponding 4s/4p orbital combinations. The $[Cu_2H]^+$ bonding may thus be viewed as a three-center, six-electron system. Consistent with this interpretation, these calculations find two filled Cu–H–Cu bonding orbitals, which are 1.97 eV and 4.72 eV below the HOMO in potential energy.

According to natural population analysis, the Wiberg bond order[34] between copper centers is 0.386 in the Löwdin basis; the copper–hydrogen bond orders are 0.534 and 0.535. Analysis of the copper–copper interaction using the atoms-in-molecules theory[35] found no bond critical point. These findings suggests that the $[(LCu)_2H]^+$ cation is an example of an open three-center interaction[36] in which the metal–metal interaction occurs mainly through the bridging hydride. For comparison, in a dicopper(I) complex with a σ-bridging acetonitrile ligand, three-center bonding does give rise to a bond critical point between the copper centers.[37]

2.2.4. Reactivity

Addition of CD_3OD to a solution of **1** in THF-d_8 results in a rapid reaction to form H–D,[38] as judged by ^{1}H NMR spectroscopy, plus a major species assigned as $\{[(IDipp)Cu]_2(\mu\text{-}OCD_3)\}^+ BF_4^-$ (Scheme 2.2).

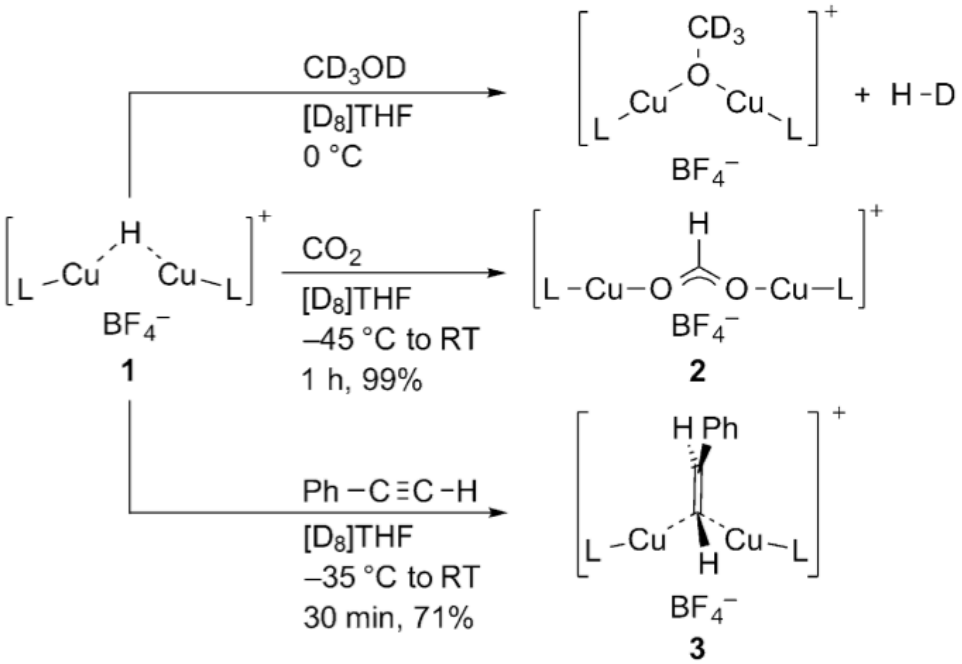

Scheme 2.2. Reactions of **1** with selected small molecules.

Complex **1** also reacts readily with CO_2 to form $\{[(IDipp)Cu]_2(\kappa\text{-}O_2CH)\}^+ BF_4^-$ (**2**). This complex, prepared independently from the terminal formate $(IDipp)CuO_2CH$ by partial formate abstraction, has been characterized crystallographically (see Figure 2.10 in experimental). Generally, the reactivity of metal hydrides toward CO_2 depends on the degree of anionic character at hydrogen.[39] In its reactivity toward CD_3OD and CO_2, the $[Cu_2H]^+$ core of **1** displays considerable hydridic character despite its overall positive charge. Consistent with this behavior, natural population analysis of **1′** find a charge of –0.123 on the bridging hydrogen.

The affinity of **1** for carbon monoxide was examined using ^1H NMR spectroscopy (Figure 2.3). Exposure of a solution of **1** in CD_2Cl_2 to an atmosphere of CO at –45 °C resulted in a shift of the hydride resonance from δ –4.29 ppm to δ –2.66 ppm. After a single freeze-pump-thaw cycle, the hydride resonance was recorded at δ –3.26 ppm, and successive freeze-pump-thaw cycles resulted in the shift of the hydride resonance beyond δ –4 ppm. A single set of IDipp-derived resonances was observed throughout.

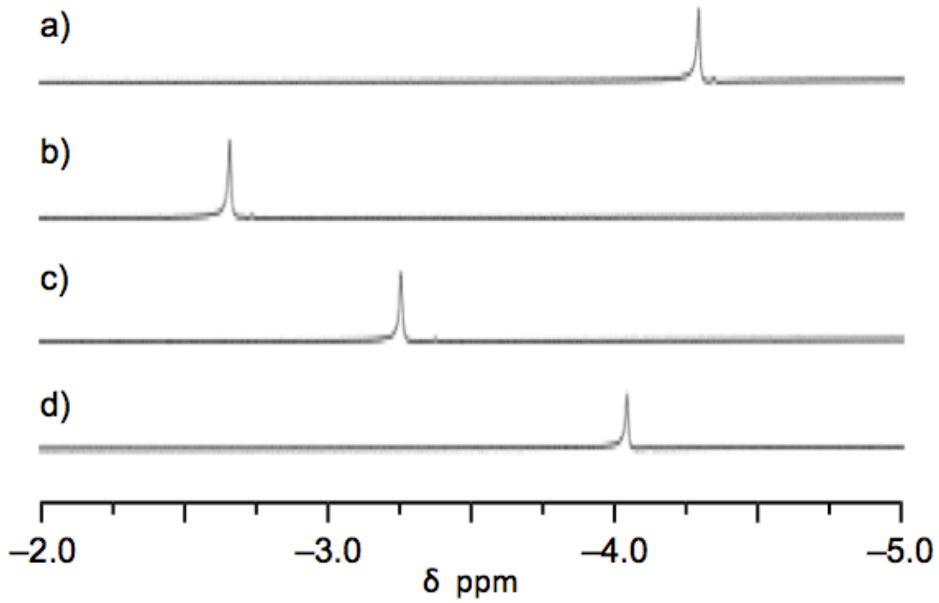

Figure 2.3. Partial ^{1}H NMR spectra showing μ-H resonances: a) of **1** before exposure to CO; b) of **1** after exposure to CO (1 atm, –45 °C, 20 min); c) of **1**/**1**•CO mixture after one degas cycle; d) of **1**/**1**•CO mixture after four degas cycles.

We conclude that the CO binds **1** weakly and reversibly to form the carbonyl adduct **1**•CO, and that carbonyl exchange between **1**•CO and **1** is rapid on the NMR timescale, giving rise to a weighted average resonance for the bridging hydride. The lability of the bound CO precluded isolation of this adduct, but the infrared spectrum of **1**•CO in CH_2Cl_2 solution displayed a sharp resonance of moderate intensity at 2,109 cm^{-1}, compared to 2,143 cm^{-1} for free CO (Figure 2.4). This small shift to a lower stretching frequency is consistent with the expected poor backbonding from an (NHC)copper(I) fragment bearing a partial positive charge.[40] Computational studies indicated that the most stable carbonyl adduct of **1′** is **1′**•CO, bearing a terminal carbonyl ligand at one of the two copper centers.

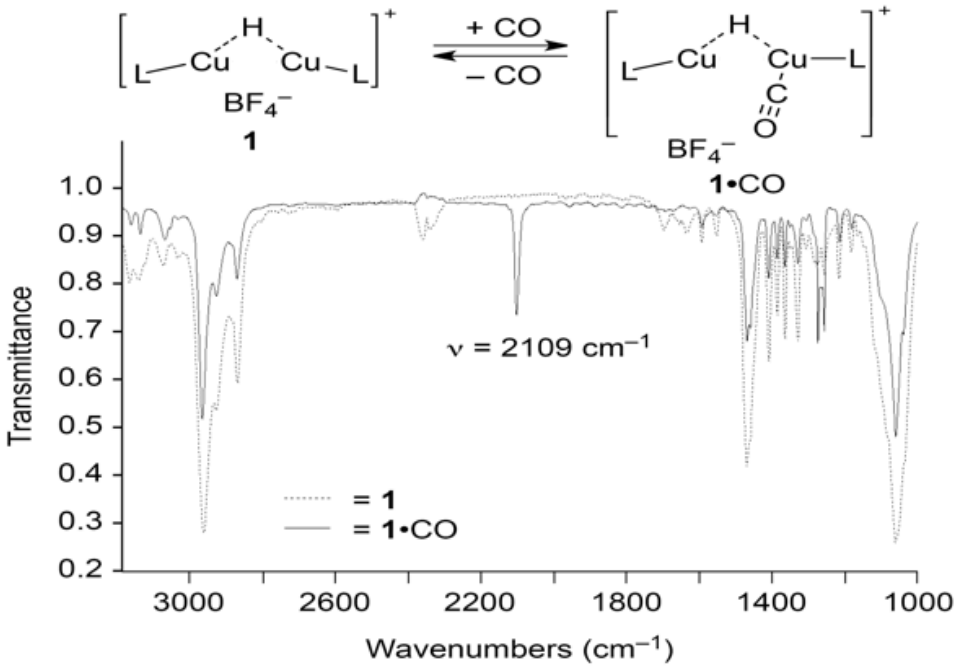

Figure 2.4. FT-IR spectra of **1** and **1**•CO in CH_2Cl_2 solution. Proposed **1**•CO structure is based on DFT calculations for **1′**•CO (L = IMe).

The reactivity of **1** with an alkyne to form a vinyl-bridged dicopper cation,[41] analogous to the *gem*-diaurated vinyl complexes studied as catalytic intermidiates,[42] was investigated. Vinyl-bridged dicopper(I) complexes are rare,[43] but copper(I) μ-aryl oligomers are well known.[44] Alkyl-bridged cations such as $[Cu_2(\mu\text{-}CH_3)]^+$ have been shown to undergo C–C bond-forming reactions with allylic halides in the gas phase.[45] Recently, *gem*-dicopper vinylidene complexes have been identified as intermediates in copper-catalyzed azide-alkyne click cycloadditions.[46]

Phenylacetylene reacts with **1** in THF solution within 30 minutes at ambient temperature, forming a product characterized by NMR spectroscopy and by X-ray crystallography as a (*trans*-phenylvinyl)-bridged dicopper(I) complex (**3**, Figure 2.5).

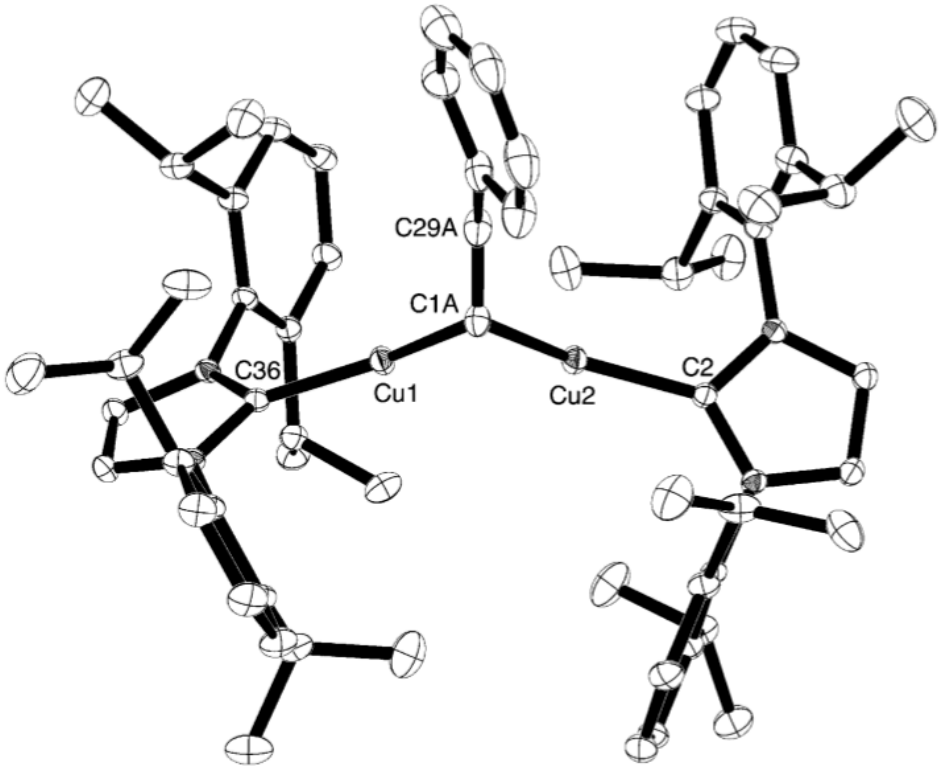

Figure 2.5. ORTEP view of **3**. Ellipsoids are set at 50% probability; the BF_4^- anion, hydrogen atoms, and THF solvent are omitted for clarity. Selected bond lengths [Å] and angles [°]: Cu1–Cu2 2.6303(4), C36–Cu1 1.923(1), Cu1–C1A 2.034(6), C1A–Cu2 2.003(6), Cu2–C2 1.925(1), C1A–C29A 1.333(8); C36–Cu1–C1A 154.3(2), C1A–Cu2–C2 151.2, C36–Cu1–Cu2 154.21(4), Cu1–Cu2–C2 156.77(4), Cu1–C1A–Cu2 81.3(2), C29A–C1A–Cu1 112.2(4), C29A–C1A–Cu2 111.7(4).

The Cu–Cu distance of 2.6303(4) Å is slightly longer than in hydride-bridged **1**. The C_{NHC}–Cu–C_{vinyl} angles are 154.3(2)° and 151.2(2)°. Key metrics of the *trans*-phenyl-vinyl moiety are similar to those of *trans*-stilbene:[47] The C=C–(Cu_2 centroid) angle is 119.5°, and the C=C distance 1.333(8) Å. The IMe-ligated analogue **3′**, which would arise from insertion of phenylacetylene into **1′**, was examined by DFT. Geometry optimization produced a structure essentially similar to that of **3**, albeit with a shorter intermetallic distance of 2.499 Å. The Wiberg bond order for the copper–copper interaction is 0.269 in the Löwdin basis. Because the calculated distance is shorter than

the experimentally determined distance this bond order, like that of **1′**, should be regarded as an upper limit. The corresponding Cu–C bond orders are 0.609 and 0.620. Again, an atoms-in-molecules analysis found no bond critical point between the copper centers, indicating that the metal–metal interaction is primarily ligand-mediated. Bonding in the $[Cu_2C_{vinyl}]^+$ core of **3′**, as in the $[Cu_2H]^+$ core of **1′**, is calculated to involve an open three-center interaction.

Complex **3** reacts with CO_2 to form $\{[(IDipp)Cu]_2(\kappa\text{-}O_2CCHCHPh)\}^+ BF_4^-$ as judged by ^1H NMR and ^{13}CNMR spectroscopy (see experimental). It also reacts with pinacolborane [4,4,5,5-tetramethyl-1,3,2-dioxaborolane; HB(pin)], forming $\{[(IDipp)Cu]_2(\mu\text{-}H)\}^+ BF_4^-$ (**1**) and (pin)BCHCHPh as judged by ^1H NMR and ^{11}B NMR spectroscopy, closing a catalytic cycle (Scheme 2.3). Future work will explore this catalytic cycle more fully.

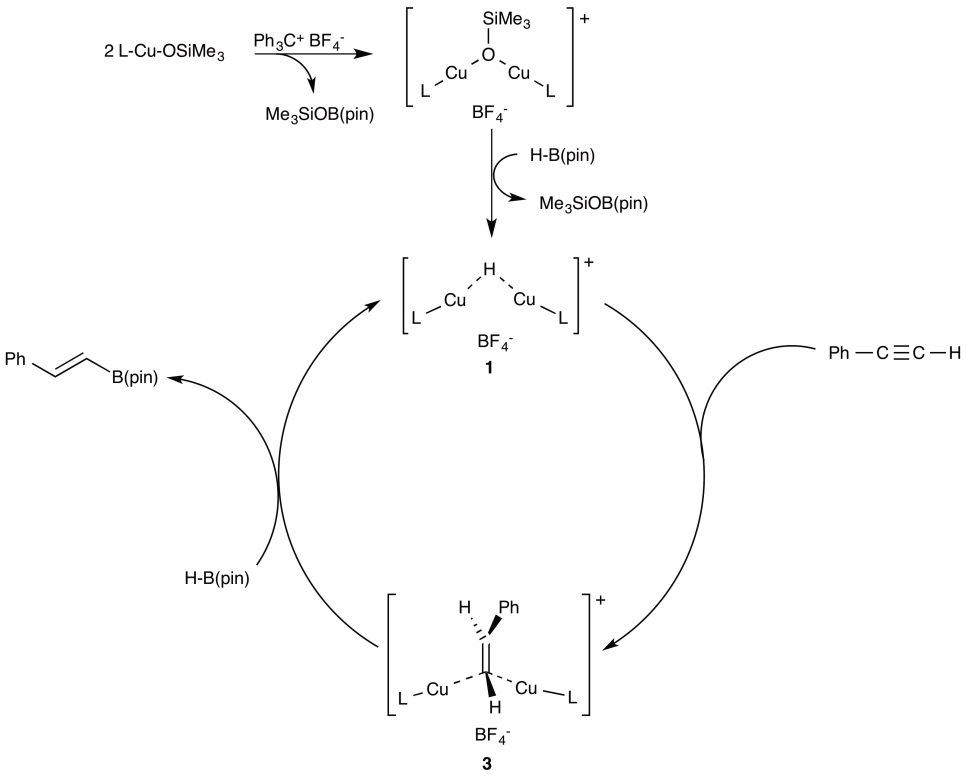

Scheme 2.3. Reaction of **3** with HB(pin), closing a catalytic cycle for alkyne hydroboration.

2.3. Conclusion

In summary, an N-heterocyclic carbene ligand supports a bent $[Cu_2H]^+$ complex with a short intermetallic distance but little direct interaction between the copper centers. The bridging hydride shows significant anionic character, reflected in its reactions with methanol and carbon dioxide. Insertion of a terminal alkyne forms a geminally dicuprated vinyl complex. Carbon monoxide binds to $\{[(IDipp)Cu]_2(\mu\text{-}H)\}^+$ BF_4^- weakly and reversibly to form a carbonyl adduct assigned as $\{[(IDipp)Cu](\mu\text{-}H)[Cu(IDipp)(CO)\}^+$ BF_4^-.

2.4. Experimental

2.4.1. General considerations

Unless otherwise indicated, manipulations were performed in an MBraun glovebox under an inert atmosphere of nitrogen, or in resealable glassware on a Schlenk line under an atmosphere of argon. Glassware and magnetic stir bars were dried in a ventilated oven at 160 °C and were allowed to cool under vacuum.

^{1}H and ^{13}C NMR spectra were obtained using a Bruker DSX 400 MHz spectrometer and a Varian Vx 400 MHz spectrometer. ^{1}H and ^{13}C NMR chemical shifts are referenced with respect to solvent signals and are reported relative to tetramethylsilane. Unless otherwise indicated, solid samples for infrared spectroscopy were prepared as pellets in potassium bromide, using a pellet die which was dried in a ventilated oven at 160 °C and cooled under vacuum prior to use. The pellets were prepared in the glovebox under an atmosphere of dry nitrogen, and were exposed to air as briefly as possible prior to data collection. Spectra were recorded using a Perkin Elmer Spectrum 1000 infrared spectrometer. Elemental analyses were performed by Atlantic Microlab, Inc. in Norcross, Georgia.

2.4.2. Materials and methods

Dichloromethane (BDH), diethyl ether (EMD Millipore Omnisolv), hexanes (EMD Millipore Omnisolv), tetrahydrofuran (THF, EMD Millipore Omnisolv), and toluene (EMD Millipore Omnisolv) were sparged with ultra high purity argon (NexAir) for 30 minutes prior to first use, dried using an MBraun solvent purification system, transferred to Straus flasks, degassed using three freeze-pump-thaw cycles, and stored under nitrogen or argon. Anhydrous benzene (EMD Millipore Drisolv) and anhydrous pentane (EMD Millipore Drisolv), both sealed under a nitrogen atmosphere, were used as

received and stored in a glovebox. Tap water was purified in a Barnstead International automated still prior to use.

Dichloromethane-d_2 (Cambridge Isotope Laboratories) was dried over calcium hydride overnight, vacuum-transferred to an oven-dried resealable Schlenk flask, and degassed by successive freeze-pump-thaw cycles. Tetrahydrofuran-d_8 (Cambridge Isotope Laboratories) was dried over sodium benzophenone ketyl, transferred under vacuum to an oven-dried sealable flask, and degassed by successive freeze-pump-thaw cycles.

Sodium *tert*-butoxide (TCI America), copper(I) chloride (Alfa-Aesar), triphenylcarbenium tetrafluoroborate (Alfa-Aesar), 2,6-diisopropylaniline (Sigma-Aldrich), acetic acid (Alfa-Aesar), paraformaldehyde (Alfa-Aesar), chlorotrimethylsilane (Sigma-Aldrich), glyoxal 40% w/w aqueous solution (Alfa-Aesar), methanol (BDH), ethyl acetate (BDH), sodium trimethylsilanolate (Sigma-Aldrich), 4,4,5,5-tetramethyl-1,3,2-dioxaborolane (Sigma-Aldrich), 4,4′-dimethylbiphenyl (Sigma-Aldrich), magnesium sulfate (Alfa-Aesar), sodium metal (Alfa-Aesar), benzophenone (Alfa-Aesar), calcium hydride (Alfa-Aesar), $^{13}CO_2$ (Cambridge Isotope Labs), nitrogen (NexAir), carbon dioxide (NexAir), carbon monoxide (GT&S Inc.) and argon (both industrial and ultra high purity grades, NexAir) were used as received. Triethoxysilane (Sigma-Aldrich) was degassed using three freeze-pump-thaw cycles prior to use. Phenylacetylene (Sigma-Aldrich) was degassed and filtered through a short column of alumina (EMD) prior to use. IDipp·HCl,[48] (IDipp)CuCl,[30b] and $[(IDipp)CuH]_2$[14] were prepared according to literature protocols and were characterized by ^1H NMR spectroscopy. Phenylsilane-d_3 was prepared by the reaction of trichlorophenylsilane

(Sigma-Aldrich) with lithium aluminum deuteride (Sigma-Aldrich) in analogy to a published protocol for the preparation of alkylsilanes.[49]

Preparation of (IDipp)Cu(OSiMe$_3$)

Sodium trimethylsilanolate (0.074 g, 0.662 mmol) was added to a suspension of (IDipp)CuCl (0.323 g, 0.662 mmol) in THF (6 mL) with stirring. After 3 hours, the reaction mixture was filtered through Celite, and the filter pad was washed with two portions of THF (3 mL each). The filtrate was concentrated, and the residue was dried for 12 hours at 40 °C under vacuum, affording the product as a white powder (0.312 g, 0.576 mmol, 87%). ^{1}H NMR (400 MHz, CD_2Cl_2): δ (ppm) 7.51 (t, *J* = 7.8 Hz, 2H, *para*-C*H*), 7.33 (d, *J* = 7.8 Hz, 4H, *meta*-C*H*), 7.14 (s, 2H, NC*H*), 2.57 (sept, *J* = 6.9 Hz, 4H, C*H*(CH$_3$)$_2$), 1.30 (d, *J* = 6.9 Hz, 12H, CH(C*H*$_3$)$_2$), 1.22 (d, *J* = 6.9 Hz, 12H, CH(C*H*$_3$)$_2$), –0.46 (s, 9H, OSi(C*H*$_3$)$_3$). ^{13}C{^{1}H} NMR (100 MHz, CD_2Cl_2): δ (ppm) 182.4 (N*C*Cu), 146.3 (*ortho*-*C*), 135.5 (*ipso*-*C*), 130.7 (*para*-*C*), 124.5 (*meta*-*C*), 123.5 (N*C*H), 29.2 (*C*H(CH$_3$)$_2$), 25.0 (CH(*C*H$_3$)$_2$), 24.2 (CH(*C*H$_3$)$_2$), 4.2 (OSi(*C*H$_3$)$_3$). IR: ν (cm^{-1}) 3161 (w), 2964 (s), 2871, 1477, 1407, 1384, 1362, 1234 (s), 987 (s), 822 (s), 753 (s), 664 (w), 513 (w), 444 (w). Anal. Calcd. for $C_{30}H_{45}N_2CuOSi$: C, 66.56; H, 5.18; N, 8.38. Found: C, 66.45; H, 5.16; N, 8.36.

Preparation of {[(IDipp)Cu]$_2$(μ-OSiMe$_3$)}$^+$ BF$_4^-$

Triphenylcarbenium tetrafluoroborate (0.152 g, 0.460 mmol) was added to a solution of (IDipp)Cu(OSiMe$_3$) (0.520 g, 0.961 mmol) in THF (10 mL). The reaction flask was covered with foil to exclude light, and the mixture was stirred for 4 hours. Anhydrous pentane (20 mL) was added to the reaction mixture, resulting in the formation

of a white precipitate. The precipitate was collected on a fritted glass filter and washed with two portions of toluene (6 mL each) and two portions of pentane (5 mL each). Residual solvents were removed under vacuum at 40 °C over 18 hours, affording the product as a white powder (0.408 g, 0.378 mmol, 82%). ^{1}H NMR (400 MHz, CD_2Cl_2): δ (ppm) 7.51 (t, *J* = 7.8 Hz, 4H, *para*-C*H*), 7.28 (d, *J* = 7.8 Hz, 8H, *meta*-C*H*), 7.13 (s, 4H, NC*H*), 2.48 (sept, *J* = 6.9 Hz, 8H, C*H*(CH_3)$_2$), 1.16 (d, *J* = 6.8 Hz, 24H, CH(C*H*$_3$)$_2$), 1.04 (d, *J* = 6.8 Hz, 24H, CH(C*H*$_3$)$_2$), –0.73 (s, 9H, OSi(C*H*$_3$)$_3$). ^{13}C{^{1}H} NMR (100 MHz, CD_2Cl_2): δ (ppm) 178.2 (N*C*Cu), 145.4 (*ortho*-*C*), 135.0 (*ipso*-*C*), 131.2 (*para*-*C*), 125.1 (*meta*-*C*), 124.8 (N*C*H), 29.1 (*C*H(CH_3)$_2$), 24.8 (CH(*C*H$_3$)$_2$), 24.3 (CH(*C*H$_3$)$_2$), 4.2 (OSi(*C*H$_3$)$_3$). IR: ν (cm^{-1}) 3171 (w), 2964 (s), 2868, 1595 (w), 1559 (w), 1470 (s), 1408, 1361 (w), 1329 (w), 1243, 1059 (s), 944 (w), 884 (s), 839, 804, 759 (w), 605 (w), 451 (w). Anal. Calcd. for $C_{57}H_{81}N_4Cu_2BF_4OSi$: C, 63.37; H, 7.56; N, 5.19. Found: C, 63.34; H, 7.57; N, 5.14.

*Preparation of {[(IDipp)Cu]$_2$(μ-H)}$^+$ BF$_4^-$ (**1**)*

A solution of {[(IDipp)Cu]$_2$(μ-OSiMe$_3$)}$^+$ BF$_4^-$ (0.125 g, 0.116 mmol) in THF (3 mL) and a solution of 4,4,5,5-tetramethyl-1,3,2-dioxaborolane (0.020 mL, 0.018 g, 0.138 mmol) in THF (1 mL) were cooled to −35°C. The 4,4,5,5-tetramethyl-1,3,2-dioxaborolane solution was added dropwise via pipette to the {[(IDipp)Cu]$_2$(μ-OSiMe$_3$)}$^+$ BF$_4^-$ solution with stirring, and the resulting mixture was allowed to stand at −35 °C for 1 hour. A layer of hexane (15 mL) was carefully added over the THF solution, and the layers were allowed to mix by diffusion at −35 °C for 18 hours, resulting in the formation of colorless crystals. The mother liquor was decanted, and the crystals were collected on a fritted glass filter. The crystals were triturated, then washed with two

portions of hexane (2 mL each), affording the product as a white powder (0.087 g, 0.088 mmol, 76%). The product decomposes slowly in solution at room temperature. ^{1}H NMR (400 MHz, THF-d_8): δ (ppm) 7.56 (s, 4H, NC*H*), 7.53 (t, *J* = 7.8 Hz, 4H, *para*-C*H*), 7.30 (d, *J* = 7.8 Hz, 8H, *meta*-C*H*), 2.48 (sept, *J* = 6.8 Hz, 8H, C*H*(CH$_3$)$_2$), 1.17 (d, *J* = 6.8 Hz, 24H, CH(C*H*$_3$)$_2$), 1.01 (d, *J* = 6.8 Hz, 24H, CH(C*H*$_3$)$_2$), –4.13 (s, 1H, Cu*H*Cu). ^{13}C{^{1}H} NMR (100 MHz, THF-d_8): δ (ppm) 178.8 (N*C*Cu), 146.0 (*ortho*-*C*), 135.1 (*ipso*-*C*), 131.3 (*para*-*C*), 125.6 (N*C*H), 124.8 (*meta*-*C*), 29.2 (*C*H(CH$_3$)$_2$), 25.4 (CH(*C*H$_3$)$_2$), 23.5 (CH(*C*H$_3$)$_2$). IR: ν (cm^{-1}) 3168 (w), 2964 (s), 2872, 1595 (w), 1467 (s), 1408, 1329, 1280 (w), 1214 (w), 1059 (s), 947 (w), 806, 757 (s), 697, 520, 451.

Note: We have been unable to obtain a satisfactory elemental analysis of **1**. The complex is extremely moisture-sensitive, and decomposes slowly at ambient temperature. After learning that carboxylation proceeds quantitatively (see p. 37), we assessed the purity of **1** by exposing a sample to CO_2, isolating but not purifying the more stable product **2**, and obtaining its elemental analysis. We reasoned that only a sufficiently pure sample of **1** would give rise to analytically pure **2**. Thus a solution of **1** (0.050 g, 0.050 mmol) in THF-d_8 (0.7mL), in a J. Young NMR tube, was degassed by three freeze-pump-thaw cycles, then pressurized with CO_2 (*ca*. 1 atm) at –45°C. The tube was allowed to warm to ambient temperature under continuous agitation. After 1 hour the mixture was transferred to a Schlenk flask and concentrated. The resulting white powder was dried at 40 °C for 18 hours under vacuum. Anal. Calcd. for $C_{55}H_{73}N_4O_2Cu_2BF_4$: C, 63.76; H, 7.10; N, 5.41. Found: C, 63.46; H, 6.92; N, 5.31.

Diffraction-quality crystals were grown by vapor diffusion of hexanes into a THF solution of $\{[(IDipp)Cu]_2(\mu\text{-}H)\}^+ BF_4^-$ at −35 °C.

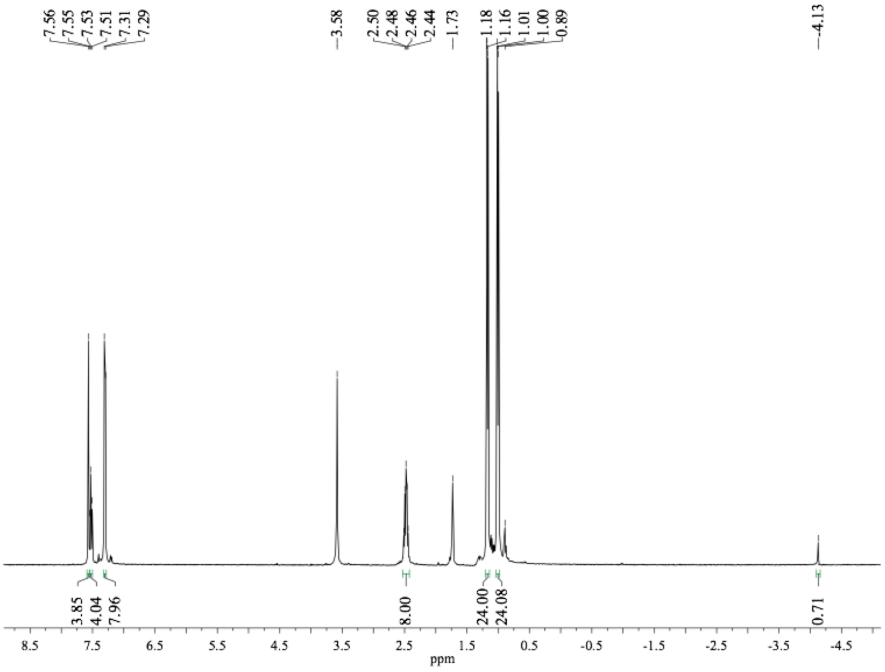

Figure 2.6. ^{1}H NMR spectrum (400 MHz, THF-d_8) of $\{[(IDipp)Cu]_2(\mu\text{-}H)\}^+ BF_4^-$. A trace of residual solvent, hexanes (δ 1.29 and 0.89 ppm), is present.

*Preparation of $\{[(IDipp)Cu]_2(\mu\text{-}^2H)\}^+ BF_4^-$ (**1**-d)*

A solution of $\{[(IDipp)Cu]_2(\mu\text{-}OSiMe_3)\}^+ BF_4^-$ (0.190 g, 0.176 mmol) in THF (3 mL) and a solution of phenylsilane-d_3 (0.033 mL, 0.029 g, 0.261 mmol) in THF (1 mL) were cooled to −35 °C. The phenylsilane-d_3 solution was added dropwise via pipette to the $\{[(IDipp)Cu]_2(\mu\text{-}OSiMe_3)\}^+ BF_4^-$ solution with stirring, and the resulting mixture was allowed to stand at −35°C for 1 hour. A layer of pentane (15 mL) was carefully added over the THF solution, and the layers were allowed to mix by diffusion at −35 °C for 18 hours, resulting in the formation of colorless crystals. The mother liquor was decanted,

and the crystals were collected on a fritted glass filter. The crystals were triturated, then washed with two portions of pentane (2 mL each), affording the product as a white powder (0.152 g, 0.153 mmol, 87%). The product decomposes slowly in solution at room temperature. The ^{2}H NMR spectrum was acquired from a sample in THF solution, with a small quantity of THF-d_8 added to allow locking and shimming. ^{1}H NMR (400 MHz, THF-d_8): δ (ppm) 7.56 (s, 4H, NC*H*), 7.53 (t, J = 8.0 Hz, 4H, *para*-C*H*), 7.30 (d, J = 7.6 Hz, 8H, *meta*-C*H*), 2.48 (sept, J = 6.8 Hz, 8H, C*H*(CH$_3$)$_2$), 1.17 (d, J = 6.8 Hz, 24H, CH(C*H*$_3$)$_2$), 1.01 (d, J = 6.8 Hz, 24H, CH(C*H*$_3$)$_2$). ^{2}H NMR (30.0 MHz, THF-d_8): δ (ppm) −4.13 (s).

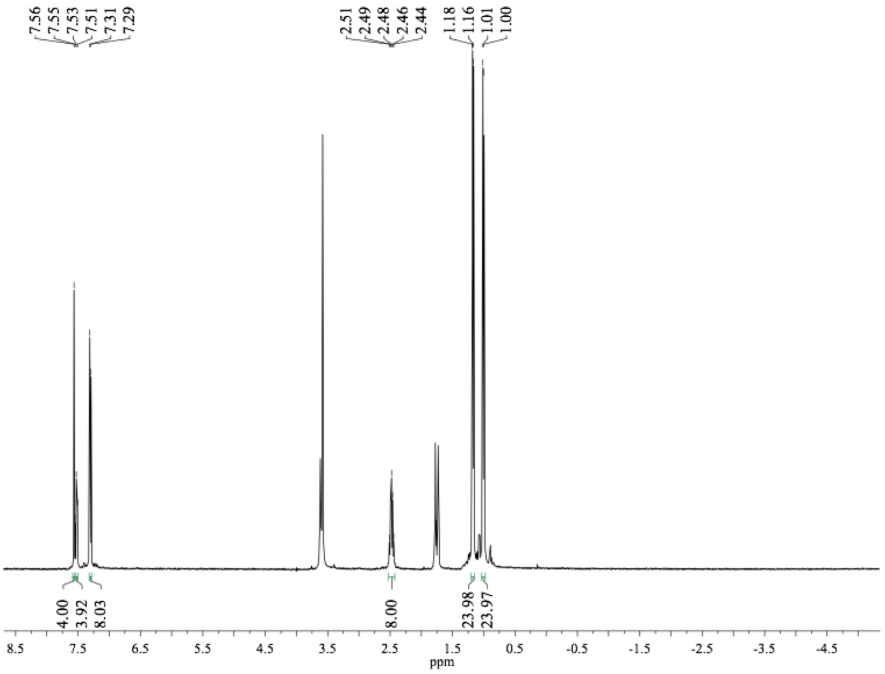

Figure 2.7. ^{1}H NMR spectrum (400 MHz, THF-d_8) of {[(IDipp)Cu]$_2$(μ-^{2}H)}$^{+}$ BF$_4^{-}$. A trace of residual solvent, THF (δ 3.62 and 1.79 ppm), is present. The ^{1}H NMR spectrum is identical to that of {[(IDipp)Cu]$_2$(μ-H)}$^{+}$ BF$_4^{-}$ except for the missing hydride resonance at δ –4.13 ppm.

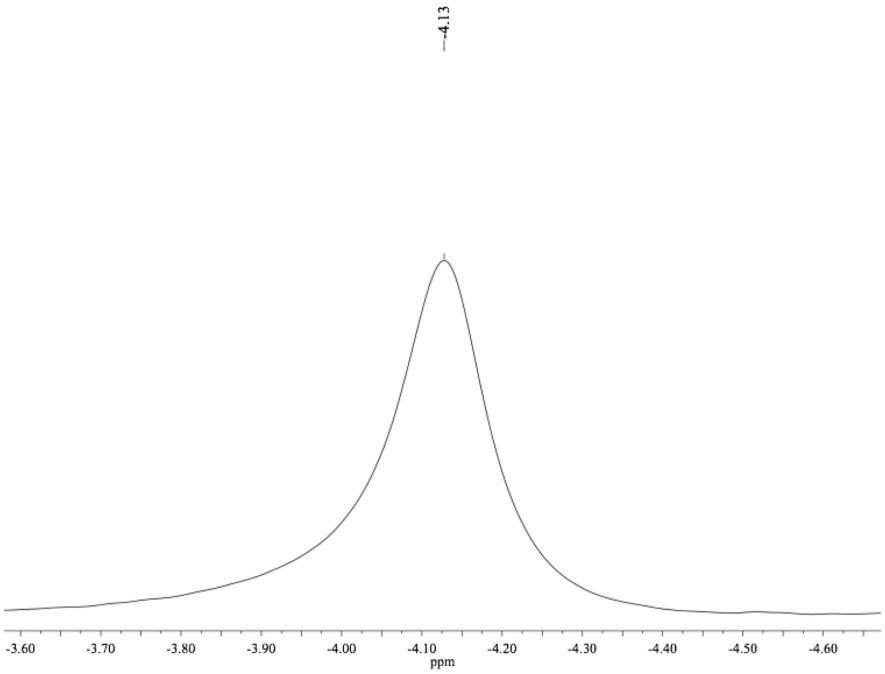

Figure 2.8. ^{2}H NMR spectrum (30.0 MHz, THF-d_8) of $\{[(IDipp)Cu]_2(\mu\text{-}^{2}H)\}^{+}$ BF_4^{-}.

Preparation of (IDipp)Cu(OOCH)

In a dried, 25-mL Schlenk flask under N_2, {[(1,3-Bis(2,6-diisopropylphenyl)imidazol-2-ylidene]copper(I) hydride}dimer was generated *in situ* from (IDipp)Cu(O*t*Bu) (0.601 g, 1.14 mmol) and triethoxysilane (0.300 mL, 0.267 g, 1.63 mmol) in diethyl ether (12 mL) at −45 °C.[14] The solution was degassed by one freeze-pump-thaw cycle, then exposed to an atmosphere of CO_2. The bright yellow solution immediately became colorless, and deposited a white precipitate. Cooling was discontinued, and the mixture was stirred for 15 minutes. The resulting solution was concentrated *in vacuo*. The residual white solid was suspended in pentane (15 mL), filtered, and washed with three portions of pentane (5 mL each). Drying under vaccum at 40 °C for 14 hours afforded the product as a white powder (0.564 g, 1.13 mmol, 99%). ^{1}H NMR (400 MHz, THF-d_8): δ (ppm) 7.79 (s, 1H, OOC*H*), 7.52 (s, 2H, NC*H*), 7.48 (t, *J*

= 7.7 Hz, 2H, *para*-C*H*), 7.34 (d, *J* = 7.6 Hz, 4H, *meta*-C*H*), 2.65 (sept, *J* = 6.8 Hz, 4H, C*H*(CH_3)$_2$), 1.31 (d, *J* = 6.8 Hz, 12H, CH(C*H*$_3$)$_2$), 1.23 (d, *J* = 6.8 Hz, 12H, CH(C*H*$_3$)$_2$). ^{13}C{^{1}H} NMR (100 MHz, THF-d_8): δ (ppm) 181.2 (N*C*Cu), 166.2 (OO*C*H), 146.4 (*ortho*-*C*), 135.7 (*ipso*-*C*), 130.8 (*para*-*C*), 124.6 (*meta*-*C*), 124.5 (N*C*H), 29.4 (*C*H(CH_3)$_2$), 24.9 (CH(*C*H$_3$)$_2$), 23.9 (CH(*C*H$_3$)$_2$). IR: ν (cm^{-1}) 3165 (w), 2964 (s), 2861 (w), 2813 (w), 2714 (w), 1628 (s), 1467, 1405, 1365, 1329 (w), 1309, 1181, 1151 (w), 1065 (w), 944 (w), 809, 760, 697 (w), 447 (w). Anal. Calcd. for $C_{28}H_{37}N_2CuO_2$: C, 67.65; H, 5.63; N, 7.50. Found: C, 67.41; H, 5.64; N, 7.47.

*Preparation of {[(IDipp)Cu]$_2$(μ-OOCH)}$^+$ BF_4^- (**2**)*

Triphenylcarbenium tetrafluoroborate (0.103 g, 0.312 mmol) was added to a solution of (IDipp)Cu(OOCH) (0.310 g, 0.624 mmol) in THF (6 mL). The reaction flask was covered with foil to exclude light, and the mixture was stirred for 3 hours. Anhydrous pentane (20 mL) was added to the THF solution, resulting in the formation of a white precipitate. The precipitate was collected on a fritted glass filter and washed with three portions of pentane (5 mL each). Residual solvents were removed under vacuum at 40 °C for 18 hours, affording the product as a white powder (0.256 g, 0.247 mmol, 79%). ^{1}H NMR (400 MHz, THF-d_8): δ (ppm) 7.64 (s, 4H, NC*H*), 7.46 (t, *J* = 7.8 Hz, 4H, *para*-C*H*), 7.33 (d, *J* = 7.8 Hz, 8H, *meta*-C*H*), 7.26 (s, 1H, OOC*H*), 2.57 (sept, *J* = 6.8 Hz, 8H, C*H*(CH_3)$_2$), 1.22 (d, *J* = 6.8 Hz, 24H, CH(C*H*$_3$)$_2$), 1.19 (d, *J* = 6.8 Hz, 24H, CH(C*H*$_3$)$_2$). ^{13}C{^{1}H} NMR (100 MHz, THF-d_8): δ (ppm) 178.7 (N*C*Cu), 171.7 (OO*C*H), 146.4 (*ortho*-*C*), 135.6 (*ipso*-*C*), 131.6 (*para*-*C*), 125.4 (N*C*H), 124.7 (*meta*-*C*), 29.4 (*C*H(CH_3)$_2$), 25.0 (CH(*C*H$_3$)$_2$), 23.7 (CH(*C*H$_3$)$_2$). IR: ν (cm^{-1}) 3168 (w), 2964 (s), 2868, 1582 (s), 1474, 1408, 1349, 1329 (w), 1273 (w), 1214 (w), 1059 (s), 944 (w), 806, 760,

694 (w), 605 (w). Anal. Calcd. for $C_{55}H_{73}N_4Cu_2BF_4O_2$: C, 63.76; H, 5.41; N, 7.10. Found: C, 63.54; H, 5.29; N, 6.94.

Diffraction-quality crystals were grown by vapor diffusion of diethyl ether vapor into a THF solution of $\{[(IDipp)Cu]_2(\mu\text{-}OOCH)\}^+ BF_4^-$.

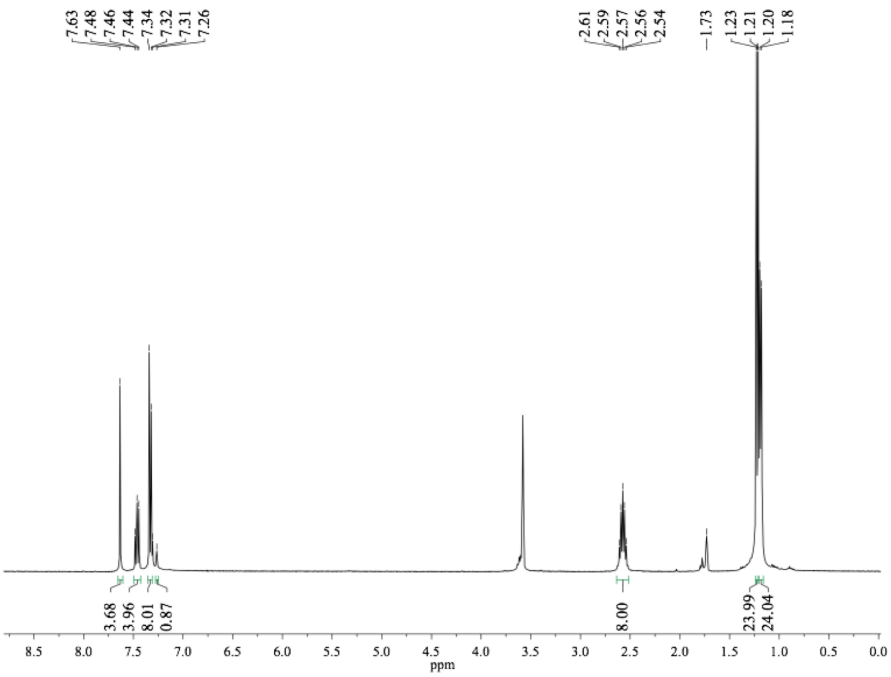

Figure 2.9. ^{1}H NMR spectrum (400 MHz, THF-d_8) of $\{[(IDipp)Cu]_2(\mu\text{-}OOCH)\}^+ BF_4^-$. A trace of benzene (δ 7.31 ppm) is present as the result of benzophenone ketyl decomposition along with residual solvent, THF (δ 3.62 and 1.79 ppm).

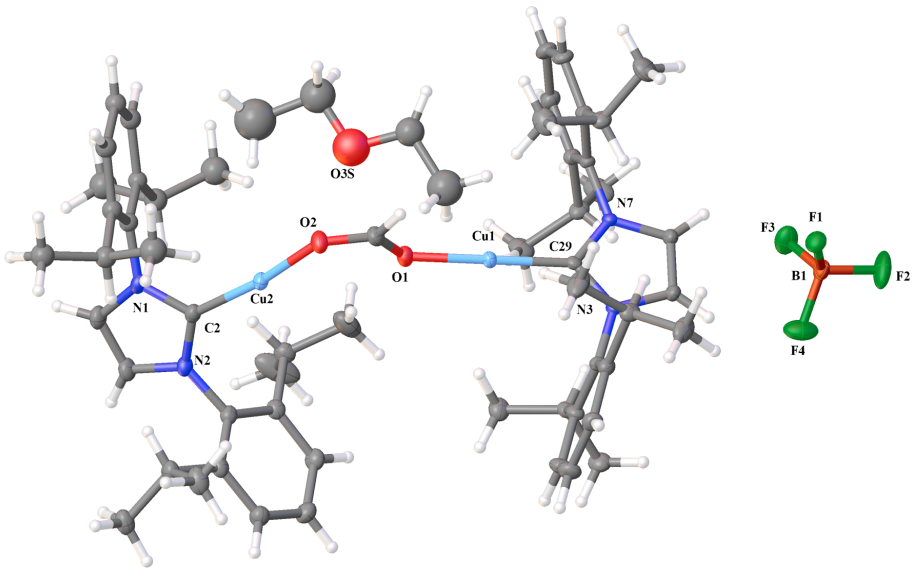

Figure 2.10. X-ray crystal structure of $\{[(IDipp)Cu]_2(\mu\text{-}OOCH)\}^+ BF_4^-$ cocrystallized with diethyl ether. Selected lengths (Å) and angles (°): C2–Cu2 1.868(1), Cu2–O2 1.857(1), O2–C1 1.252(2), C1–O1 1.255(2), O1–Cu1 1.861(1), Cu1–C29 1.865(1); C2–Cu2–O2 171.23(7), Cu2–O2–C1 125.6(2), C1–O1–Cu1 125.7(1), O1–Cu1–C29 177.69(6).

Preparation of $\{[(IDipp)Cu]_2(\mu\text{-}trans\text{-}CHCHPh)\}^+ BF_4^-$ ***(3)***

Phenylacetylene (0.014 mL, 0.013 g, 0.127 mmol) was added to a solution of $\{[(IDipp)Cu]_2(\mu\text{-}H)\}^+ BF_4^-$ (0.127 g, 0.128 mmol) in THF (4 mL) cooled to −35 °C. Cooling was discontinued, and the mixture was stirred for 30 minutes. The resulting red solution was concentrated *in vacuo*. The residual grey solid was taken up in hexanes (15 mL) and stirred briefly. The solid was allowed to settle before the mother liquor was decanted. Residual solvents were removed under vacuum for 2 hours, affording the product as a grey powder (0.099 g, 0.090 mmol, 71%). ^{1}H NMR (400 MHz, THF-d_8): δ (ppm) 7.52 (s, 4H, NC*H*), 7.43 (t, J = 7.8 Hz, 4H, *para*-C*H*), 7.21 (d, J = 7.6 Hz, 8H, *meta*-C*H*), 6.82 (m, 2H, Ph *ortho*-C*H*), 6.28 (d, J = 20 Hz, 1H, CC*H*Ph), 5.64 (d, J = 20 Hz, 1H, CuC*H*Cu), 2.45 (sept, J = 6.8 Hz, 8H, C*H*$(CH_3)_2$), 1.11 (d, J = 6.8 Hz, 24H,

$CH(CH_3)_2$), 0.93 (d, J = 6.8 Hz, 24H, $CH(CH_3)_2$). $^{13}C\{^1H\}$ NMR (100 MHz, THF-d_8): δ (ppm) 179.3 (N*C*Cu), 161.2 (Cu*C*Cu), 145.9 (*ortho-C*), 137.7 (C*C*Ph), 135.2 (*ipso-C*), 131.1 (*para-C*), 129.5 (Ph *para-C*), 128.5 (Ph *meta-C*), 127.6 (Ph *ortho-C*), 126.5 (Ph *ipso-C*), 125.3 (N*C*H), 124.8 (*meta-C*), 29.2 ($CH(CH_3)_2$), 24.9 ($CH(CH_3)_2$), 23.7 ($CH(CH_3)_2$). IR: ν (cm^{-1}) 3168 (w), 3069 (w), 2961 (s), 2872, 1530 (w), 1470 (s), 1411, 1365, 1326, 1283 (w), 1217 (w), 1181 (w), 1063 (s), 941 (w), 803, 763 (s), 701 (w), 657 (w), 520 (w), 447 (w).

Note: We have been unable to obtain a satisfactory elemental analysis for this complex. Like **1**, complex **3** is extremely sensitive to air and moisture. Attempts to obtain its high-resolution mass spectrum were unsuccessful due to decomposition. We have reproduced ^1H and ^{13}C NMR spectra, which we believe represent the purity of the sample prepared as described above.

Diffraction-quality crystals were grown by cautious layering of hexanes onto a THF solution of $\{[(IDipp)Cu]_2(\mu\text{-}CHCHPh)\}^+ BF_4^-$.

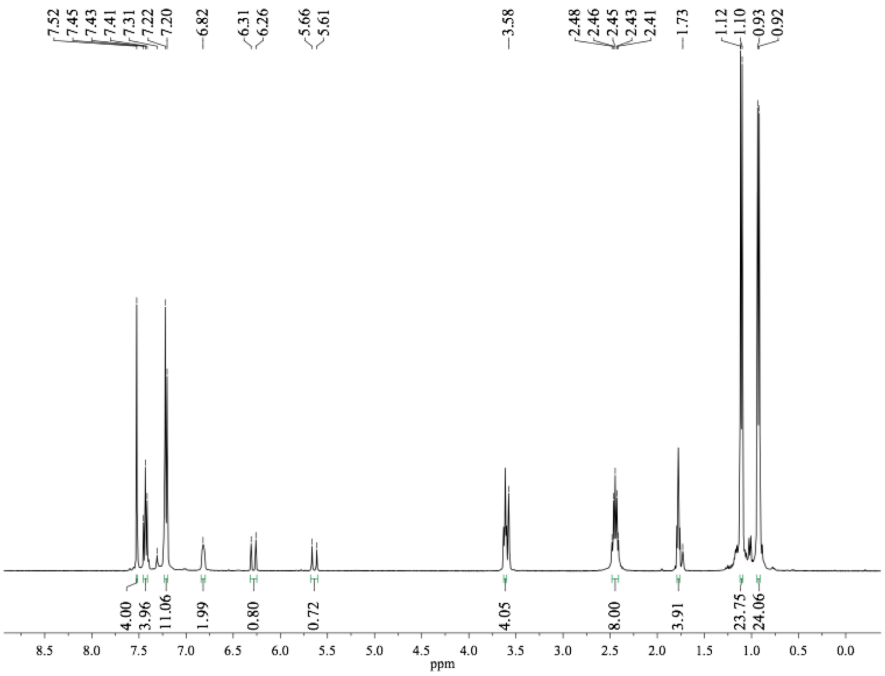

Figure 2.11. ^{1}H NMR spectrum (400 MHz, THF-d_8) of $\{[(IDipp)Cu]_2(\mu\text{-}CHCHPh)\}^+$ BF_4^-. The resonances for the phenyl *ortho*- and *meta*-protons are coincident with those for the *meta*-protons of the ligand aryl groups, resulting in an integral of 11H. A trace of benzene (δ 7.31 ppm) is present as the result of benzophenone ketyl decomposition along with residual solvent, THF (δ 3.62 and 1.79 ppm).

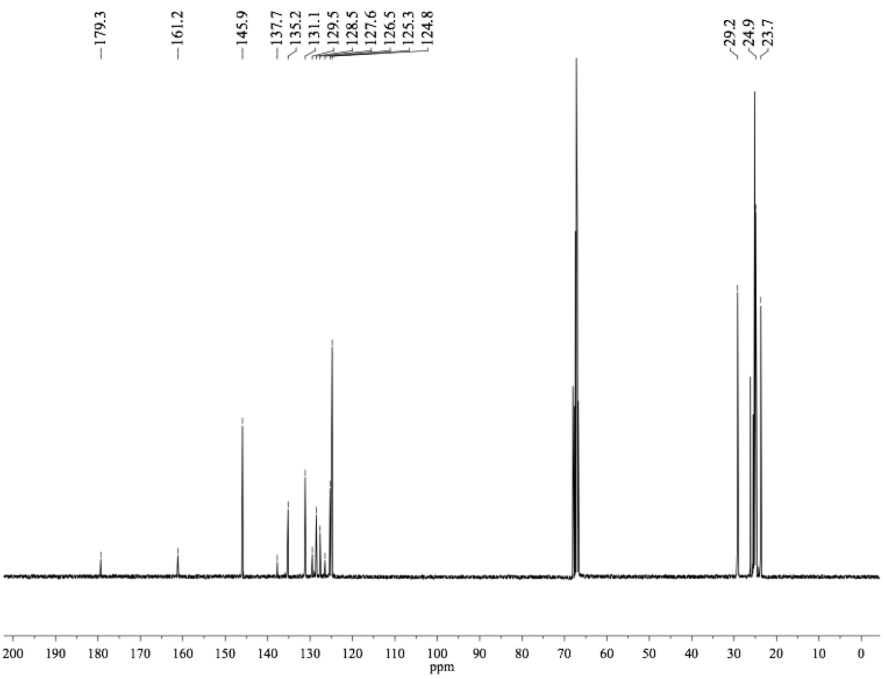

Figure 2.12. $^{13}C\{^{1}H\}$ NMR spectrum (100 MHz, THF-d_8) of $\{[(IDipp)Cu]_2(\mu\text{-}CHCHPh)\}^+ BF_4^-$. A trace of residual solvent, THF (δ 68.0 and 26.2 ppm), is present.

Reaction of $\{[(IDipp)Cu]_2(\mu\text{-}H)\}^+ BF_4^-$ with CO_2

A solution of $\{[(IDipp)Cu]_2(\mu\text{-}H)\}^+ BF_4^-$, (0.030 g, 0.030 mmol) in THF-d_8 (0.7 mL) cooled to −35 °C in an NMR tube equipped with a J. Young valve was degassed by three freeze-pump-thaw cycles, then pressurized with CO_2 (*ca.* 1 atm) at –45 °C. The tube was agitated continuously to ensure mixing. The reaction progress was checked at intervals by ^1H NMR spectroscopy. After 1 hour, the ^1H NMR spectrum was identical to that of authentic $\{[(IDipp)Cu]_2(\mu\text{-}OOCH)\}^+ BF_4^-$, prepared as described above. The internal 4,4′-dimethylbiphenyl (0.011g, 0.060 mmol) was added to the NMR tube. The yield for $\{[(IDipp)Cu]_2(\mu\text{-}OOCH)\}^+ BF_4^-$ (99%) was determined by integration of peak areas with respect to those of 4,4′-dimethylbiphenyl in the ^1H NMR spectrum. A separate sample of $\{[(IDipp)Cu]_2(\mu\text{-}H)\}^+ BF_4^-$ was exposed to $^{13}CO_2$, and the ^1H and ^{13}C NMR spectra were recorded after 1 hour.

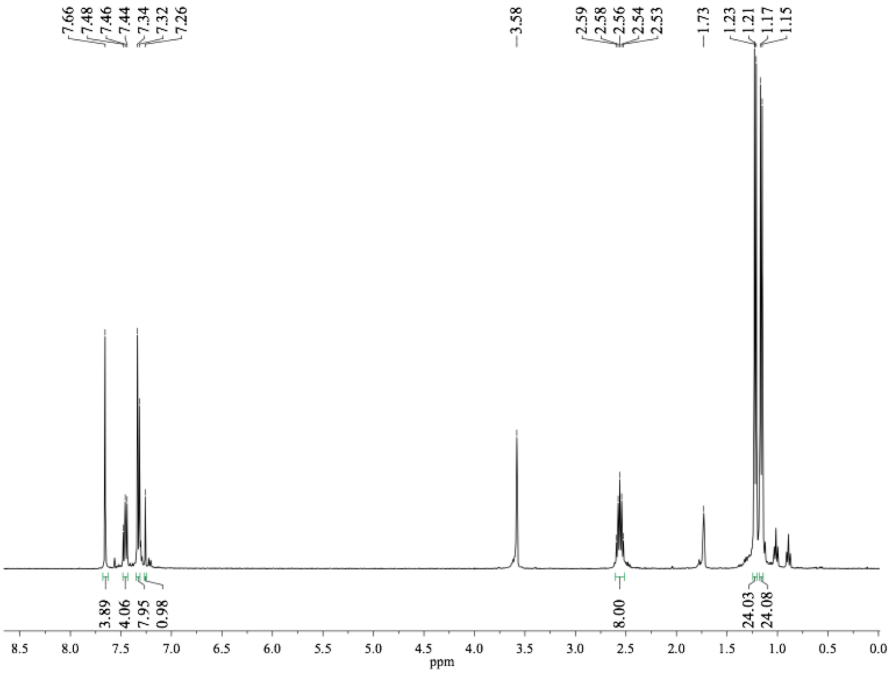

Figure 2.13. ^{1}H NMR spectrum (400 MHz) of $\{[(IDipp)Cu]_2(\mu\text{-}H)\}^+$ BF_4^- in THF-d_8 solution after one hour's exposure to CO_2 (*ca.* 1 atm). A trace of residual solvent, hexanes (δ 1.29 and 0.89 ppm), is present.

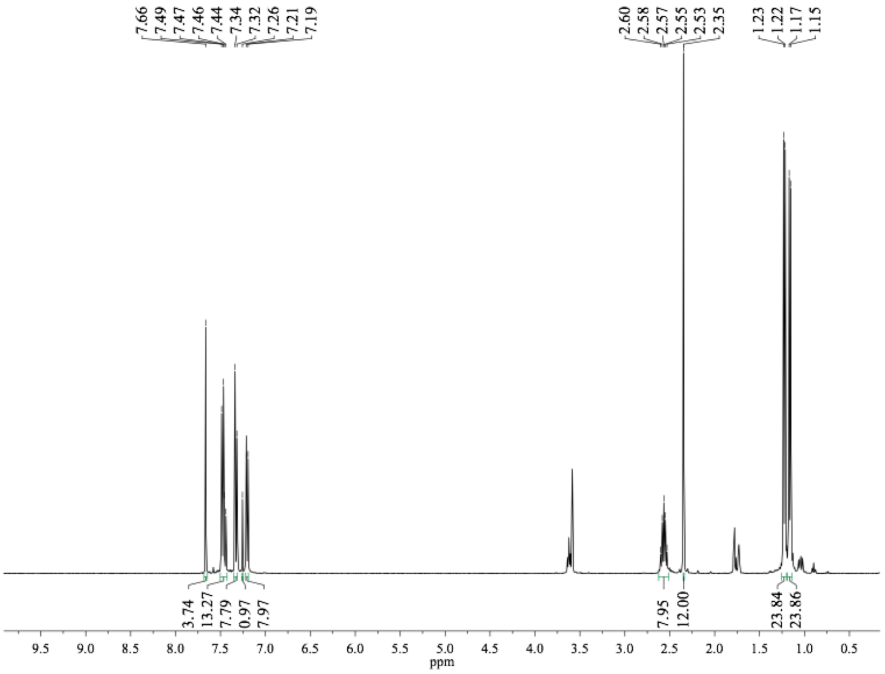

Figure 2.14. ^{1}H NMR spectrum (400 MHz) of $\{[(IDipp)Cu]_2(\mu\text{-}H)\}^+$ BF_4^- in THF-d_8 solution after one hour's exposure to CO_2 (*ca.* 1 atm). One equivalent of 4,4′-dimethylbiphenyl [δ (ppm) 7.48 (d, 4H, J = 7.8 Hz), 7.20 (d, 4H, J = 7.8 Hz), 2.35 (s, 6H)] and residual solvent, THF (δ 3.62 and 1.79 ppm), are present.

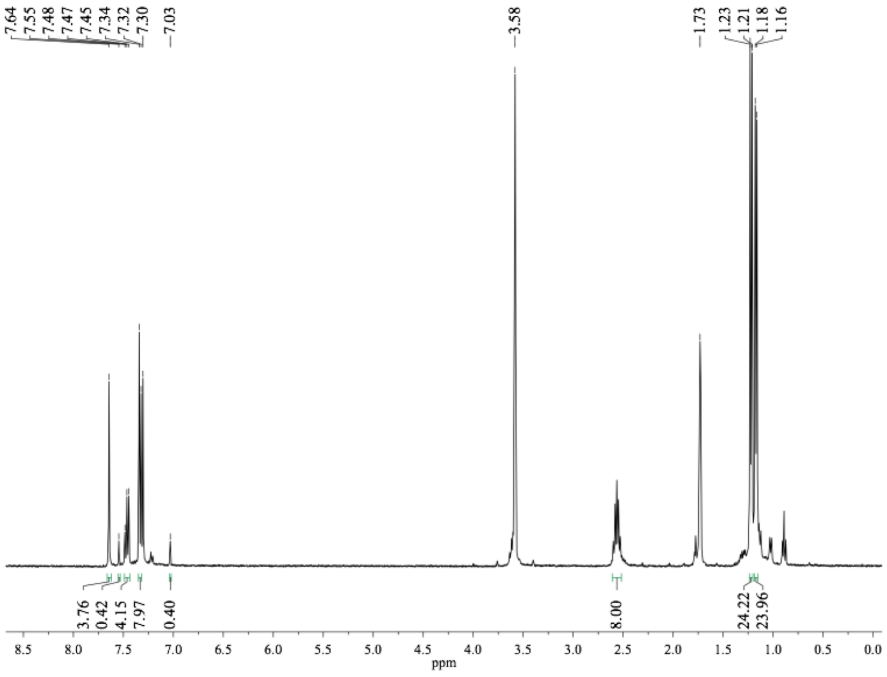

Figure 2.15. ^{1}H NMR spectrum (400 MHz) of $\{[(IDipp)Cu]_2(\mu\text{-}H)\}^+$ BF_4^- in THF-d_8 solution after one hour's exposure to $^{13}CO_2$ (*ca.* 1 atm). The presence of ^{13}C-formate is indicated by a doublet ($J(^1H\text{-}^{13}C)$ = 206 Hz) at δ 7.29 ppm. Trace benzene (δ 7.30 ppm), resulting from benzophenone ketyl decomposition, and residual solvent, THF (δ 3.62 and 1.79 ppm) and hexanes (δ 1.29 and 0.89 ppm), are present.

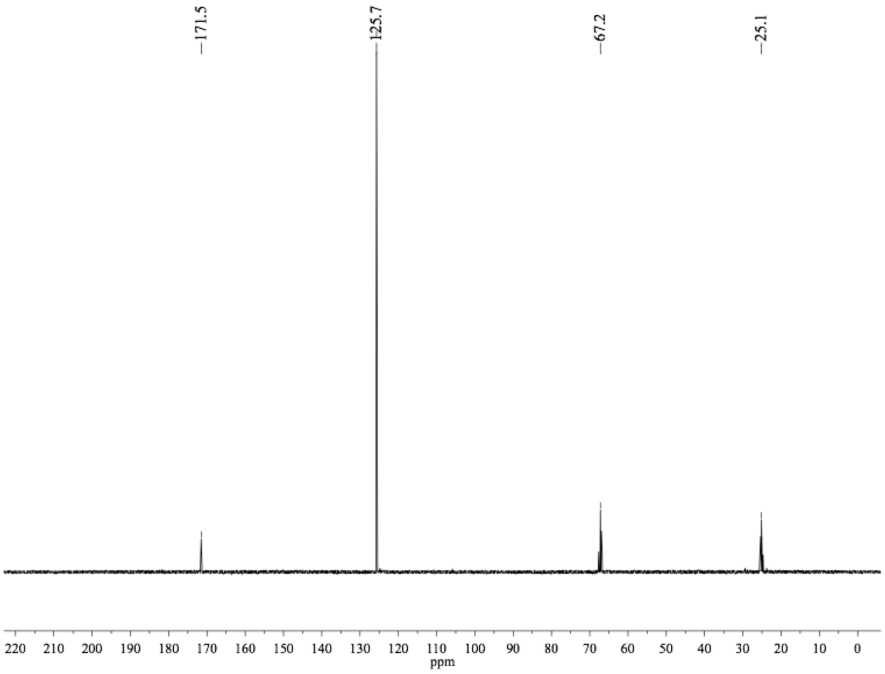

Figure 2.16. $^{13}C\{^{1}H\}$ NMR spectrum (100 MHz) of $\{[(IDipp)Cu]_2(\mu\text{-}H)\}^+ BF_4^-$ in THF-d_8 solution after one hour's exposure to $^{13}CO_2$ (*ca.* 1 atm). The presence of ^{13}C-formate is indicated by a singlet at δ 171.5 ppm. The singlet at δ 125.7 ppm corresponds to $^{13}CO_2$.

Reaction of $\{[(IDipp)Cu]_2(\mu\text{-}H)\}^+ BF_4^-$ with CO

A solution of $\{[(IDipp)Cu]_2(\mu\text{-}H)\}^+ BF_4^-$, (0.025 g, 0.025 mmol) in THF-d_8 (0.7 mL) cooled to −35 °C in an NMR tube equipped with a J. Young valve was degassed by three freeze-pump-thaw cycles, then pressurized with CO (*ca.* 1 atm) at −45 °C. The tube was agitated continuously for 10 minutes to ensure mixing. ^{1}H NMR and ^{13}C spectra were promptly recorded. The chemical shift of the hydride was observed at δ –2.47 ppm, compared to δ –4.12 ppm for the parent hydride complex in the ^{1}H NMR spectrum. In the ^{13}C NMR spectrum, the resonance at δ 176.6 ppm was assigned as that of the copper-bound carbonyl carbon.

The lability of the CO adduct was investigated by conducting a series of freeze-pump-thaw cycles to degas the solution sample. The reaction of $\{[(IDipp)Cu]_2(\mu\text{-}H)\}^+$

BF_4^- with CO was carried out as described previously, except in CD_2Cl_2 solution. The initial shift of the hydride peak, upon addition of CO, seen in $\{[(IDipp)Cu]_2(\mu\text{-}H)\}^+ BF_4^-$ in CD_2Cl_2 from –4.29 ppm to –2.66 ppm was observed in the ^1H NMR spectrum. After one freeze-pump-thaw cycle, a shift of the hydride resonance from –2.66 ppm to –3.26 ppm was observed. Subsequent freeze-pump-thaw cycles resulted in further shifts of the hydride resonance from –3.26 ppm to –3.65 ppm, from –3.65 ppm to –3.86 ppm and from –3.86 ppm to –4.04 ppm. These resonances are believed to represent weighted averages of chemical shifts for the parent hydride and a labile carbonyl complex. This interpretation suggests that the carbonyl adduct forms reversibly, and that exchange of CO between copper hydride complexes is rapid on the NMR timescale.

The carbonyl adduct of $\{[(IDipp)Cu]_2(\mu\text{-}H)\}^+ BF_4^-$ was prepared *in situ* as a solution in dichloromethane. The solution was injected into a sealed liquid cell, with KBr windows, in the glovebox under an atmosphere of dry nitrogen. A sharp absorption at 2109 cm^{-1}, corresponding to stretching vibrations of a copper bound CO, was observed in the IR spectrum of the solution product.

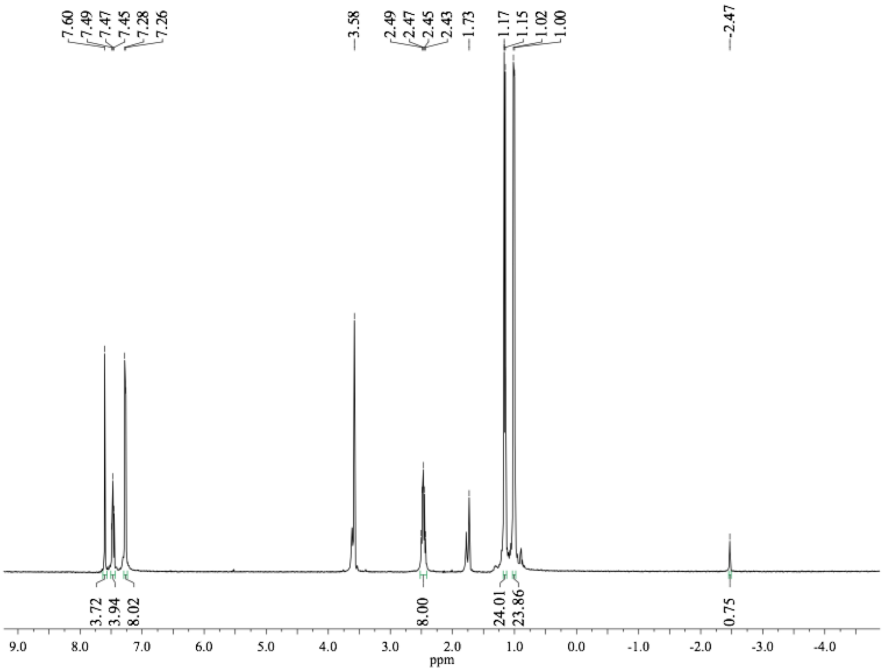

Figure 2.17. ^{1}H NMR spectrum (400 MHz, THF-d_8) of the reaction of $\{[(IDipp)Cu]_2(\mu\text{-}H)\}^+ BF_4^-$ with 1 atm CO after twenty minutes. A shift of the hydride peak seen in $\{[(IDipp)Cu]_2(\mu\text{-}H)\}^+ BF_4^-$ from –4.12 ppm to –2.47 ppm can be seen. A trace of residual solvent, THF (δ 3.62 and 1.79 ppm) and hexanes (δ 1.29 and 0.89 ppm), is present.

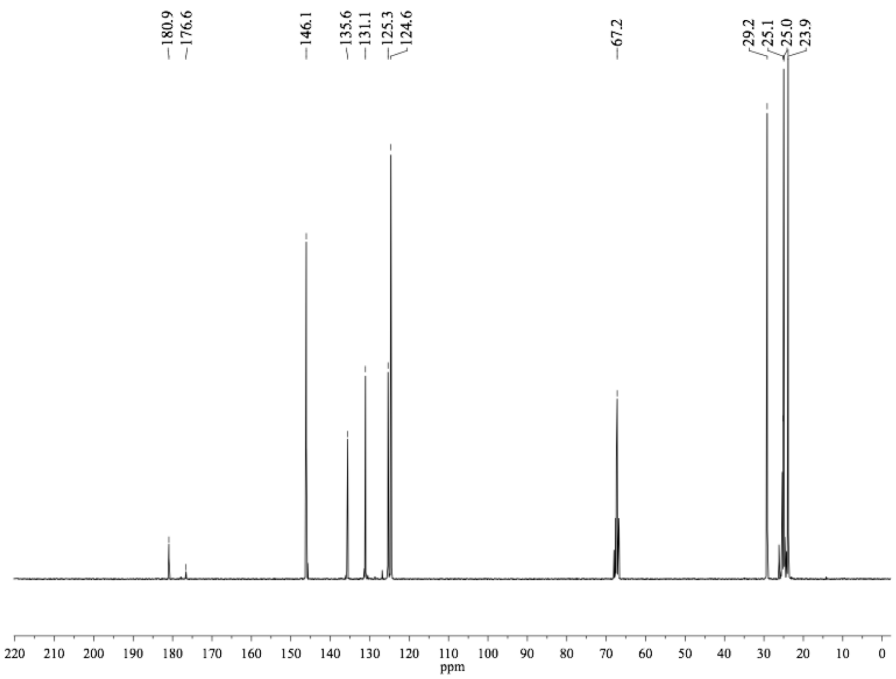

Figure 2.18. $^{13}C\{^{1}H\}$ NMR spectrum (100 MHz, THF-d_8) of the reaction of $\{[(IDipp)Cu]_2(\mu\text{-}H)\}^+ BF_4^-$ with 1 atm CO after twenty minutes. The singlet at δ 176.6 ppm is assigned to the copper-bound carbonyl carbon atom.

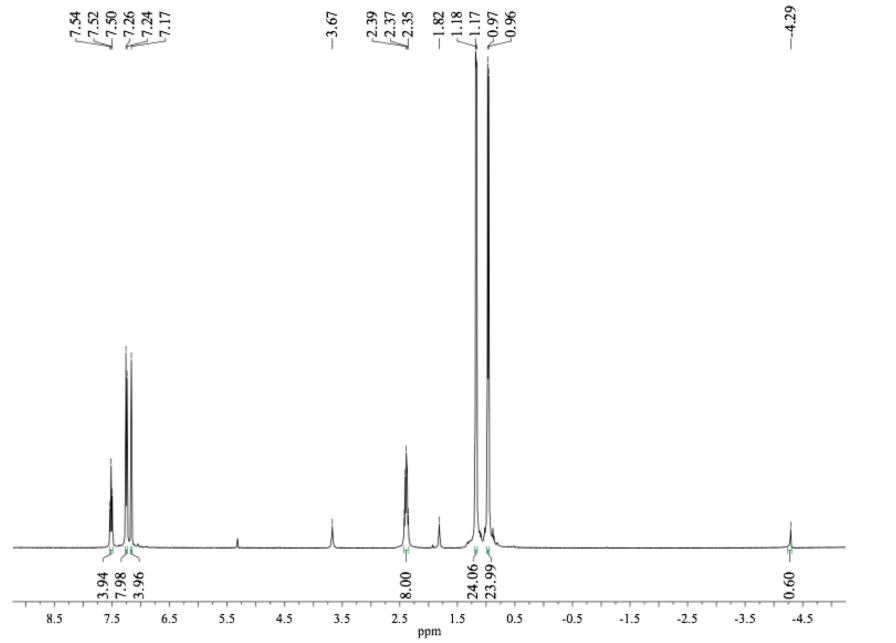

Figure 2.19. ^{1}H NMR spectrum (400 MHz, CD_2Cl_2) of $\{[(IDipp)Cu]_2(\mu\text{-}H)\}^+ BF_4^-$. A trace of residual solvent, THF (δ 3.67 and 1.82 ppm), is present.

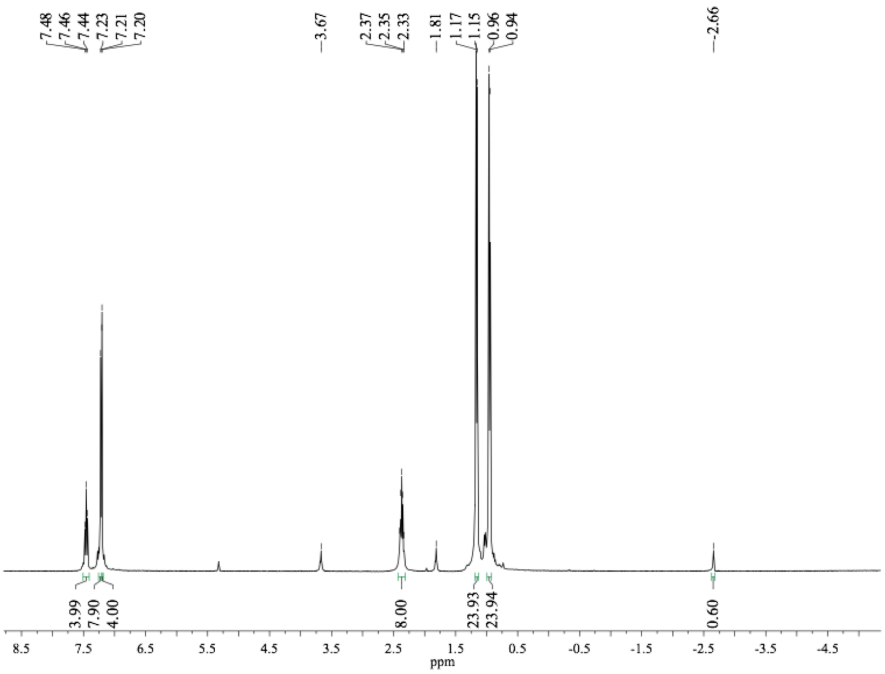

Figure 2.20. ^{1}H NMR spectrum (400 MHz, CD_2Cl_2) of the reaction of $\{[(IDipp)Cu]_2(\mu\text{-}H)\}^+ BF_4^-$ with 1 atm CO after twenty minutes. A shift of the hydride peak seen in $\{[(IDipp)Cu]_2(\mu\text{-}H)\}^+ BF_4^-$ from –4.29 ppm to –2.66 ppm can be seen. A trace of residual solvent, THF (δ 3.62 and 1.79 ppm), is present.

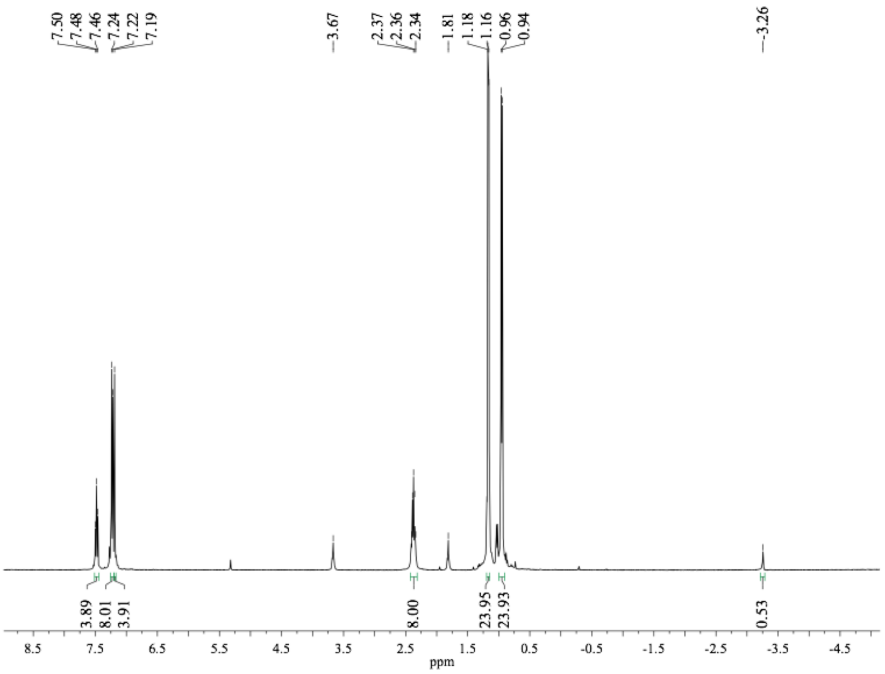

Figure 2.21. ^{1}H NMR spectrum (400 MHz, CD_2Cl_2) of the reaction of $\{[(IDipp)Cu]_2(\mu\text{-}H)\}^+ BF_4^-$ with 1 atm CO after one freeze-pump-thaw cycle. A shift of the hydride peak from –2.66 ppm to –3.26 ppm can be seen. A trace of residual solvent, THF (δ 3.67 and 1.81 ppm), is present.

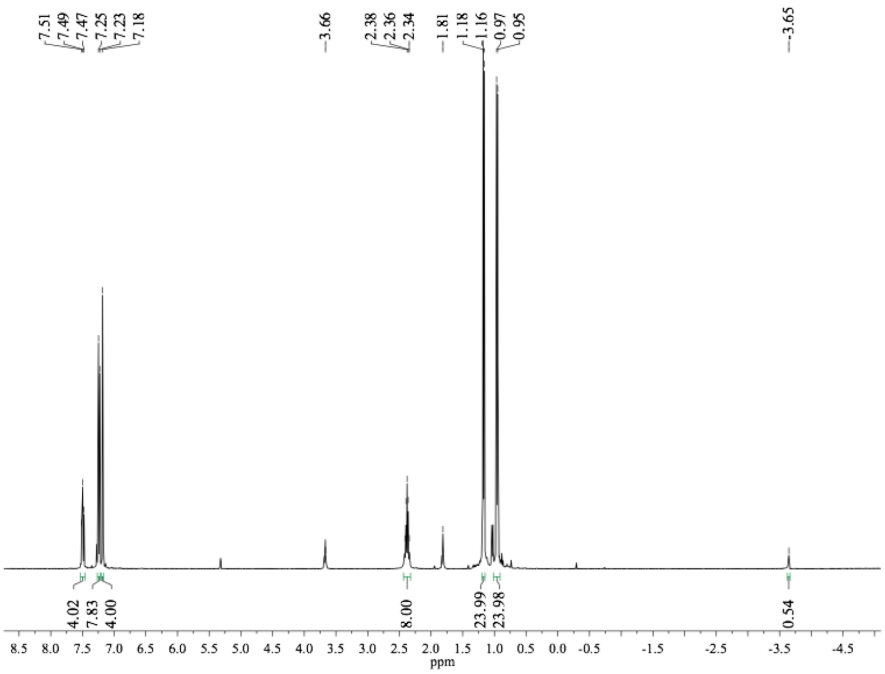

Figure 2.22. ^{1}H NMR spectrum (400 MHz, CD_2Cl_2) of the reaction of $\{[(IDipp)Cu]_2(\mu\text{-}H)\}^+ BF_4^-$ with 1 atm CO after two freeze-pump-thaw cycles. A shift of the hydride peak from –3.26 ppm to –3.65 ppm can be seen. A trace of residual solvent, THF (δ 3.66 and 1.81 ppm), is present.

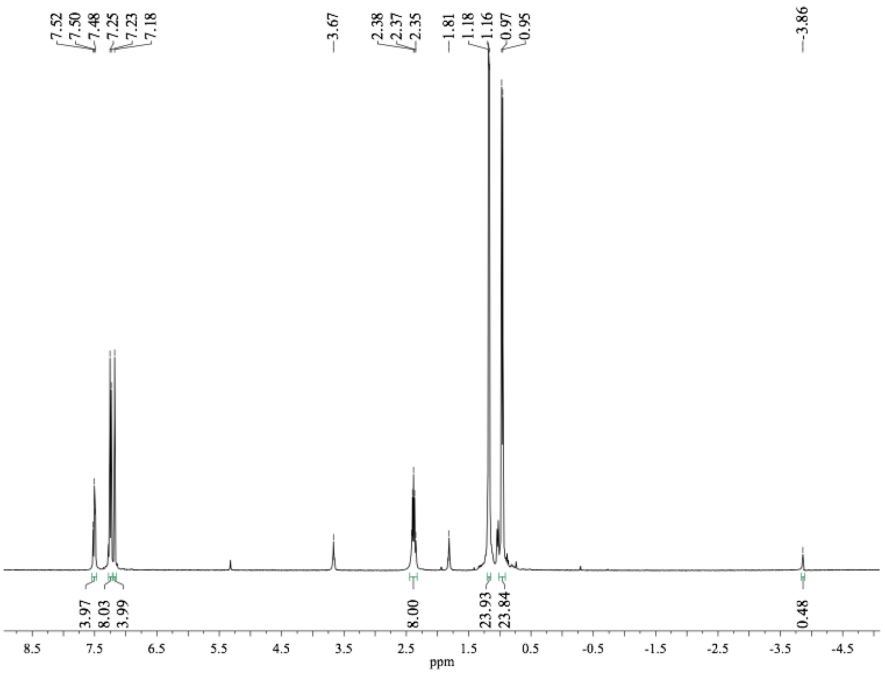

Figure 2.23. ^{1}H NMR spectrum (400 MHz, CD_2Cl_2) of the reaction of $\{[(IDipp)Cu]_2(\mu\text{-}H)\}^+$ BF_4^- with 1 atm CO after three freeze-pump-thaw cycles. A shift of the hydride peak from –3.65 ppm to –3.86 ppm can be seen. A trace of residual solvent, THF (δ 3.67 and 1.81 ppm), is present.

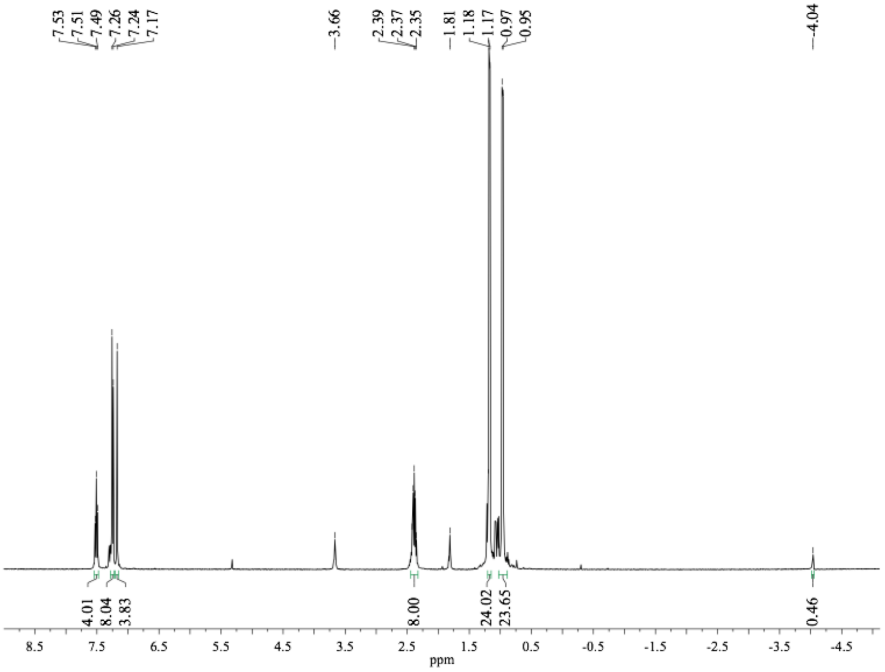

Figure 2.24. ^{1}H NMR spectrum (400 MHz, CD_2Cl_2) of the reaction of $\{[(IDipp)Cu]_2(\mu\text{-}H)\}^+ BF_4^-$ with 1 atm CO after four freeze-pump-thaw cycles. A shift of the hydride peak from –3.86 ppm to –4.04 ppm can be seen. A trace of residual solvent, THF (δ 3.66 and 1.81 ppm), is present.

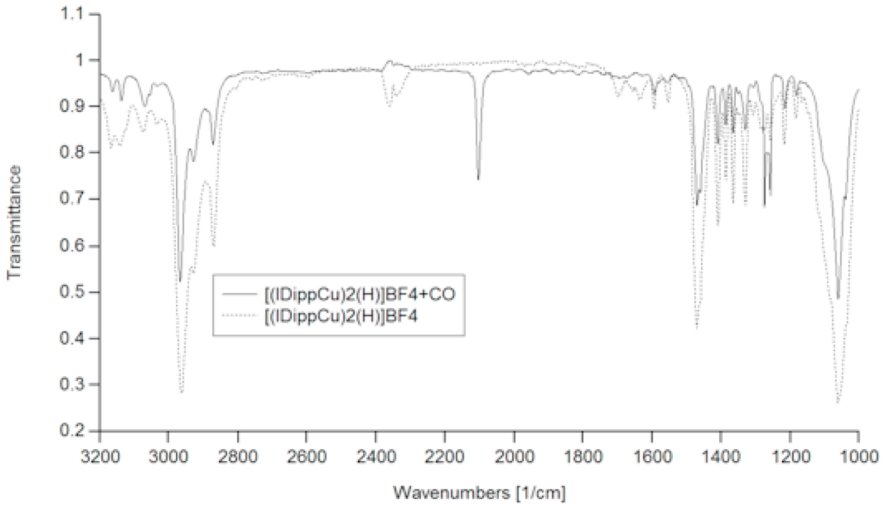

Figure 2.25. Overlay of the infrared absorption spectra of $\{[(IDipp)Cu]_2(\mu\text{-}H)\}^+ BF_4^-$ (dotted spectrum) and the reaction $\{[(IDipp)Cu]_2(\mu\text{-}H)\}^+ BF_4^-$ with 1 atm CO (black spectrum). The sharp absorption at 2109 cm^{-1}, corresponding to stretching vibrations of a copper-bound CO, is believed to indicate the presence of a copper(I) carbonyl complex.

Reaction of {[(IDipp)Cu]$_2$(μ-trans-CHCHPh)}$^+$ BF_4^- with CO_2

A solution of {[(IDipp)Cu]$_2$(μ-trans-CHCHPh)}$^+$ BF_4^-, (0.025 g, 0.023 mmol) in THF-d_8 (0.7 mL) in an NMR tube equipped with a J. Young valve was degassed by three freeze-pump-thaw cycles, then pressurized with CO_2 (*ca.* 1 atm) at ambient temperature. The tube was agitated continuously to ensure mixing. The reaction progress was checked at intervals by ^{1}H NMR spectroscopy. After 30 hours, the reaction was complete. ^{1}H NMR (400 MHz, THF-d_8): δ (ppm) 7.67 (s, 4H, NC*H*), 7.51 (t, *J* = 8 Hz, 4H, *para*-C*H*), 7.39 (m, 3H, Ph *meta*-C*H*, Ph *para*-C*H*), 7.36 (d, *J* = 8 Hz, 8H, *meta*-C*H*), 7.21 (d, *J* = 16 Hz, 1H, CHC*H*Ph), 7.12 (m, 2H, Ph *ortho*-C*H*), 5.39 (d, *J* = 16 Hz, 1H, C*H*CHPh), 2.59 (sept, *J* = 8 Hz, 8H, C*H*(CH$_3$)$_2$), 1.24 (d, *J* = 4 Hz, 24H, CH(C*H*$_3$)$_2$), 1.16 (d, *J* = 8 Hz, 24H, CH(C*H*$_3$)$_2$). ^{13}C{^{1}H} NMR (100 MHz, THF-d_8): δ (ppm) 177.7 (N*C*Cu), 176.7 (O$_2$*C*CCPh), 146.4 (*ortho*-*C*), 145.8 (O$_2$C*C*CPh), 135.5 (*ipso*-*C*), 134.9 (O$_2$CC*C*Ph) 131.3 (*para*-*C*), 130.8 (Ph *para*-*C*), 129.2 (Ph *meta*-*C*), 128.9 (Ph *ortho*-*C*), 125.8 (N*C*H), 124.8 (*meta*-*C*), 121.7 (Ph *ipso*-*C*), 29.4 (*C*H(CH$_3$)$_2$), 25.2 (CH(*C*H$_3$)$_2$), 23.7 (CH(*C*H$_3$)$_2$).

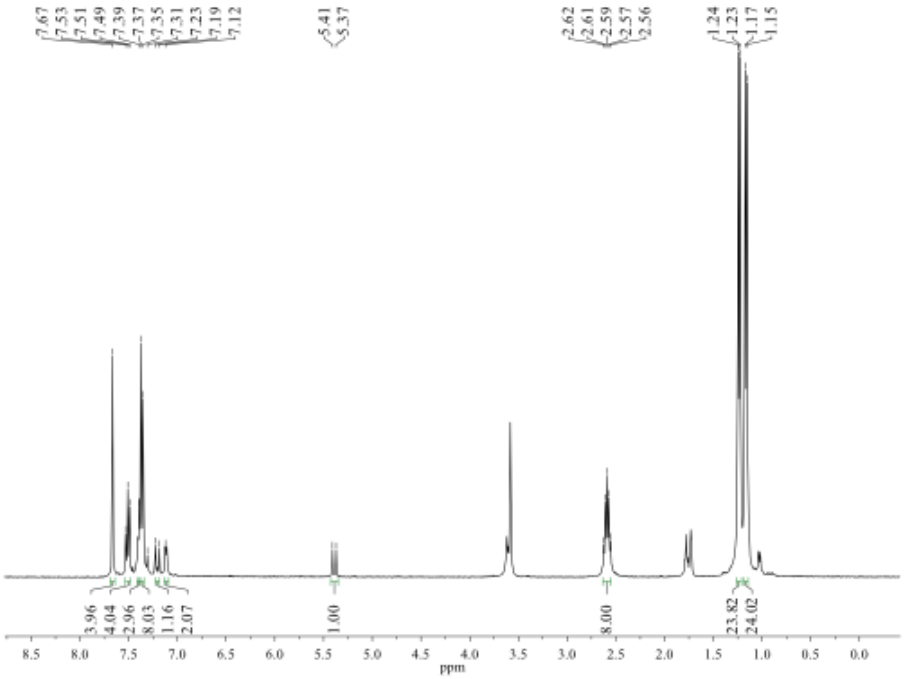

Figure 2.26. ^{1}H NMR spectrum (400 MHz) of $\{[(IDipp)Cu]_2(\mu\text{-trans-CHCHPh})\}^{+}$ BF_4^{-} in THF-d_8 solution after thirty hours' exposure to CO_2 (*ca.* 1 atm). A trace of benzene (δ 7.31 ppm) is present as the result of benzophenone ketyl decomposition along with residual solvent, THF (δ 3.62 and 1.79 ppm).

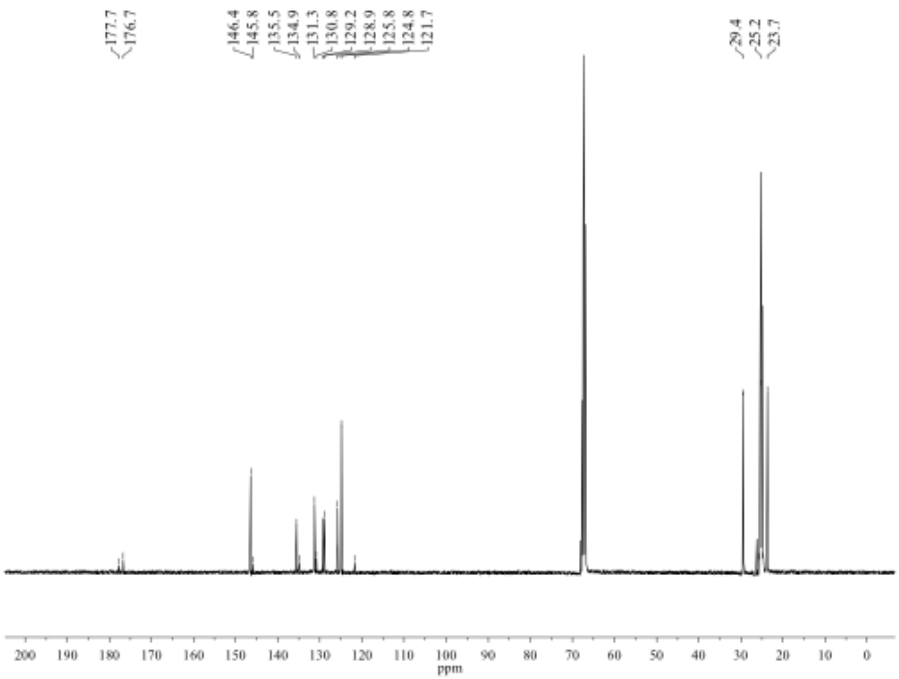

Figure 2.27. $^{13}C\{^{1}H\}$ NMR spectrum (100 MHz) of $\{[(IDipp)Cu]_2(\mu\text{-}CHCHPh)\}^+ BF_4^-$ in THF-d_8 solution after thirty hours' exposure to $^{13}CO_2$ (*ca.* 1 atm). A trace of residual solvent, THF (δ 68.0 and 26.2 ppm), is present.

Reaction of $\{[(IDipp)Cu]_2(\mu\text{-}trans\text{-}CHCHPh)\}^+ BF_4^-$ with HB(pin)

A solution of $\{[(IDipp)Cu]_2(\mu\text{-}trans\text{-}CHCHPh)\}^+ BF_4^-$ (0.029 g, 0.027 mmol) in THF-d_8 (1 mL) and 4,4,5,5-tetramethyl-1,3,2-dioxaborolane (0.006 mL, 0.005 g, 0.041 mmol) were cooled to −35 °C. The 4,4,5,5-tetramethyl-1,3,2-dioxaborolane was added to the $\{[(IDipp)Cu]_2(\mu\text{-}trans\text{-}CHCHPh)\}^+ BF_4^-$ solution. The reaction progress was checked at intervals by ^{1}H NMR spectroscopy. After 40 minutes, the ^{1}H NMR spectrum displayed a single set of IDipp resonances identical to those of authentic **1** and resonances for PhCHCHB(pin). ^{1}H NMR (400 MHz, THF-d_8): δ (ppm) 7.48 (m, 2H, Ph *ortho*-C*H*), 7.37 (m, 1H, CHC*H*Ph), 7.33 (m, 3H, Ph *meta-H*, Ph *para-H*), 6.13 (d, J = 20 Hz, 1H, C*H*CHPh), 1.27 (s, 12H *(pin)*B). ^{11}B NMR (53 MHz, THF-d_8): δ (ppm) 30.05.

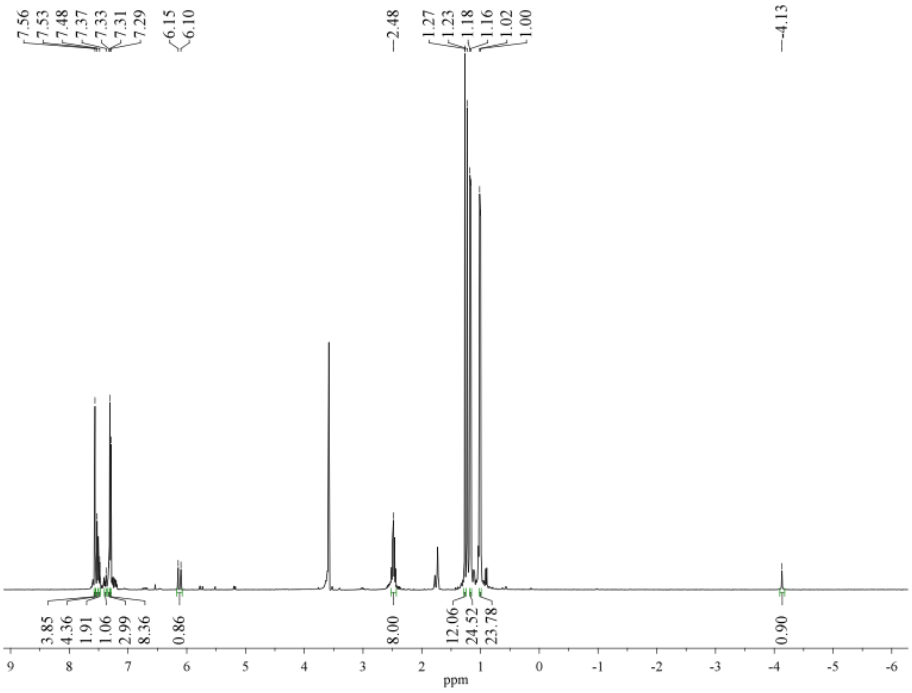

Figure 2.28. ^{1}H NMR spectrum (400 MHz, THF-d_8) of the reaction of {[(IDipp)Cu]$_2$(μ-trans-CHCHPh)}$^{+}$ BF_4^{-} with HB(pin) after 40 min. Excess HB(pin) (δ 1.23 ppm) is present along with a trace of residual solvent, THF (δ 3.67 and 1.81 ppm).

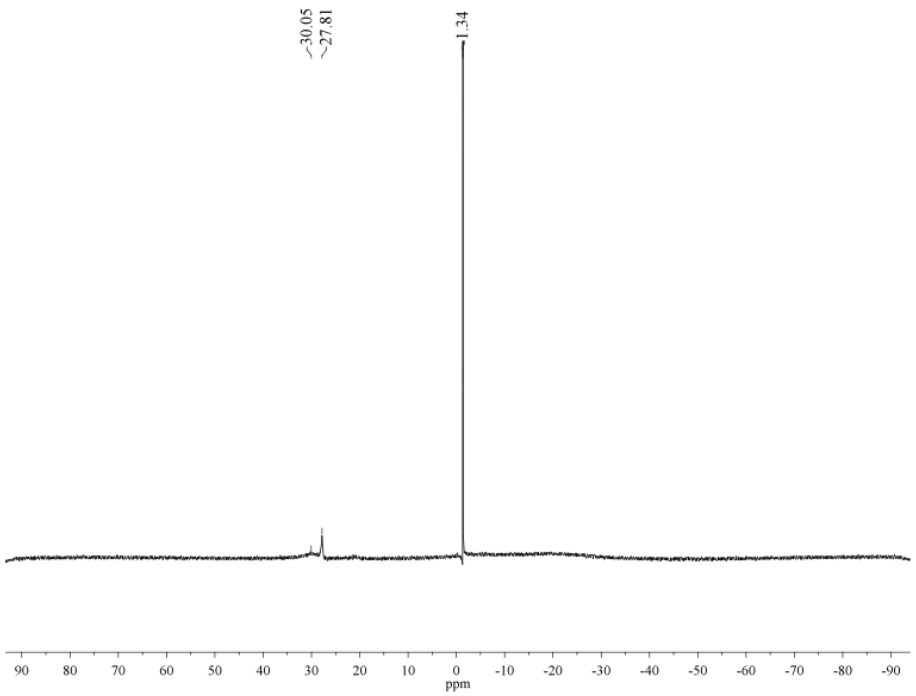

Figure 2.29. ^{11}B NMR spectrum (53 MHz, THF-d_8) of the reaction of {[(IDipp)Cu]$_2$(μ-trans-CHCHPh)}$^+$ BF_4^- with HB(pin) after 40 min. Excess HB(pin) (δ 27.81) is present along with BF_4^- (δ −1.34 ppm).

Methanolysis of {[(IDipp)Cu]$_2$(μ-H)}$^+$ BF_4^-

A solution of {[(IDipp)Cu]$_2$(μ-H)}$^+$ BF_4^-, (0.060 g, 0.060 mmol) in THF-d_8 (0.7 mL) cooled to −35 °C was transferred to an NMR tube equipped with a J. Young valve. The tube was then opened, and methanol-d_4 (2.5 μL, 0.062 mmol) was added. The resulting mixture was agitated, then allowed to stand at –20 °C. The reaction was monitored by ^{1}H NMR spectroscopy. After 1 hour, the ^{1}H NMR spectrum displayed a 1:1:1 triplet resonance for H–D at δ 4.50 ppm. After 18 hours, the starting complex had been completely consumed, and a single new set of IDipp resonances, assigned to {[(IDipp)Cu]$_2$(μ-OCD$_3$)}$^+$ BF_4^-, was observed.

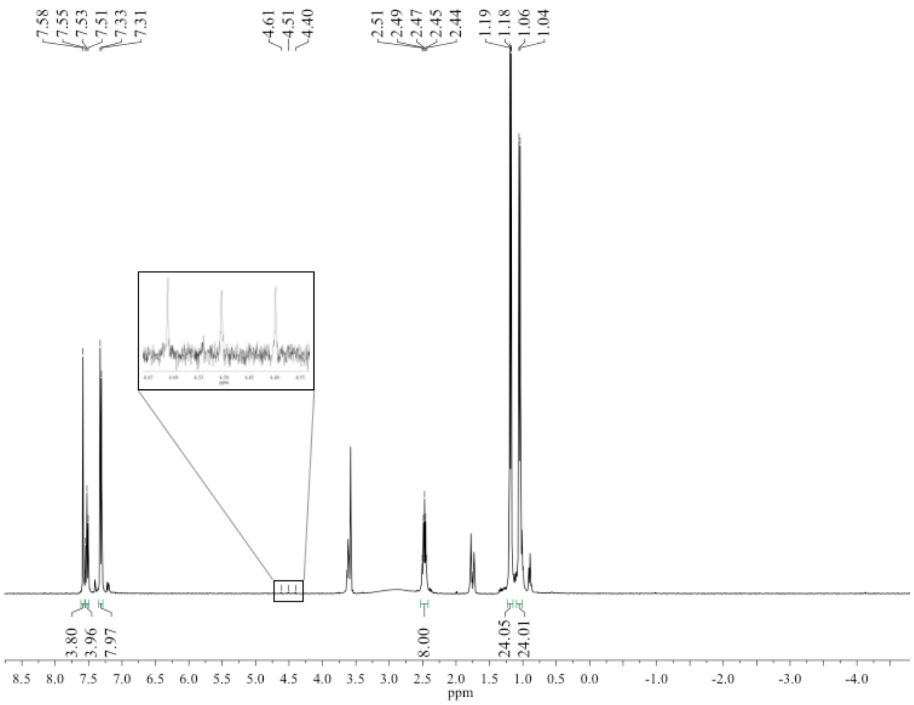

Figure 2.30. ^{1}H NMR spectrum (400 MHz, THF-d_8) of the reaction of $\{[(IDipp)Cu]_2(\mu\text{-}H)\}^+$ BF_4^- with CD_3OD after 18 h. In addition to the methanolysis product and H–D, some decomposition product $[(IDipp)_2Cu]^+$ is also evident. A trace of residual solvent, THF (δ 3.67 and 1.81 ppm), is present.

X-ray crystallography

For each complex, a suitable crystal was selected and mounted on a Bruker APEX2 diffractometer with 1.6 kW graphite monochromated MO radiation. Using Olex2,[50] the structure was solved with Superflip[51] structure solution program using Charge Flipping and refined with the ShelXL[52] refinement package using Least Squares minimization.

Table 2.1. Crystallographic details for $\{[(IDipp)Cu]_2(\mu\text{-}H)\}^+ BF_4^-\bullet(C_4H_8O)$.

$C_{58}H_{81}BCu_2F_4N_4O$
$M = 1064.18$
0.664 x 0.367 x 0.102 mm^3
Monoclinic, space group P 1 21 1
$a = 10.6145(17)$ Å
$b = 25.817(4)$ Å
$c = 21.735(4)$ Å
$\alpha = 90°$
$\beta = 102.304(3)°$
$\gamma = 90°$
$V = 5819.3(17)$ $Å^3$
$Z = 4$
$D_c = 1.224$ mg/mm^3
$\mu(MoK\alpha) = 0.784$ mm^{-1}
$T = 110(2)$ K
$1.918° \leq 2\Theta \leq 55.832°$
56366 reflections measured, 24826 unique ($R_{int} = 0.0823$) which were used in all calculations.
Final *GooF* = 1.019
Final $R_1 = 0.0730$ ($I > 2\sigma(I)$)
wR_2 (all data) = 0.1852

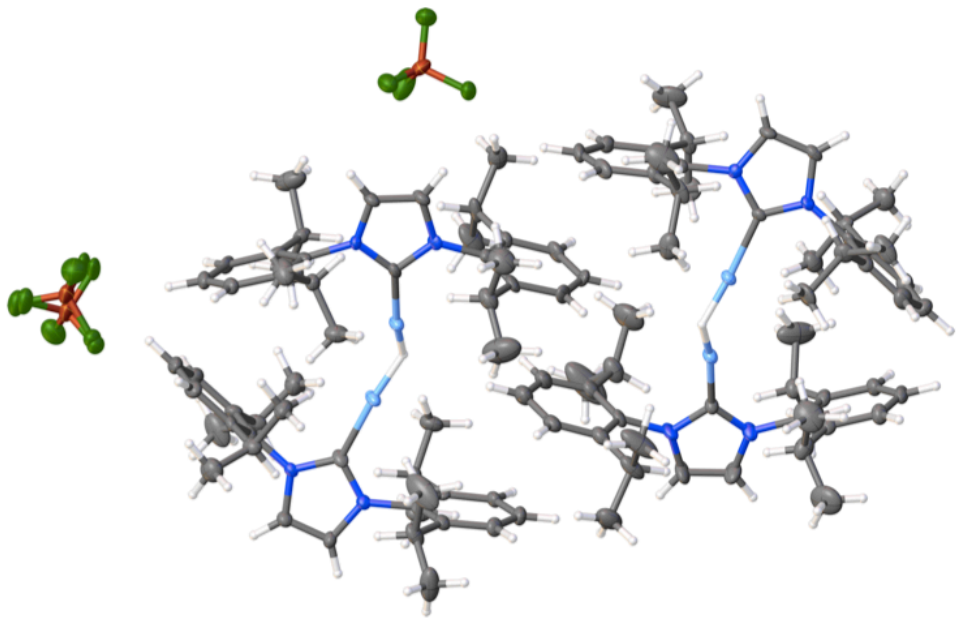

Figure 2.31. Solid-state structure of $\{[(IDipp)Cu]_2(\mu\text{-}H)\}^+ BF_4^-\bullet(C_4H_8O)$, showing both molecules in the asymmetric unit.

Table 2.2. Crystallographic details for $\{[(IDipp)Cu]_2(\mu\text{-}OOCH)\}^+ BF_4^- \bullet 0.5[(C_2H_5)_2O]$.

$C_{57}H_{78}BCu_2F_4N_4O_{2.5}$
$M = 1073.12$
0.763 x 0.365 x 0.344 mm^3
Triclinic, space group P-1
$a = 11.3551(9)$ Å
$b = 15.4000(12)$ Å
$c = 18.2742(15)$ Å
$\alpha = 78.0770(10)°$
$\beta = 75.9800(10)°$
$\gamma = 68.6460(10)°$
$V = 2862.7(4)$ $Å^3$
$Z = 2$
$D_c = 1.245$ mg/mm^3
$\mu(MoK\alpha) = 0.799$ mm^{-1}
$T = 110(2)$ K
$3.44° \leq 2\Theta \leq 63.142°$
31405 reflections measured, 18214 unique ($R_{int} = 0.0261$) which were used in all calculations.
Final *GooF* = 1.045
Final $R_1 = 0.0494$ ($I > 2\sigma(I)$)
wR_2 (all data) = 0.1454

Table 2.3. Crystallographic details for $\{[(IDipp)Cu]_2(\mu\text{-}CHCHPh)\}^+ BF_4^-\bullet 2(C_4H_8O)$.

$C_{70}H_{95}BCu_2F_4N_4O_2$
$M = 1238.38$
0.75 x 0.619 x 0.41 mm^3
Monoclinic, space group $P2_1/n$
$a = 12.6587(11)$ Å
$b = 31.464(3)$ Å
$c = 17.2399(15)$ Å
$\alpha = 90°$
$\beta = 100.3810(10)°$
$\gamma = 90°$
$V = 6754.1(11)$ $Å^3$
$Z = 4$
$D_c = 1.218$ mg/mm^3
$\mu(MoK\alpha) = 0.686$ mm^{-1}
$T = 173(2)$ K
$2.728° \leq 2\Theta \leq 60.242°$
52180 reflections measured, 19858 unique ($R_{int} = 0.0365$) which were used in all calculations.
Final *GooF* = 1.049
Final $R_1 = 0.0636$ ($I > 2\sigma(I)$)
wR_2 (all data) = 0.1756

Density-Functional Theory Studies

Density-functional theory calculations were spin-restricted, and all were performed within Gaussian09 A.02.[53] Geometries were fully optimized using the parameter-free PBE0 functional.[54] Comparative calculations were undertaken using the dispersion-corrected functional of Grimme.[55] Selected metrics and natural atomic charges calculated with the two functionals are summarized in Tables S8 and S9. Calculated structures were local minima of their respective potential energy hypersurfaces; calculated harmonic frequencies were all real. Converged densities passed an internal stability check. Calculations included continuum THF solvation ($\varepsilon = 7.4257$) through the integral equation formalism of Tomasi's polarizable continuum model

(IEFPCM).[56,57] Atomic orbitals on nonmetal atoms were described with the TZVP basis set of Godbout, Andzelm, and coworkers.[58] Orbital contours are plotted at 0.03 a.u. Mulliken population[59] analysis was conducted with the AOMix program of Gorelsky.[60,61] The wave functions were also analyzed with atoms-in-molecules calculations[35] using AIMA11.[62]

Table 2.4. Optimized Cartesian (PBE0) coordinates for **1′**.

Center Number	Atomic Number	Atomic Type	Coordinates (Angstroms) X	Y	Z
1	29	0	9.137870	10.090662	4.120996
2	29	0	11.630912	9.817769	4.046385
3	6	0	7.440665	9.463547	4.796854
4	7	0	6.771893	8.348586	4.431248
5	6	0	5.589629	8.227810	5.121770
6	6	0	5.514551	9.297027	5.946361
7	7	0	6.653087	10.036937	5.732055
8	1	0	4.911975	7.404345	4.970654
9	1	0	4.758748	9.588639	6.656209
10	6	0	6.959250	11.276013	6.418602
11	1	0	7.002491	11.109275	7.495129
12	1	0	7.928023	11.630072	6.071231
13	1	0	6.201563	12.027972	6.196657
14	6	0	7.231361	7.403000	3.433765
15	1	0	6.541897	7.379153	2.589394
16	1	0	8.212711	7.721018	3.086574
17	1	0	7.309440	6.406271	3.868457
18	6	0	13.188360	8.844223	4.643803
19	7	0	13.610598	8.666654	5.914198
20	6	0	14.763218	7.918676	5.956216
21	1	0	15.258363	7.666955	6.879167
22	7	0	14.099537	8.190526	3.891510
23	6	0	15.072851	7.616975	4.674774
24	1	0	15.890560	7.050361	4.261771
25	6	0	12.942348	9.200794	7.083972
26	1	0	12.035679	9.707365	6.758152
27	1	0	12.677372	8.393289	7.766784
28	1	0	13.588563	9.914193	7.596165
29	6	0	14.064995	8.108211	2.444926
30	1	0	14.036222	7.065382	2.128596
31	1	0	13.167726	8.614524	2.094013
32	1	0	14.942262	8.594649	2.017554
33	1	0	10.449559	10.715865	3.472076

Table 2.5. Optimized Cartesian (PBE0) coordinates for **3′**.

Center Number	Atomic Number	Atomic Type	Coordinates (Angstroms) X	Y	Z
1	29	0	9.3406	9.1559	3.1628
2	29	0	11.8226	9.2159	3.4514
3	6	0	7.8021	8.9615	4.3187
4	7	0	6.5515	9.4313	4.1191
5	6	0	5.7232	9.1082	5.1680
6	6	0	6.4745	8.4131	6.0515
7	7	0	7.7383	8.3364	5.5149
8	1	0	4.6852	9.3943	5.1965
9	1	0	6.2191	7.9712	7.0001
10	6	0	8.8491	7.6508	6.1439
11	1	0	9.7368	7.8093	5.5335
12	1	0	9.0213	8.0531	7.1426
13	1	0	8.6451	6.5817	6.2127
14	6	0	6.1345	10.1930	2.9588
15	1	0	5.8897	11.2169	3.2437
16	1	0	6.9542	10.2053	2.2430
17	1	0	5.2644	9.7253	2.4981
18	6	0	13.0560	9.1122	4.9379
19	7	0	12.9302	9.6985	6.1490
20	6	0	14.0069	9.4148	6.9554
21	1	0	14.0946	9.7925	7.9604
22	7	0	14.2342	8.4547	5.0051
23	6	0	14.8325	8.6261	6.2310
24	1	0	15.7807	8.1804	6.4810
25	6	0	11.8140	10.5331	6.5457
26	1	0	12.1506	11.5537	6.7304
27	1	0	11.0857	10.5354	5.7365
28	1	0	11.3493	10.1342	7.4479
29	6	0	14.7977	7.6631	3.9298
30	1	0	14.8720	6.6169	4.2285
31	1	0	14.1429	7.7441	3.0645
32	1	0	15.7872	8.0376	3.6667
33	6	0	10.7544	9.4093	1.8029
34	6	0	10.8259	8.3839	0.9160
35	1	0	10.7936	10.4095	1.3595
36	1	0	10.7909	7.3604	1.2901
37	6	0	10.9482	8.4544	-0.5435
38	6	0	10.9943	7.2605	-1.2711
39	6	0	11.0206	9.6618	-1.2478
40	6	0	11.1075	7.2672	-2.6535
41	1	0	10.9388	6.3158	-0.7389
42	6	0	11.1339	9.6702	-2.6272
43	1	0	10.9879	10.6034	-0.7115
44	6	0	11.1778	8.4735	-3.3367
45	1	0	11.1410	6.3300	-3.1978
46	1	0	11.1891	10.6150	-3.1566
47	1	0	11.2663	8.4846	-4.4173

Table 2.6. Optimized Cartesian (B97D) coordinates for **1′**.

Center Number	Atomic Number	Atomic Type	Coordinates (Angstroms) X	Y	Z
1	29	0	9.151628	10.162186	4.094336
2	29	0	11.630580	9.871288	3.983368
3	6	0	7.484247	9.493627	4.802679
4	7	0	6.841299	8.340946	4.458391
5	6	0	5.664524	8.187389	5.171817
6	6	0	5.563084	9.272078	5.991489
7	7	0	6.680931	10.053442	5.751736
8	1	0	5.014366	7.335205	5.035974
9	1	0	4.807515	9.550858	6.711646
10	6	0	6.960179	11.322570	6.426425
11	1	0	7.000723	11.165255	7.509462
12	1	0	7.926935	11.690202	6.071807
13	1	0	6.178849	12.052057	6.187649
14	6	0	7.327512	7.391067	3.455612
15	1	0	6.628217	7.346470	2.613664
16	1	0	8.303711	7.737030	3.104631
17	1	0	7.428833	6.397717	3.905388
18	6	0	13.149450	8.856243	4.607518
19	7	0	13.530725	8.645294	5.899893
20	6	0	14.672956	7.865085	5.967522
21	1	0	15.129004	7.588535	6.907232
22	7	0	14.079718	8.185187	3.870409
23	6	0	15.020602	7.573287	4.681864
24	1	0	15.838709	6.992104	4.281312
25	6	0	12.831322	9.189754	7.065811
26	1	0	11.916402	9.676894	6.716893
27	1	0	12.576592	8.377899	7.755124
28	1	0	13.467089	9.922220	7.575177
29	6	0	14.084875	8.123377	2.407474
30	1	0	14.057306	7.078274	2.081578
31	1	0	13.196462	8.645994	2.042467
32	1	0	14.984799	8.609836	2.015978
33	1	0	10.455132	10.797364	3.413689

Table 2.7. Optimized Cartesian (B97D) coordinates for **3′**.

Center Number	Atomic Number	Atomic Type	Coordinates (Angstroms) X	Y	Z
1	29	0	9.307217	9.201677	3.067617
2	29	0	11.756474	9.217443	3.323164
3	6	0	7.905092	8.988682	4.380827
4	7	0	6.623561	9.452457	4.356892
5	6	0	5.939282	9.108586	5.511459
6	6	0	6.813078	8.404466	6.285163
7	7	0	8.004590	8.345107	5.580584
8	1	0	4.909272	9.388928	5.678159
9	1	0	6.692469	7.945486	7.255719
10	6	0	9.202120	7.640010	6.042807
11	1	0	10.023002	7.876169	5.358741
12	1	0	9.456648	7.972596	7.05474
13	1	0	9.023630	6.558950	6.044470
14	6	0	6.055775	10.245313	3.264712
15	1	0	5.909712	11.281808	3.588685
16	1	0	6.754986	10.217451	2.424568
17	1	0	5.096478	9.815221	2.959059
18	6	0	12.873499	9.104821	4.894735
19	7	0	12.668244	9.738428	6.086204
20	6	0	13.649120	9.410978	7.007622
21	1	0	13.661156	9.818180	8.008442
22	7	0	14.004887	8.371806	5.097790
23	6	0	14.494525	8.543237	6.382281
24	1	0	15.384927	8.042105	6.733714
25	6	0	11.573432	10.676829	6.340627
26	1	0	11.964103	11.697265	6.420541
27	1	0	10.872574	10.616482	5.502897
28	1	0	11.063704	10.403533	7.270253
29	6	0	14.609081	7.494789	4.092775
30	1	0	14.532938	6.449807	4.413267
31	1	0	14.067928	7.632392	3.152650
32	1	0	15.661582	7.762890	3.953942
33	6	0	10.690940	9.422792	1.639614
34	6	0	10.817194	8.388261	0.747773
35	1	0	10.731624	10.426238	1.193694
36	1	0	10.782208	7.364907	1.131985
37	6	0	10.999796	8.459192	-0.706624
38	6	0	11.098957	7.254773	-1.436395
39	6	0	11.083878	9.677417	-1.415992
40	6	0	11.274199	7.262379	-2.822088
41	1	0	11.035629	6.308109	-0.900852
42	6	0	11.258794	9.685547	-2.798722
43	1	0	11.012319	10.620769	-0.879790
44	6	0	11.354750	8.479106	-3.509094
45	1	0	11.347932	6.322238	-3.365212
46	1	0	11.321867	10.633812	-3.329164
47	1	0	11.491551	8.490638	-4.588513

Table 2.8. Selected crystallographic and calculated metrics; calculated bond orders.

Compound **1**

Interatomic distance (Å)	X-ray[a]	PBE0 (**1′**)	B97D (**1′**)
Cu···Cu	2.5331(15) 2.5354(15)	2.509	2.498
Cu–μ_2-H	1.45(2), 1.45(2) 1.45(2), 1.45(2)	1.591 1.591	1.602 1.601
Interatomic angle (°)			
∠Cu–μ_2-H–Cu	122(3), 121(3)	104.1	102.5
Wiberg bond orders, Löwdin basis			
Cu···Cu		0.386	0.417
Cu1–H		0.534	0.530
Cu2–H		0.535	0.530

Compound **3**

Interatomic distance (Å)	X-ray	PBE0 (**3′**)	B97D (**3′**)
Cu···Cu	2.6303(4)	2.499	2.462
Cu–μ_2-C	2.034(6) 2.003(6)	1.978 1.974	2.001 2.003
Interatomic angle (°)			
∠Cu–μ_2-C–Cu	81.3(2)	78.5	75.9
Wiberg bond orders, Löwdin basis			
Cu···Cu		0.269	
Cu1–μ_2-C		0.609	
Cu2–μ_2-C		0.620	

[a] Two crystallographically independent molecules in the asymmetric unit of **1**.

Table 2.9. Natural atomic charges of selected atoms in **1′**.

	PBE0	B97D
μ_2–H	–0.12	–0.4
Cu	–0.02	0.4
Cu	–0.02	0.4

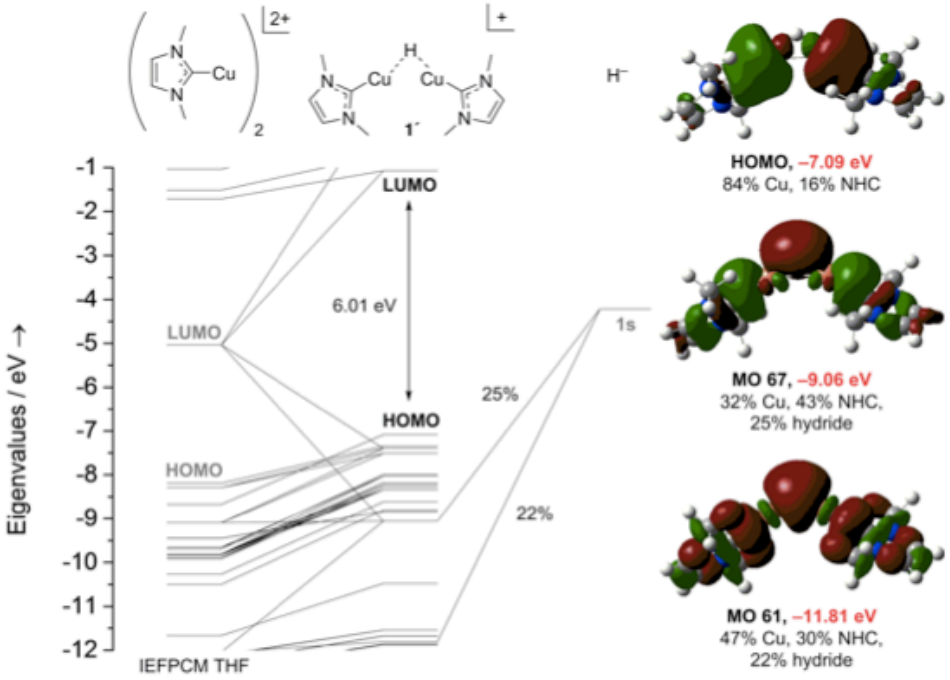

Figure 2.32. Partial Kohn–Sham orbital energy level diagram of **1′** calculated with the parameter-free PBE0 functional. Plots of selected orbitals, with eigenvalues and percentage compositions in terms of electron density of fragments, appear at right. Implicit (IEFPCM) THF solvation is included.

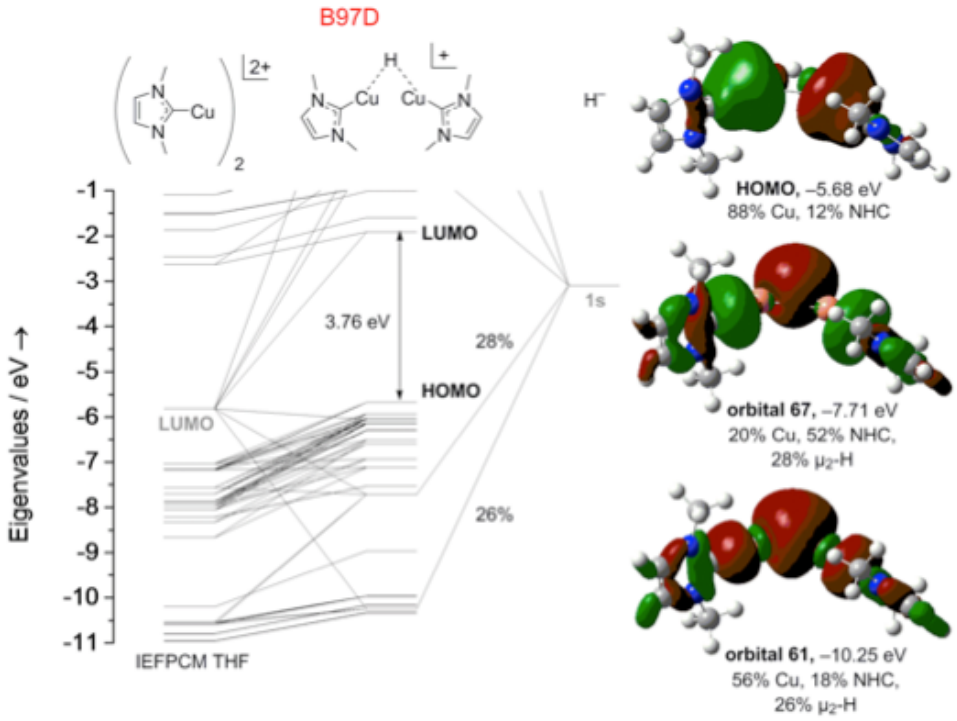

Figure 2.33. Partial Kohn–Sham orbital energy level diagram of **1′** calculated with the dispersion-corrected B97D functional. Plots of selected orbitals, with eigenvalues and percentage compositions in terms of electron density of fragments, appear at right. Implicit (IEFPCM) THF solvation is included.

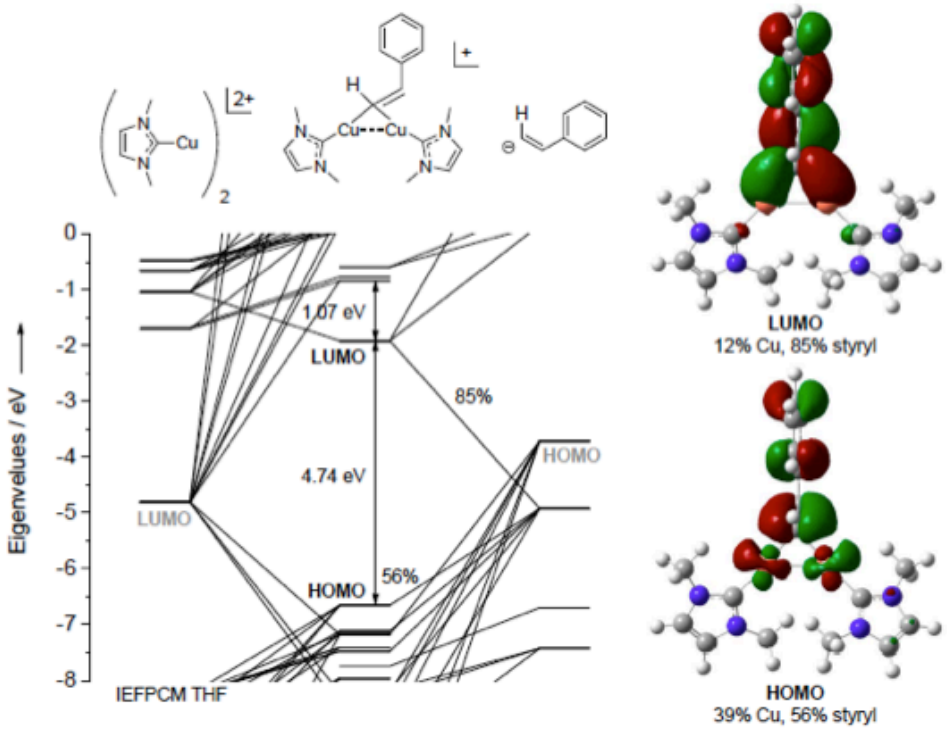

Figure 2.34. Partial Kohn–Sham orbital energy level diagram of **3′** calculated with the parameter-free PBE0 functional. Plots of selected orbitals, with percentage compositions in terms of electron density of fragments, appear at right. Implicit (IEFPCM) THF solvation is included.

2.5. References

1. C. Deutsch, N. Krause, B.H. Lipshutz, Chem. Rev. 108 (2008) 2916.

2. A. Wurtz, C.R. Hebd. Seances Acad. Sci. 18 (1844) 702.

3. H. Müller, A.J. Bradley, J. Chem. Soc. 129 (1926) 1669.

4. M.R. Churchill, S.A. Bezman, J.A. Osborn, J. Wormald, J. Am. Chem. Soc. 93 (1971) 2063.

5. a) C.F. Albert, P.C. Healy, J.D. Kildea, C.L. Raston, B.W. Skelton, A.H. White, Inorg. Chem. 28 (1989) 1300; b) D.M. Ho, R. Bau, Inorg. Chim. Acta. 84 (1984) 213.

6. a) G.V. Goeden, J.C. Huffman, K.G. Caulton, Inorg. Chem. 25 (1986) 2484; b) T.H. Lemmen, K. Folting, J.C. Huffman, K.G. Caulton, J. Am. Chem. Soc. 107 (1985) 7774; c) G.V. Goeden, K.G. Caulton, J. Am. Chem. Soc. 103 (1981) 7354.

7. a) T.M. Koenig, J.F. Daeuble, D.M. Brestensky, J.M. Stryker, Tetrahedron Lett. 31 (1990) 3237; b) D.M. Brestensky, J.M. Stryker, Tetrahedron Lett. 30 (1989) 5677; c) W.S. Mahoney, D.M. Brestensky, J.M. Stryker, J. Am. Chem. Soc. 110 (1988) 291; d) H. Brunner, W. Miehling, J. Organomet. Chem. 275 (1984) C17.

8. Selected recent examples: a) T. Vergote, F. Nahra, D. Peeters, O. Riant, T. Leyssens, J. Organomet. Chem. 730 (2013) 95; b) T.O. Schrader, B.R. Johnson, L. Lopez, M. Kasem, T. Gharbaoui, D. Sengupta, D. Buzard, C. Basmadjian, R.M. Jones, Org. Lett. 14 (2012) 6306; c) A. Albright, R.E. Gawley, J. Am. Chem. Soc. 133 (2011) 19680; d) F. Yu, J.-N. Zhou, X.-C. Zhang, Y.-Z. Sui, F.-F. Wu, L.-J. Xie, A.S.C. Chan, J. Wu, Chem. Eur. J. 17 (2011) 14234.; e) R. Moser, Z.V. Bošković, C.S. Crowe, B.H. Lipshutz, J. Am. Chem. Soc. 132 (2010) 7852.

9. For a review see: S. Rendler, M. Oestreich, Angew. Chem. 119 (2007) 504; Angew. Chem. Int. Ed. 46 (2007) 498.

10. Selected references: a) S. Werkmeister, K. Junge, M. Beller, Green Chem. 14 (2012) 2371; b) H. Shimizu, N. Sayo, T. Saito, Synlett (2009) 1295; c) H. Shimizu, D. Igarashi, W. Kuriyama, Y. Yusa, N. Sayo, T. Saito, Org. Lett. 9 (2007) 1655; d) J.-X. Chen, J.F. Daeuble, J.M. Stryker, Tetrahedron, 56 (2000) 2789; e) J.-X. Chen, J.F. Daeuble, D.M. Brestensky, J.M. Stryker, Tetrahedron 56 (2000) 2153.

11. R.S. Dhayal, J.-H. Liao, Y.-R. Lin, P.-K. Liao, S. Kahlal, J.-Y. Saillard, C.W. Liu, J. Am. Chem. Soc. 135 (2013) 4704.

12. Z. Mao, J.-S. Huang, C.-M. Che, N. Zhu, S.K.-Y. Leung, Z.-Y. Zhou, J. Am. Chem. Soc. 127 (2005) 4562.

13. B.H. Lipshutz, B.A. Frieman, Angew. Chem. 117 (2005) 6503; Angew. Chem. Int. Ed. 44 (2005) 6345.

14. N.P. Mankad, D.S. Laitar, J.P. Sadighi, Organometallics 23 (2004) 3369.

15. For a related species see: A. Welle, S. Díez-González, B. Tinant, S.P. Nolan, O. Riant, Org. Lett. 8 (2006) 6059.

16. G.D. Frey, B. Donnadieu, M. Soleilhavoup, G. Bertrand. Chem. Asian J. 6 (2011) 402.

17. E.Y. Tsui, P. Müller, J.P. Sadighi, Angew. Chem. 120 (2008) 9069; Angew. Chem. Int. Ed. 47 (2008) 8937.

18. B.K. Tate, C.M. Wyss, J. Bacsa, K. Kluge, L. Gelbaum, J.P. Sadighi, Chem. Sci. 4 (2013) 3068.

19. P. Pyykkö, Chem. Rev. 97 (1997) 597.

20. a) N. Kuganathan, J.C. Green, Chem. Commun. (2008) 2432; b) H.L. Hermann, G. Boche, P. Schwerdtfeger, Chem. Eur. J. 7 (2001) 5333; c) C. Mealli, S.S.M.C. Godinho, M.J. Calhorda, Organometallics 20 (2001) 1734; d) C. Kölmel, R. Ahlrichs, J. Phys. Chem. 94 (1990) 5536; e) K.M. Merz, Jr., R. Hoffmann, Inorg. Chem. 27 (1988) 2120.

21. a) S.-L. Zheng, M. Messerschmidt, P. Coppens, Angew. Chem. 117 (2005) 4690; Angew. Chem. Int. Ed. 44 (2005) 4614; b) A. Sundararaman, L.N. Zakharov, A.L. Rheingold, F. Jäkle, Chem. Commun. (2005) 1708; c) J.-P. Zhang, Y.-B. Wang, X.-C. Huang, Y.-Y. Lin, X.-M. Chen, Chem. Eur. J. 11 (2005) 552; d) R. D. Köhn, G. Seifert, Z. Pan, M.F. Mahon, G. Kociok-Köhn, Angew. Chem. 115 (2003) 818; Angew. Chem. Int. Ed. 42 (2003) 793; e) J.-M. Poblet, M. Bénard, Chem. Commun. (1998) 1179; f) K. Singh, J.R. Long, P. Stravropoulos, J. Am. Chem. Soc. 119 (1997) 2942; g) M.K. Ehlert, S.J. Rettig, A. Storr, R.C. Thompson, J. Trotter, Can. J. Chem. 68 (1990) 1444.

22. J.C. Green, M.L.H. Green, G. Parkin, Chem. Commun. 48 (2012) 11481.

23. a) R. Clérac, F.A. Cotton, L.M. Daniels, J. Gu, C.A. Murillo, H.-C. Zhou, Inorg. Chem. 39 (2000) 4488; b) F.A. Cotton, X. Feng, D.J. Timmons, Inorg. Chem. 37 (1998) 4066; c) J. Beck, J. Strähle, Angew. Chem. 97 (1985) 419; Angew. Chem. Int. Ed. Engl. 24 (1985) 409.

24. For studies of bonding in bent [M_2(μ-H)] complexes, see for example: a) M. Savoca, J. Langer, O. Dopfer, Angew. Chem. 125 (2013) 1608; Angew. Chem. Int. Ed. 52 (2013) 1568; b) Z. Zhu, R.J. Wright, M.M. Olmstead, E. Rivard, M. Brynda, P.P. Power, Angew. Chem. 118 (2006) 5939; Angew. Chem. Int. Ed. 45 (2006) 5807; c) M.-H. Baik, R.A. Friesner, G. Parkin, Polyhedron 23 (2004) 2879; d) B. Jeżowska-

Trzebiatowska, B. Nissen-Sobocińska, J. Organomet. Chem. 322 (1987) 331; e) R. Bau, R.G. Teller, S.W. Kirtley, T.F. Koetzle, Acc. Chem. Res. 12 (1979) 176.

25. Linear [Ni-H-Ni] complexes: D.A. Vicic, T.J. Anderson, J.A. Cowan, A.J. Schultz, J. Am. Chem. Soc. 126 (2004) 8132.

26. Calculations of linear $\{M_2(\mu\text{-}H)\}^+$ structures for alkali metals: S.J. Grabowski, R. Hoffmann, ChemPhysChem 13 (2012) 2286.

27. R.A. Flurer, K.L. Busch, J. Am. Chem. Soc. 113 (1991) 3656.

28. R. Gáspár, I. Tamássy-Lentei, Acta Phys. Acad. Sci. Hung. 50 (1981) 343.

29. Calculations of copper–copper bonding in cyclic copper hydrides: A.C. Tsipis, C.A. Tsipis, J. Am. Chem. Soc. 125 (2003) 1136.

30. a) H. Kaur, F.K. Zinn, E.D. Stevens, S.P. Nolan, Organometallics 23 (2004) 1157; b) V. Jurkauskas, J.P. Sadighi, S.L. Buchwald, Org. Lett. 5 (2003) 2417.

31. CCDC 953635 (**1**), 953636 (**2**), and 953634 (**3**) contain the supplementary crystallographic data. These data can be obtained free of charge from The Cambridge Crystallographic Data Centre via www.ccdc.cam.ac.uk/data_request/cif.

32. A. Bondi, J. Phys. Chem. 68 (1964) 441.

33. X-ray diffraction tends to underestimate M–H distances; see for example Ref. [24e]. The Cu-H-Cu bending in **1** may thus be more pronounced than the experimentally determined angle suggests.

34. K.B. Wiberg, Tetrahedron 24 (1968) 1083.

35. R.F.W. Bader, Atoms in Molecules: A Quantum Theory, Oxford University Press, Oxford (1990).

36. a) M.R. Churchill, D.G. DeBoer, F.J. Rotella, Inorg. Chem. 15 (1976) 1843; b) M.R. Churchill, S.W.-Y. Ni, J. Am. Chem. Soc. 95 (1973) 2150.

37. T.C. Davenport, T.D. Tilley, Angew. Chem. 123 (2011) 12413; Angew. Chem. Int. Ed. 50 (2011) 12205.

38. B.D. Nageswara Rao, L.R. Anders, Phys. Rev. 140 (1965) A112.

39. a) J.T. Muckerman, P. Achord, C. Creutz, D.E. Polyansky, E. Fujita, Proc. Natl. Acad. Sci. U.S.A. 109 (2012) 15657; b) C.J. Curtis, A. Miedaner, W.W. Ellis, D.L. DuBois, J. Am. Chem. Soc. 124 (2002) 1918; c) D.J. Darensbourg, H. Pickner Wiegreffe, P.W. Wiegreffe, J. Am. Chem. Soc. 112 (1990) 9252; d) S. Sakaki, K. Ohkubo, Inorg. Chem. 28 (1989) 2583.

40. C. Dash, A. Das, M. Yousufuddin, H.V.R. Dias, Inorg. Chem. 52 (2013) 1584.

41. Reactions of alkynes with neutral copper hydride: a) K. Semba, T. Fujihara, J. Terao, Y. Tsuji, Chem. Eur. J. 18 (2012) 4179; b) T. Fujihara, T. Xu, K. Semba, J. Terao, Y. Tsuji, Angew. Chem. 123 (2011) 543; Angew. Chem. Int. Ed. 50 (2011) 523; c) T. Konno, J. Chae, T. Tanaka, T. Ishihara, H. Yamanaka, J. Fluorine Chem. 127 (2006) 36; d) J.F. Daeuble, C. McGettigan, J.M. Stryker, Tetrahedron Lett. 31 (1990) 2397; see also Ref. [14].

42. Selected references: a) A. Zhdanko, M.E. Maier, Organometallics 32 (2013) 2000; b) D. Weber, T.D. Jones, L.L. Adduci, M.R. Gagné, Angew. Chem. 124 (2012) 2502; Angew. Chem. Int. Ed. 51 (2012) 2452; c) A.S.K. Hashmi, I. Braun, P. Nösel, J. Schädlich, M. Wieteck, M. Rudolph, F. Rominger, Angew. Chem. 124 (2012) 4532; Angew. Chem. Int. Ed. 51 (2012) 4456; d) T.J. Brown, D. Weber, M.R. Gagné, R.A. Widenhoefer, J. Am. Chem. Soc. 134 (2012) 9134; e) G. Seidel, C.W. Lehmann, A. Fürstner, Angew. Chem. 122 (2010) 8644; Angew. Chem. Int. Ed. 49 (2010) 8466; f) D. Weber, M.A. Tarselli, M.R. Gagné, Angew. Chem. 121 (2009) 5843; Angew. Chem. Int. Ed. 48 (2009) 5733.

43. P. Schulte, U. Behrens, F. Olbrich, Z. Anorg. Allg. Chem. 626 (2000) 1692.

44. For a review of mesitylcopper and related complexes, see: M. Stollenz, F. Meyer, Organometallics 31 (2012) 7708.

45. G.N. Khairallah, T. Waters, R.A.J. O'Hair, Dalton Trans. (2009) 2832.

46. B.T. Worrell, J.A. Malik, V.V. Fokin, Science 340 (2013) 457.

47. J.A. Bouwstra, A. Schouten, J. Kroon, Acta Crystallogr. Sect. C 40 (1984) 428.

48. L. Hintermann, Beilstein Journal of Organic Chemistry 3 (2007) No. 22 (doi: 10/1186/1860-5397-3-22).

49. A.E. Finholt, C. Bond, Jr., K.E. Wilzbach, H.I. Schlesinger, J. Am. Chem. Soc. 69 (1947) 2692.

50. O.V. Dolomanov, L.J. Bourhis, R.J. Gildea, J.A.K. Howard, H. Puschmann, OLEX2: a complete structure solution, refinement and analysis program. J. Appl. Cryst. 42 (2009) 339.

51. SHELXS-97 (Sheldrick, 2008).

52. SHELXL-97 (Sheldrick, 2008).

53. Gaussian 09, Revision A.02, M.J. Frisch, G.W. Trucks, H.B. Schlegel, G.E. Scuseria, M.A. Robb, J.R. Cheeseman, G. Scalmani, V. Barone, B. Mennucci, G.A. Petersson, H. Nakatsuji, M. Caricato, X. Li, H.P. Hratchian, A.F. Izmaylov, J. Bloino, G. Zheng, J.L. Sonnenberg, M. Hada, M. Ehara, K. Toyota, R. Fukuda, J. Hasegawa, M. Ishida, T. Nakajima, Y. Honda, O. Kitao, H. Nakai, T. Vreven, J.A. Montgomery, Jr., J.E. Peralta, F. Ogliaro, M. Bearpark, J.J. Heyd, E. Brothers, K.N. Kudin, V.N. Staroverov, R. Kobayashi, J. Normand, K. Raghavachari, A. Rendell, J.C. Burant, S.S. Iyengar, J. Tomasi, M. Cossi, N. Rega, J.M. Millam, M. Klene, J.E. Knox, J.B. Cross, V. Bakken, C. Adamo, J. Jaramillo, R. Gomperts, R.E. Stratmann, O. Yazyev, A.J. Austin, R. Cammi, C. Pomelli, J.W. Ochterski, R.L. Martin, K. Morokuma, V.G. Zakrzewski, G.A. Voth, P. Salvador, J.J. Dannenberg, S. Dapprich, A.D. Daniels, Ö. Farkas, J.B. Foresman, J.V. Ortiz, J. Cioslowski, D.J. Fox, Gaussian, Inc., Wallingford CT (2009).

54. J.P. Perdew, K. Burke, M. Ernzerhof, Phys. Rev. Lett. 77 (1996) 3865.

55. S. Grimme, J. Comput. Chem. 27 (2006) 1787.

56. S. Miertus, E. Scrocco, J. Tomasi, Chem. Phys. 55 (1981) 117.

57. B. Mennucci, E. Cancès, J. Tomasi, J. Phys. Chem. B 101 (1997) 10506.

58. N. Godbout, D.R. Salahub, J. Andzelm, E. Wimmer, Can. J. Chem. 70 (1992) 560.

59. R.S. Mulliken, J. Chem. Phys. 23 (1955) 1833.

60. S.I. Gorelsky, AOMix: Program for Molecular Orbital Analysis; York University: Toronto (1997) http://www.sg-chem.net.

61. S.I. Gorelsky, A.B.P. Lever, J. Organomet. Chem. 635 (2001) 187.

62. http://aim.tkgristmill.com/

CHAPTER 3

Bonding and Reactivity of a μ-Boryl Dicopper Cation

Part of this thesis chapter has been adapted with permission from an article co-written by the author:

C.M. Wyss, J. Bitting, J. Bacsa, T.G. Gray, J.P. Sadighi, "Bonding and Reactivity of a μ-Boryl Dicopper Cation." Prepared in Manuscript Form to Organometallics.

3.1. Introduction

Transition metal boryl complexes have been the focus of intensive research as intermediates in hydroboration[1] and diboration[2] reactions of unsaturated organic substrates, as well as in the selective C–H bond activation of hydrocarbons.[3] Transition metal boryl complexes that have been structurally characterized are almost exclusively mononuclear and there are few reports on homo- and heterometallic boryl-bridged complexes.[4] Copper boryl complexes have proven to be highly effective catalysts in the reduction of CO_2,[5] in the hydroboration and diboration of unsaturated organics,[6] and in the borylation of carbon–halogen bonds.[7] Structural and theoretical examinations of such complexes offer insight into the nature of the metal–boron bond, with the goal of improving catalytic efficiency.[8] The only copper boryls isolated and structurally characterized to date are mononuclear examples.[5,9] Herein, we describe the synthesis and structural characterization of a boryl-bridged dicopper cation, $\{[(SIDipp)Cu]_2(\mu\text{-}BO_2C_6H_4)\}^+ BF_4^-$, supported by an N-heterocyclic carbene. The complex adopts a bent arrangement about the boryl with a short intermetallic distance of 2.4082(2) Å. Density functional theory (DFT) calculations were applied to give further insight into the nature

of the metal–boron bonds in comparison to the mononuclear analogue.[5] The two electrons contributed by the bridging boryl are shared between the boron and the two copper centers in the $[(LCu)_2B]^+$ core. This three-center, two-electron bonding orbital is lower-lying in energy than the Cu–B σ-bonding molecular orbital in the mononuclear analogue, consistent with a less nucleophilic Cu–B bond.

3.2. Results and Discussion

3.2.1. Synthesis of $\{[(SIDipp)Cu]_2(\mu\text{-}BO_2C_6H_4)\}^+ BF_4^-$

The siloxide-bridged $\{[(SIDipp)Cu]_2(\mu\text{-}OSiMe_3)\}^+ BF_4^-$ reacts with bis(catecholato)diboron (catB–Bcat) to form $\{[(SIDipp)Cu]_2(\mu\text{-}BO_2C_6H_4)\}^+ BF_4^-$ (**1**) and the hydrocarbon-soluble byproduct $Me_3SiOB(cat)$ (Scheme 3.1).

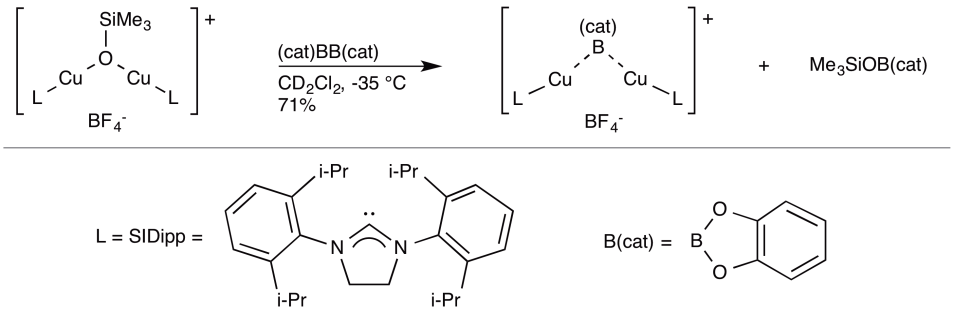

Scheme 3.1. Synthesis of boryl-bridged dicopper complex **1**. Dashed lines indicate delocalized two-electron bonding.

The ^1H NMR spectrum in CD_2Cl_2 displays a single set of resonances arising from the SIDipp ligands. The resonances assigned to the bridging B(cat) moiety appear upfield of those observed for (cat)BB(cat). The ^{11}B NMR spectrum shows only a single peak at –1.47 ppm arising from the BF_4^- counterion. The resonance for the bridging boryl could not be assigned definitively. For comparison, the ^{11}B NMR spectrum of the copper boryl

complex (IDipp)CuB(pin) displays a very broad singlet at 41.7 ppm.[5] We speculate that coupling between boron and an additional quadrupolar nucleus, ^{63}Cu or ^{65}Cu, might broaden this resonance into the baseline. An equilibrium between the boryl-bridged cation and the terminal boryl plus solvated $[(IDipp)Cu]^+$ could further broaden this resonance. In the solid-state, complex **1** is stable at –32 °C; however, dichloromethane solutions of **1** slowly deposit metallic copper at room temperature.

3.2.2. Reactivity and structural aspects

We first examined the reactivity of complex **1** with CO_2 to compare the reactivity of **1** and the terminal copper boryl complex (IDipp)CuB(pin),[5] which readily reacts with CO_2. In marked contrast to the terminal copper boryl complex, **1** was not observed to react with CO_2 to form CO and the corresponding borate byproduct.

In light of the rich chemistry between terminal boryls and alkynes,[8d-e,10] we wanted to investigate the reactivity of the boryl-bridged cation with alkynes. We first looked at its reactivity toward phenylacetylene. A solution of $\{[(SIDipp)Cu]_2(\mu\text{-}BO_2C_6H_4)\}^+$ BF_4^- in CD_2Cl_2 became bright yellow upon addition of phenylacetylene. After 8 hours at –35 ºC, the solution had become colorless. The ^{11}B NMR spectrum indicated the formation of H–B(cat), and the ^{1}H NMR spectrum was consistent with the formation of $\{[(SIDipp)Cu]_2(\mu\text{-}CCC_6H_5)\}^+$ BF_4^- (Scheme 3.2).[11] This is an unusual example of a boryl complex acting as a Brønsted base.

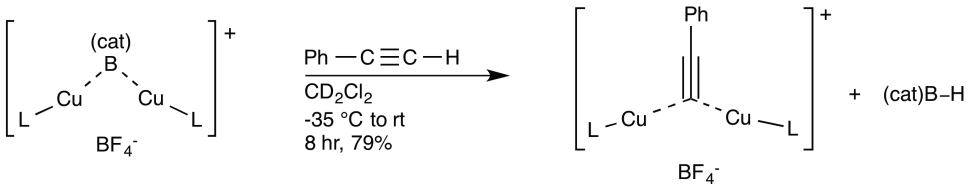

Scheme 3.2. Reaction of **1** with phenylacetylene. The alkynyl is represented as σ-bridging because the ligands are equivalent on the NMR timescale, however, this may actually be an average of degenerate σ,π-bridged structures.[12]

To see whether a non-acidic alkyne would insert to form a B–C bond, we attempted the reaction of **1** with 3-hexyne. Upon addition of 3-hexyne to a solution of $\{[(SIDipp)Cu]_2(\mu\text{-}BO_2C_6H_4)\}^+ BF_4^-$ in CD_2Cl_2 an intense yellow color, similar to that seen on addition of phenylacetylene, appeared. This color change, combined with subtle changes in the ^1H NMR spectrum, led us to believe that the alkyne may be weakly bound to **1**, and not inserted as has been demonstrated with terminal boryls and alkynes.[6b,8d-e] We attempted to crystallize a μ,η^2-alkyne complex from a solution of **1** in CH_2Cl_2 at –32 °C, using 3-hexyne as co-solvent. The resulting colorless crystals unfortunately contained no alkyne, but proved well suited for analysis by X-ray diffraction (Figure 3.1).

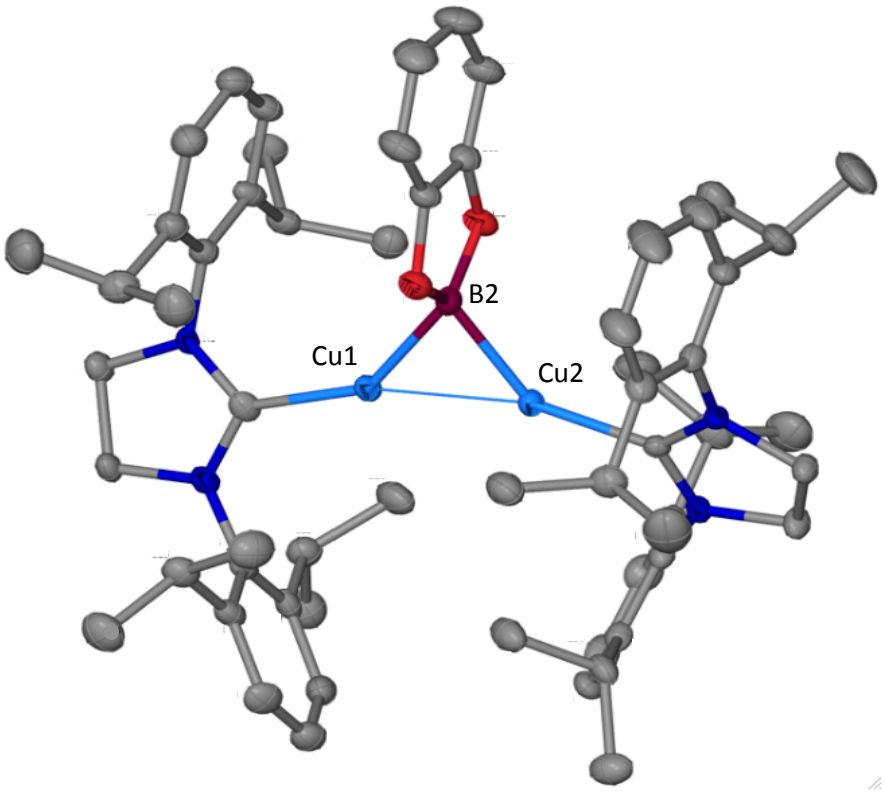

Figure 3.1. ORTEP view of $\{[(SIDipp)Cu\}_2(\mu\text{-}BO_2C_6H_5)\}^+ BF_4^-$. Ellipsoids are set at 50% probability; the BF_4^- anion, hydrogen atoms, and co-crystallized solvent are omitted for clarity. Selected bond lengths (Å) and angles (°): Cu1–Cu2 2.4082(2), C1–Cu1 1.941(5), Cu1–B2 2.051(6), B2–Cu2 2.041(6), Cu2–C28 1.923(5); C1–Cu1–B2 143.7(2), Cu1–B2–Cu2 72.1(2), B2–Cu2–C28 142.7(2).

The complex adopts a bent arrangement about the boryl, with a Cu–B–Cu angle of 72.1(2)° and an intermetallic Cu–Cu distance of 2.4082(2) Å. This is considerably less than twice the van der Waals radius of copper, 1.4 Å,[13] and shorter than the intermetallic Cu–Cu distances of 2.541(2) Å found for a hydride-bridged dicopper cation, $\{[(SIDipp)Cu]_2(\mu\text{-}H)\}^+ OTf^-$.[14] It should be noted that crystal packing effects arising from the change in anion could also contribute to the difference in the Cu–Cu distances. The C–Cu–B angles in **1** are 143.7(2)° and 142.7(2)°, and the C–Cu–Cu angles are 162.0(2)° and 163.2(2)°.

In light of the deprotonation of phenylacetylene by **1,** we reasoned that the protonolysis of the boryl by an alcohol should form the alkoxide-bridged dicopper cation plus catecholborane. Subsequent metathesis of hydride and alkoxide would be expected to generate the hydrido-bridged dicopper complex plus alkoxy(catechol)borate. Complex **1** reacts readily with CH_3OH, in THF-d_8 at –32 °C, to form $\{[(SIDipp)Cu]_2(\mu\text{-}H)\}^+ BF_4^-$ and $CH_3OB(cat)$ as judged by ^{1}HNMR spectroscopy (Scheme 3.3). The ^{1}H NMR spectrum of the major product was identical to that of $\{[(SIDipp)Cu]_2(\mu\text{-}H)\}^+ BF_4^-$, prepared independently by the route developed for $\{[(IDipp)Cu]_2(\mu\text{-}H)\}^+ BF_4^-$.[15]

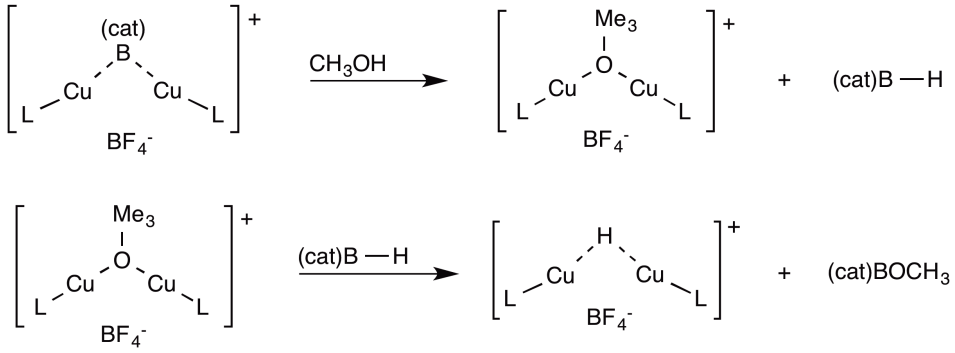

Scheme 3.3. Proposed reaction route of **1** with methanol.

3.2.3. Density functional theory calculations

Density functional theory (DFT) calculations were applied to $\{[(SIDipp)Cu]_2(\mu\text{-}BO_2C_6H_4)\}^+ BF_4^-$ to elucidate the copper–copper and copper–boron interactions (Figure 3.2).

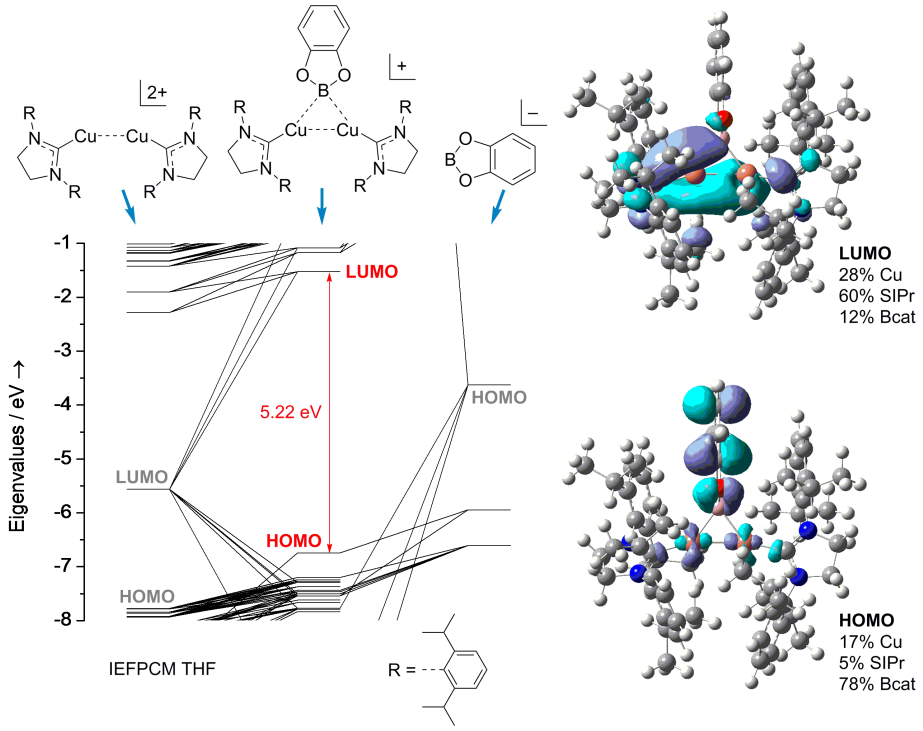

Figure 3.2. Partial Kohn–Sham orbital energy diagram **1**. Plots of selected orbitals, with percentage compositions in terms of fragments, appear at the right. Implicit THF solvation is included.

The copper–copper distance was calculated at 2.34458 Å, somewhat less than the value from the solid-state structure. According to natural population analysis, the Wiberg bond order between copper centers is 0.366 in the Löwdin basis. This should be regarded as a maximum since the calculated copper–copper distance is shorter than the experimentally determined value. The copper–boron bond orders are 0.656 and 0.659. The highest occupied Kohn–Sham orbital (HOMO) of **1** is largely derived from the filled B(cat) π-system (78% B(cat), 17% Cu, 5% NHC), and the lowest unoccupied orbital (LUMO) is largely NHC-derived (60% NHC, 28% Cu, 12% B(cat)). The HOMO-LUMO gap was calculated to be 5.22 eV. Marder, Lin and coworkers studied (IDipp)CuB(pin) by DFT and found the HOMO to be the Cu–B σ-bonding molecular orbital.[8c] Theoretical studies

suggest that the flow of electrons in the insertion of aldehydes,[8a] CO_2,[8b], alkenes,[8c] and alkynes,[8d-e] is from the Cu–B σ-bond to each coordinated substrate. Many reactivity studies show the boryl ligand in copper-promoted borylations displaying such nucleophilic behavior.[16]

The electron density between the two Cu centers and B in the $[(LCu)_2B]^+$ core of **1** is spread among the three atom centers in a three-center two-electron bond and is lower-lying in energy than the Cu–B σ-bonding molecular orbital in the mononuclear analogue. This could lead to a less nucleophilic Cu–B bond, accounting in part for the difference in reactivity between **1** and (IDipp)CuB(pin). It should also be taken into consideration that the –B(pin) ligand is a stronger σ donor than –B(cat), as reflected by the stronger trans-influence calculated for square-planar platinum(II) complexes of the type *trans*-$[PtL(Cl)(PMe_3)_2]$.[17] It has also been shown theoretically that the insertion barrier of an alkene substrate molecule into a Cu–B(pin) bond is slightly smaller than the insertion barrier into a Cu–B(cat) bond. The smaller barrier suggests that the nucleophilicity of the –B(pin) ligand is somewhat greater than that of the –B(cat) ligand.[18]

3.3. Conclusion

In summary, an N-heterocyclic carbene ligand supports a bent $[Cu_2B(cat)]^+$ complex with a short intermetallic distance. Density functional theory (DFT) calculations determined that the two electrons contributed by the bridging boryl are shared among the two copper centers and boron in the $[(LCu)_2B]^+$ core in a three-center, two-electron bond. The boryl-bridged dicopper cation deprotonates phenylacetylene to form a

phenylacetylide dicopper complex, and readily reacts with methanol to form the hydride-bridged dicopper cation.

3.4. Experimental

3.4.1. General considerations

Unless otherwise indicated, manipulations were performed in an MBraun glovebox under an inert atmosphere of nitrogen, or in sealable glassware on a Schlenk line under an atmosphere of argon. Glassware and magnetic stir bars were dried in a ventilated oven at 160 °C and were allowed to cool under vacuum.

^{1}H, ^{13}C, and ^{11}B NMR spectra were obtained using a Bruker DSX 400 MHz spectrometer and a Varian Vx 400 MHz spectrometer. ^{1}H and ^{13}C NMR chemical shifts are referenced with respect to solvent signals and are reported relative to tetramethylsilane. Samples for infrared spectroscopy were prepared as pellets in potassium bromide, using a pellet die which was dried in a ventilated oven at 160 °C and cooled under vacuum prior to use. The pellets were prepared in the glovebox under an atmosphere of dry nitrogen, and were exposed to air as briefly as possible prior to data collection. Spectra were recorded using a Perkin Elmer Spectrum 1000 infrared spectrometer. Elemental analyses were performed by Atlantic Microlab in Norcross, Georgia.

3.4.2. Materials and methods

Dichloromethane (BDH), hexane (EMD Millipore Omnisolv), tetrahydrofuran (THF, EMD Millipore Omnisolv), and toluene (EMD Millipore Omnisolv) were sparged with ultra high purity argon (NexAir) for 30 minutes prior to first use, dried using an

MBraun solvent purification system, transferred to Straus flasks, degassed using three freeze-pump-thaw cycles, and stored under nitrogen or argon. Methanol (EMD Millipore) was vacuum-transferred to an oven-dried resealable flask containing 3Å molecular sieves, and degassed by successive freeze-pump-thaw cycles. Anhydrous benzene (EMD Millipore Drisolv, sealed under a nitrogen atmosphere) was used as received and stored in a glovebox. Tap water was purified in a Barnstead International automated still prior to use.

Dichloromethane-d_2 (Cambridge Isotope Labs) was dried over excess calcium hydride overnight, vacuum-transferred to an oven-dried resealable flask, and degassed by successive freeze-pump-thaw cycles. Benzene-d_6 (Cambridge Isotope Labs) and tetrahydrofuran-d_8 (Cambridge Isotope Laboratories) were dried over sodium benzophenone ketyl, vacuum-transferred into oven-dried resealable flasks, and degassed by successive freeze-pump-thaw cycles.

Sodium *tert*-butoxide (TCI America), copper(I) chloride (Alfa-Aesar), triphenylcarbenium tetrafluoroborate (Alfa-Aesar), 4,4,5,5-tetramethyl-1,3,2-dioxaborolane (Sigma-Aldrich), 2,6-diisopropylaniline (Sigma-Aldrich), diisopropylethylamine (Alfa-Aesar), acetic acid, (Alfa-Aesar), sodium trimethylsilanolate (Sigma-Aldrich), bis(catecholato)diboron (Sigma-Aldrich), sodium metal (Alfa-Aesar), benzophenone (Alfa-Aesar), calcium hydride (Alfa-Aesar), acetone (BDH), 1,2-dichloroethane (EMD Millipore Omnisolv), triethyl orthoformate (Alfa-Aesar), nitrogen (NexAir), and argon (both industrial and ultra high purity grades, NexAir) were used as received. Phenylacetylene (Sigma-Aldrich) was filtered over alumina (EMD) prior to use. SIDipp·HCl[19], (SIDipp)CuCl[20], and (SIDipp)Cu(O*t*Bu)[20] were prepared according to

literature protocols and were characterized by ^{1}H NMR spectroscopy.

Preparation of (SIDipp)Cu(OSiMe$_3$)

Sodium trimethylsilanolate (0.321 g, 2.861 mmol) was added to a suspension of (SIDipp)CuCl (1.400 g, 2.859 mmol) in THF (40 mL) with stirring. After stirring for 3 hours, the reaction mixture was filtered through Celite, and the filter pad was washed with three portions of THF (5 mL each). The solvent was removed from the filtrate under vacuum, and the residue was dried for 12 hours at 40 °C under vacuum, affording the product as a white powder (1.259 g, 2.326 mmol, 81%). The product hydrolyzes readily in the presence of atmospheric moisture. ^{1}H NMR (400 MHz, CD_2Cl_2): δ (ppm) 7.42 (t, *J* = 8 Hz, 2 H, *para*-C*H*), 7.28 (d, *J* = 4 Hz, 4 H, *meta*-C*H*), 3.99 (s, 4 H, NCH_2), 3.07 (sept., *J* = 8 Hz, 4 H, C*H*(CH_3)$_2$), 1.37 (d, *J* = 8 Hz, 12 H, CH(CH_3)$_2$), 1.34 (d, *J* = 8 Hz, 12 H, CH(CH_3)$_2$), –0.50 (s, 9H, OSi(CH_3)$_3$). ^{13}C{^{1}H} NMR (100 MHz, CD_2Cl_2): δ (ppm) 204.9 (br. N*C*Cu), 147.3 (*ortho*-*C*), 135.4 (*ipso*-*C*), 129.8 (*para*-*C*), 124.7 (*meta*-*C*), 54.0 (N*C*H_2), 29.2 (*C*H(CH_3)$_2$), 25.6 (CH(*C*H_3)$_2$), 24.1 (CH(*C*H_3)$_2$), 4.0 (OSi(*C*H_3)$_3$). IR: ν (cm^{-1}) 2960 (w), 2866, 1482, 1459, 1384, 1365, 1344, 1327, 1302, 1273 (s), 1248, 1234 (w), 1180, 1058, 1003 (w), 936, 819, 809, 769, 761, 739 (s), 663 (s), 619 (s), 550, 503, 447. Anal. Calcd. for $C_{30}H_{47}N_2CuOSi$: C, 66.32; H, 8.72; N, 5.16. Found: C, 66.24; H, 8.88; N, 5.12.

Preparation of {[(SIDipp)Cu]$_2$(μ-OSiMe$_3$)}$^+$ BF_4^-

Triphenylcarbenium tetrafluoroborate (0.240 g, 0.727 mmol) was added to a solution of (SIDipp)Cu(OSiMe$_3$) (0.800 g, 1.478 mmol) in THF (12 mL). The reaction flask was covered with foil to exclude light, and the mixture was stirred for 4 hours.

Anhydrous hexanes (30 mL) were added to the THF solution, resulting in the formation of a white precipitate. The precipitate was collected on a fritted glass filter and washed with two portions of toluene (6 mL each) and two portions of hexanes (5 mL each). Residual solvents were removed under vacuum at 40 °C for 18 hours, affording the product as a white powder (0.718 g, 0.662 mmol, 91%). The product hydrolyzes readily in the presence of atmospheric moisture. ^{1}H NMR (400 MHz, CD_2Cl_2): δ (ppm) 7.40 (t, *J* = 8 Hz, 4 H, *para*-C*H*), 7.21 (d, *J* = 8 Hz, 8 H, *meta*-C*H*), 3.90 (s, 8 H, NCH_2), 2.91 (sept., *J* = 8 Hz, 8 H, C*H*(CH_3)$_2$), 1.27 (d, *J* = 8 Hz, 24 H, CH(CH_3)$_2$), 1.07 (d, *J* = 8 Hz, 24 H, CH(CH_3)$_2$), –0.84 (s, 9H, OSiMe(CH_3)$_3$). ^{13}C{^{1}H} NMR (100 MHz, CD_2Cl_2): δ (ppm) 201.7 (br. N*C*Cu), 146.5 (*ortho*-*C*), 134.9 (*ipso*-*C*), 130.2 (*para*-*C*), 125.2 (*meta*-*C*), 54.7 (N*C*H_2), 29.0 (*C*H(CH_3)$_2$), 25.4 (CH(*C*H_3)$_2$), 24.3 (CH(*C*H_3)$_2$), 3.9 (OSi(*C*H_3)$_3$). IR: ν (cm^{-1}) 2957 (w), 2867, 1482, 1455 (w), 1363, 1327, 1273, 1247, 1180, 1050, 922, 880 (s), 838 (s), 805, 757 (s), 604, 550 (s), 520, 450. Anal. Calcd. for $C_{57}H_{85}N_4Cu_2BF_4OSi$: C, 63.14; H, 7.90; N, 5.17. Found: C, 63.34; H, 8.02; N, 5.00.

*Preparation of {[(SIDipp)Cu]$_2$(μ-$BO_2C_6H_4$)}$^+$ BF_4^- (**1**)*

Bis(catecholato)diboron (0.055g, 0.231 mmol) was added to a solution of {[(SIDipp)Cu]$_2$(μ-$OSiMe_3$)}$^+$ BF_4^- (0.250 g, 0.231 mmol) in dichloromethane (4 mL), previously cooled to –35°C. The resultant mixture was stored at –35 °C for 18 hours. A layer of hexanes (15 mL) was carefully added over the dichloromethane solution, and the layers were allowed to mix by diffusion at –35 °C for 14 hours, resulting in the formation of colorless crystals. The mother liquor was decanted, and the crystals were collected on a fritted glass filter. The crystals were triturated, then washed with three portions of hexanes (4 mL each), affording the product as a white powder (0.181 g, 0.164 mmol,

71%). The product hydrolyzes readily in the presence of atmospheric moisture and undergoes decomposition in solution at room temperature. ^{1}H NMR (400 MHz, CD_2Cl_2): δ (ppm) 7.09 (t, *J* = 8 Hz, 4 H, *para*-C*H*), 6.95 (d, *J* = 8 Hz, 10 H, *meta*-C*H*), 6.72 (m, 2H, cat *ortho*-C*H*), 3.87 (s, 8 H, NCH_2), 2.79 (sept., *J* = 8 Hz, 8 H, C*H*$(CH_3)_2$), 1.20 (d, *J* = 8 Hz, 24 H, CH(CH_3)$_2$), 0.97 (d, *J* = 8 Hz, 24 H, CH(CH_3)$_2$) the multiplet corresponding to the catecholate *meta*-C*H* coincides with the *meta*-C*H* doublet of the ligand N-aryl group, resulting in an integration of 10 H. ^{13}C{^{1}H} NMR (100 MHz, CD_2Cl_2): δ (ppm) 200.3 (br. N*C*Cu), 148.1 (BO*C*), 146.5 (*ortho*-*C*), 133.4 (*ipso*-*C*), 130.0 (*para*-*C*), 124.7 (*meta*-*C*), 121.9 (cat *meta*-*C*), 112.7 (cat *ortho*-*C*), 54.2 (N*C*H_2), 29.0 (*C*H$(CH_3)_2$), 25.5 (CH(*C*H_3)$_2$), 23.7 (CH(*C*H_3)$_2$). ^{11}B NMR (CD_2Cl_2): δ (ppm) –1.47 (*B*F_4). Note: The resonance for Cu*B*Cu was too broad to be definitively assigned. IR: ν (cm^{-1}) 2960 (w), 2868 (w), 1484, 1458 (w), 1384, 1362, 1325, 1272, 1230 (s), 1137, 1099, 1046 (w), 1015 (w), 934, 915, 878, 806 (s), 743, 618, 547, 519, 447. Anal. Calcd. for $C_{60}H_{80}N_4Cu_2B_2F_4O_2$: C, 64.69; H, 7.24; N, 5.03. Found: C, 64.44; H, 6.96; N, 4.90.

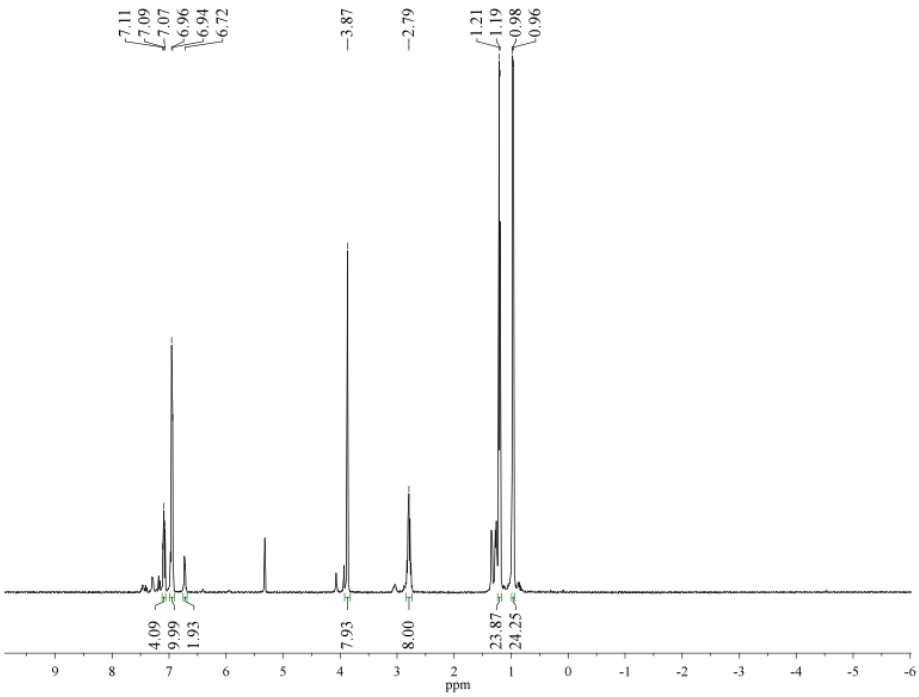

Figure 3.3. ^{1}H NMR spectrum (400 MHz, CD_2Cl_2) of $\{[(SIDipp)Cu]_2(\mu\text{-}BO_2C_6H_4)\}^+$ BF_4^-. A trace of residual solvent, hexanes (δ 1.29 and 0.89 ppm), is present.

Preparation of $\{[(SIDipp)Cu]_2(\mu\text{-}CCC_6H_5)\}^+$ BF_4^-

Phenylacetylene (0.010 mL, 0.091 mmol) was added to a solution of $\{[(SIDipp)Cu]_2(\mu\text{-}BO_2C_6H_4)\}^+$ BF_4^- (0.050 g, 0.045 mmol) in dichloromethane (1 mL) that was cooled to –35 °C. The resultant mixture was stored at –35 °C for 8 hours. A layer of hexane (18 mL) was carefully added over the dichloromethane solution, and the layers were allowed to mix by diffusion at room temperature for 14 hours, resulting in the formation of colorless crystals. The mother liquor was decanted, and the crystals were collected on a fritted glass filter. The crystals were triturated, then washed with two portions of hexane (4 mL each), affording the product as a white powder (0.039 g, 0.036 mmol, 79%). ^{1}H NMR (400 MHz, CD_2Cl_2): δ (ppm) 7.37 (t, *J* = 8 Hz, 4 H, *para*-C*H*), 7.20 (m, 1 H, Ph *para*-C*H*), 7.16 (d, *J* = 8 Hz, 8 H, *meta*-C*H*), 6.99 (t, *J* = 8 Hz, 2 H, Ph

meta-C*H*), 6.26 (d, *J* = 8 Hz, 2 H, Ph *ortho*-C*H*), 3.96 (s, 8 H, NCH_2), 2.91 (sept., *J* = 8 Hz, 8 H, C*H*(CH_3)$_2$), 1.26 (d, *J* = 8 Hz, 24 H, CH(CH_3)$_2$), 0.99 (d, *J* = 8 Hz, 24 H, CH(CH_3)$_2$). ^{13}C{^{1}H} NMR (100 MHz, CD_2Cl_2): δ (ppm) 201.7 (br. N*C*Cu), 146.9 (*ortho-C*), 134.4 (*ipso-C*), 132.2 (Ph *ortho-C*), 130.2 (*para-C*), 129.3 (Ph *para-C*), 128.6 (Ph *meta-C*), 124.9 (*meta-C*), 122.3 (C*C*Ph), 119.3 (Cu*C*Cu), 54.3 (N*C*H_2), 29.1 (*C*H(CH_3)$_2$), 25.4 (CH(*C*H_3)$_2$), 23.9 (CH(*C*H_3)$_2$). IR: ν (cm^{-1}) 2958 (w), 2867 (w), 1589, 1483, 1456 (w), 1384, 1362 (s), 1324, 1304, 1271, 1234, 1180, 1044 (w), 934, 889, 805 (s), 757 (s), 738, 707, 691, 620, 548, 536, 519, 446. Anal. Calcd. for $C_{62}H_{81}N_4Cu_2BF_4$: C, 67.93; H, 7.45; N, 5.11. Found: C, 67.59; H, 7.35; N, 4.90.

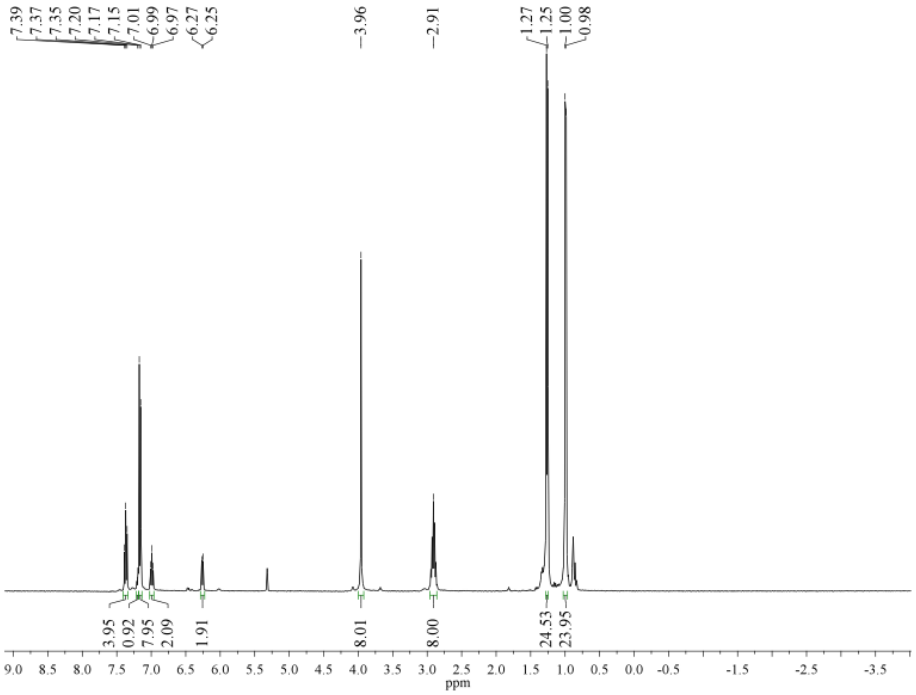

Figure 3.4. ^{1}H NMR spectrum (400 MHz, CD_2Cl_2) of $\{[(SIDipp)Cu]_2(\mu\text{-}CCC_6H_5)\}^+$ BF_4^-. A trace of residual solvent, hexanes (δ 1.29 and 0.89 ppm), is present.

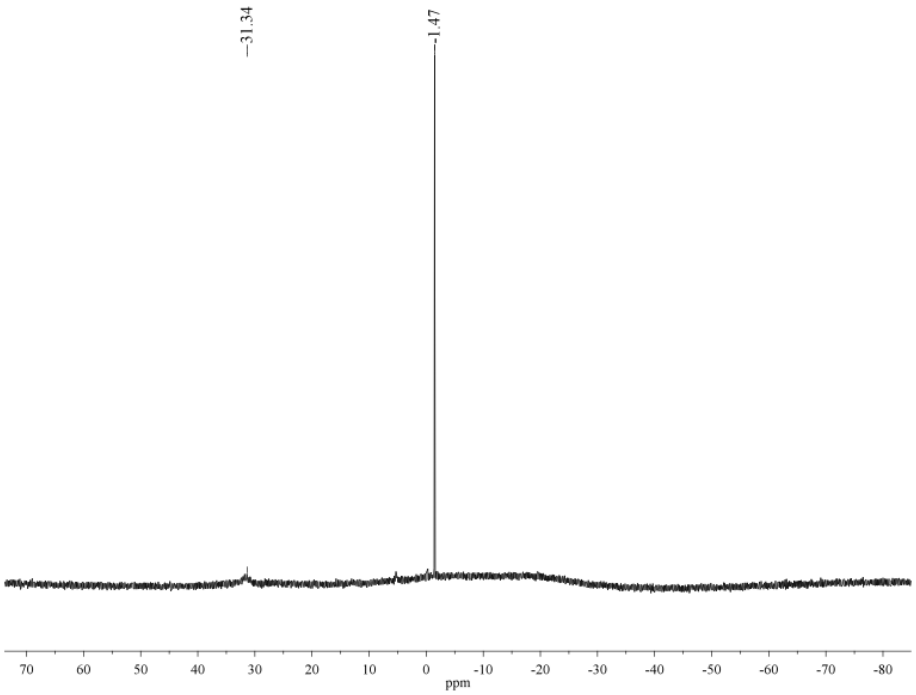

Figure 3.5. ^{11}B NMR spectrum (400 MHz, CD_2Cl_2) of the reaction of $\{[(SIDipp)Cu]_2(\mu\text{-}BO_2C_6H_5)\}^+ BF_4^-$ with phenylacetylene.

Preparation of $\{[(SIDipp)Cu]_2(\mu\text{-}H)\}^+ BF_4^-$

Prepared independently using modified procedure previously described for $\{[(IDipp)Cu]_2(\mu\text{-}H)\}^+ BF_4^-$.[15] ^{1}H NMR (400 MHz, THF-d_8): δ (ppm) 7.37 (t, J = 8 Hz, 4H, *para*-C*H*), 7.19 (d, J = 8 Hz, 8H, *meta*-C*H*), 4.07 (s, 8H, NC*H*), 3.03 (sept, J = 8 Hz, 8H, C*H*(CH_3)$_2$), 1.26 (d, J = 8 Hz, 24H, CH(C*H*$_3$)$_2$), 1.00 (d, J = 8 Hz, 24H, CH(C*H*$_3$)$_2$), –4.40 (s, 1H, Cu*H*Cu).

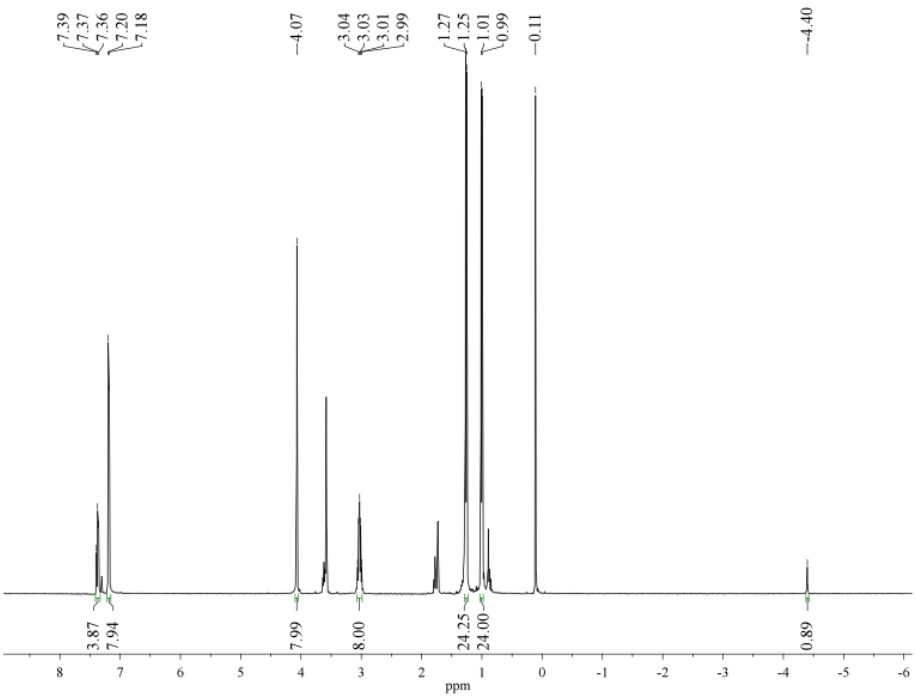

Figure 3.6. ^{1}H NMR spectrum (400 MHz, THF-d_8) of $\{[(SIDipp)Cu]_2(\mu\text{-}H)\}^+ BF_4^-$. The reaction side product, $Ph_3COSiMe_3$ (δ 0.11), is present, along with a trace of residual solvent, hexanes (δ 1.29 and 0.89 ppm) and THF (δ 3.62 and 1.79 ppm).

Reaction of $\{[(SIDipp)Cu]_2(\mu\text{-}BO_2C_6H_4)\}^+ BF_4^-$ with CH_3OH

A solution of $\{[(SIDipp)Cu]_2(\mu\text{-}BO_2C_6H_4)\}^+ BF_4^-$, (0.016 g, 0.014 mmol) in THF-d_8 (0.7 mL) cooled to –35 °C was transferred to an NMR tube equipped with a J. Young valve. The tube was then opened, and methanol (0.6 μL, 0.015 mmol) was added. The resulting mixture was agitated and the reaction was immediately checked by ^{1}H NMR spectroscopy. The ^{1}H NMR spectrum displayed authentic $\{[(SIDipp)Cu]_2(\mu\text{-}H)\}^+ BF_4^-$ and (cat)$BOCH_3$. Qualitatively similar results to those obtained in THF are observed in CD_2Cl_2 solution.

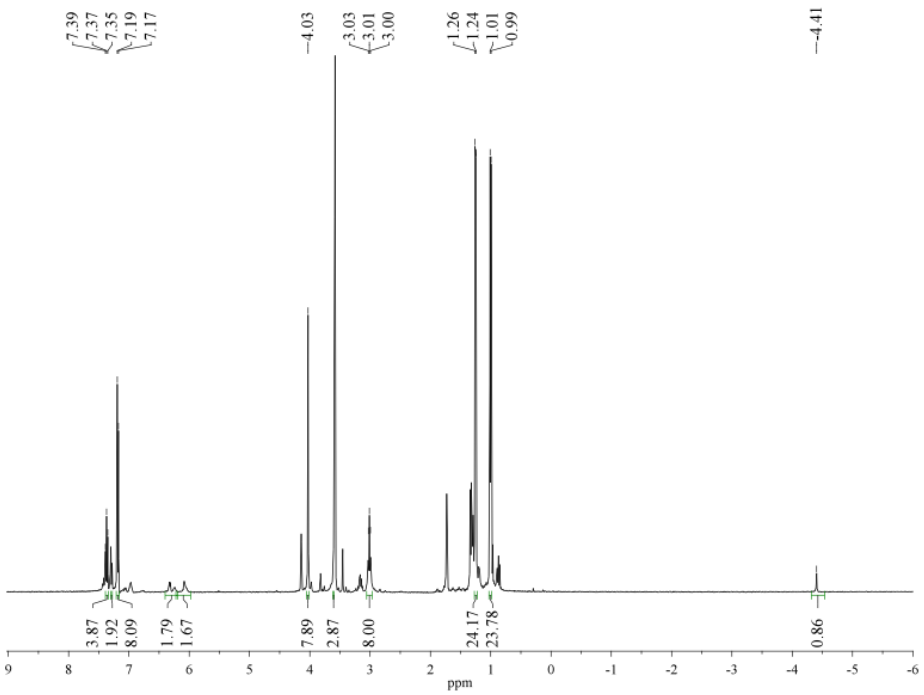

Figure 3.7. ^{1}H NMR spectrum (400 MHz, THF-d_8) of the reaction of $\{[(SIDipp)Cu]_2(\mu\text{-}BO_2C_6H_4)\}^+$ BF_4^- with CH_3OH. In addition to $\{[(SIDipp)Cu]_2(\mu\text{-}H)\}^+$ BF_4^- and (cat)$BOCH_3$, some $\{[(SIDipp)Cu]_2(\mu\text{-}OCH_3)\}^+$ BF_4^- is also evident due to the slight excess of CH_3OH. A trace of residual co-solvent, hexanes (δ 1.29 and 0.89 ppm), is present.

3.5. References

1. For reviews see: a) K. Burgess, M.J. Ohlmeyer, Chem. Rev. 91 (1991) 1179; b) C.M. Crudden, D. Edwards, Eur. J. Org. Chem. (2003) 4695; c) I. Beletskaya, A. Pelter, Tetrahedron 53 (1997) 4957.

2. For reviews see: a) T.B. Marder, N.C. Norman, Top. Catal. 5 (1998) 63; b) T. Ishiyama, N. Miyaura, Chem. Rec. 3 (2004) 271; c) I. Beletskaya, C. Moberg, Chem. Rev. 106 (2006) 2320; d) V. Lillo, A. Bonet, E. Fernández, Dalton Trans. (2009) 2899.

3. a) J.-Y. Cho, M.K. Tse, D. Holmes, R.E. Maleczka, Jr., M.R. Smith, III, Science 295 (2002) 305; b) R.E. Maleczka, Jr., F. Shi, D. Holmes, M.R. Smith, III, J. Am. Chem. Soc. 125 (2003) 7792; c) H. Chen, S. Schlecht, T.C. Semple, J.F. Hartwig, Science 287 (2000) 1995; d) C.S. Wei, C.A. Jiménez-Hoyos, M.F. Videa, J.F. Hartwig, M.B. Hall, J. Am. Chem. Soc. 132 (2010) 3078; e) T.J. Mazzacano, N.P. Mankad, J. Am. Chem. Soc. 135 (2013) 17258.

4. a) J.M. Murphy, J.D. Lawrence, K. Kawamura, C. Incarvito, J.F. Hartwig, J. Am. Chem. Soc. 128 (2006) 13684; b) S.A. Westcott, T.B. Marder, R.T. Baker, R.L. Harlow, J.C. Calabrese, K.C. Lam, Z. Lin, Polyhedron 23 (2004) 2665; c) A. Korostylev, I. Gridnev, J.M. Brown, J. Organomet. Chem. 680 (2003) 329; d) H. Braunschweig, K. Radacki, D. Rais, G.R. Whittell, Angew. Chem. Int. Ed. 44 (2005) 1192; e) D. Curtis, M.J.G. Lesley, N.C. Norman, A.G. Orpen, J. Starbuck, J. Chem. Soc., Dalton Trans. (1999) 1687; f) R.S. Anju, D.K. Roy, K. Geetharani, B. Mondal, B. Varghese, S. Ghosh, Dalton Trans. 42 (2013) 12828.

5. D.S. Laitar, P. Müller, J.P. Sadighi, J. Am. Chem. Soc. 127 (2005) 17196.

6. a) D.S. Laitar, E.Y. Tsui, J.P. Sadighi, J. Am. Chem. Soc. 128 (2006) 11036; b) L. Zhang, J. Cheng, B. Carry, Z. Hou, J. Am. Chem. Soc. 134 (2012) 14314; c) Y. Sasaki, C. Zhong, M. Sawamura, H. Ito, J. Am. Chem. Soc. 132 (2010) 1226; d) H. Ito, Y. Sasaki, M. Sawamura, J. Am. Chem. Soc. 130 (2008) 15774; e) M.A. Beenen, C. An, J.A. Ellman, J. Am. Chem. Soc. 130 (2008) 6910; f) K. Semba T. Fujihara, J. Terao, Y. Tsuji, Angew. Chem. Ed. 52 (2013) 12400; g) Y. Lee, A.H. Hoveyda, J. Am. Chem. Soc. 131 (2009) 3160; h) D.S. Laitar, E.Y. Tsui, J.P. Sadighi, Organometallics 25 (2006) 2405.

7. a) C. Kleeberg, L. Dang, Z. Lin, T.B. Marder, Angew. Chem. Int. Ed. 48 (2009) 5350; b) C.-T. Yang, Z-Q. Zhang, H. Tajuddin, C.-C. Wu, J. Liang, J.-H Liu, Y. Fu, M. Czyzewska, P.G. Steel, T.B. Marder, L. Liu, Angew. Chem. Int. Ed. 51 (2012) 528; c) H. Iwamoto, K. Kubota, E. Yamamoto, H. Ito, Chem. Commun. 51 (2015) 9655.

8. a) H. Zhao, L. Dang, T.B. Marder, Z. Lin, J. Am. Chem. Soc. 130 (2008) 5586; b) H. Zhao, Z. Lin, T.B. Marder, J. Am. Chem. Soc. 128 (2006) 15637; c) L. Dang, H. Zhao, Z. Lin, T.B. Marder, Organometallics 26 (2007) 2824; d) H. Jang, A.R. Zhugralin, Y. Lee, A.H. Hoveyda, J. Am. Chem. Soc. 133 (2011) 7859; e) J.H. Moon, H.-Y. Jung, Y.J. Lee, S.W. Lee, J. Yun, J.Y. Lee, Organometallics 34 (2015) 2151.

9. a)T. Kajiwara, T. Terabayashi, M. Yamashita, K. Nozaki, Angew. Chem. Int. Ed. 47 (2008) 6606; b) Y. Segawa, M. Yamashita, K. Nozaki, Angew. Chem. Int. 46 (2007) 6710; c) C. Borner, C. Kleeberg, Eur. J. Inorg. Chem. (2014) 2486; d) Y. Okuno, M. Yamashita, K. Nozaki, Angew. Chem. Int. Ed. 50 (2011) 920; e) K. Semba, M. Shinomiya, T. Fujihara, J. Terao, Y. Tsuji, Chem. Eur. J. 19 (2013) 7125.

10. a) G.R. Clark, G.J. Irvine, W.R. Roper, L.J. Wright, Organometallics 16 (1997) 5499; b) S. Onozawa, M. Tanaka, Organometallics 20 (2001) 2956; c) C.

Gunanathan, M. Hölscher, F. Pan, W. Leitner, J. Am. Chem. Soc. 134 (2012) 14349; d) T. Sagawa, Y. Asano, F. Ozawa, Organometallics 21 (2002) 5879.

11. a) V.W.-W. Yam, W.-K. Lee, K.K. Cheung, H.-K. Lee, W.-P. Leung, J. Chem. Soc., Dalton Trans. (1996) 2889; b) J. Diez, M.P. Gamasa, J. Gimeno, A. Aguirre, S. García-Granda, J. Holubova, L.R. Favello, Organometallics 18 (1999) 662; c) A.J. Edwards, M.A. Paver, P.R. Raithby, M.-A. Rennie, C.A. Russell, D.S. Wright, Organometallics 13 (1994) 4967; d) P. Olbrich, U. Behrens, E. Weiss, J. Organomet. Chem. 472 (1994) 365.

12. Selected examples: a) W.-H. Chan, Z.-Z. Zhang, T.C.W. Mak, C.-M. Che, J. Organomet. Chem. 556 (1998) 169; b) F. Olbrich, U. Behrens, E. Weiss, J. Organomet. Chem. 472 (1994) 365; c) V.W.-W. Yam, S.W.-K. Choi, C.-L. Chan, K.-K. Cheung, Chem. Commun. (1996) 2067.

13. A. Bondi, J. Phys. Chem. 68 (1964) 441.

14. A.M. Suess, M.R. Uehling, W. Kaminsky, G. Lalic, J. Am. Chem. Soc. 137 (2015) 7747.

15. C.M. Wyss, B.K. Tate, J. Bacsa, T.G. Gray, J.P. Sadighi, Angew. Chem. Int. Ed. 52 (2013) 12920.

16. For a review see: L. Dang, Z. Lin, T.B. Marder, Chem. Commun. (2009) 3987.

17. J. Zhu, Z. Lin, T.B. Marder, Inorg. Chem. 44 (2005) 9384.

18. L. Dang, H. Zhao, Z. Lin, T.B. Marder, Organometallics 27 (2008) 1178.

19. K.M. Kuhn, R.H. Grubbs, Org. Lett. 10 (2008) 2075.

20. D.S. Laitar, *Synthetic and Catalytic Studies of Group 11 N-Heterocyclic Carbene Complexes*. Dissertation, Massachusetts Institute of Technology. Cambridge Massachusetts, 2006.

CHAPTER 4

Dinuclear μ-Fluoro Cations of Copper, Silver and Gold

Part of this thesis chapter has been adapted with permission from an article co-written by the author:

C.M. Wyss, B.K. Tate, J. Bacsa, M. Wieliczko, J.P. Sadighi, "Dinuclear μ-Fluro Cations of Copper, Silver and Gold." *Polyhedron* **2014**, *84*, 87-95.

4.1. Introduction

Bonds between fluoride and low-valent late transition metals, although not intrinsically weak,[1-3] are often highly labile. The hard/soft acid-base concept[4] suggests that the hard fluoride ion, with its tendency toward ionic bonding, is mismatched with low-valent late transition metal cations, for which more covalent bonds are usually favored. Partly as a result, complexes of copper, silver and gold with the fluoride ion are rare compared to those with the heavier halides.

The accessibility of group 11 metal fluoride complexes depends on the charge at the metal center: Copper(II) fluoride itself is a stable salt, whereas copper(I) fluoride disproportionates to copper(II) fluoride and copper metal.[5] Likewise, coordination complexes based on copper(II) fluoride are known,[6-8] but structurally characterized copper(I) fluoride complexes were long limited to $(Ph_3P)_3CuF$[9-11] and the remarkable μ_3-fluoride $[Cu_3(\mu_3\text{-}F)(\mu\text{-dtbpm})_3]^{2+}$ $\{[PF_6]^-\}_2$ [dtbpm = bis(di-*tert*-butylphosphino)methane].[12] Silver(I) forms a stable binary fluoride, and many silver(I) fluoride complexes have been characterized.[13-18] Gold(III)[19] and gold(V)[20] form reactive binary fluorides, but molecular gold fluorides were unknown[21] until the

availability of N-heterocyclic carbene (NHC) ligands[22,23] enabled the isolation of a two-coordinate gold(I) fluoride.[24] The NHC ligand framework also proved amenable to the synthesis of linear fluorides of copper(I) and silver(I).[25]

Group 11 metal fluoride complexes exhibit distinctive reactivity. Addition of an (NHC)gold(I) fluoride across the triple bond of internal alkynes forms a *trans*-β-fluorovinylgold species, enabling the catalytic hydrofluorination of alkynes to vinyl fluorides.[26] Several (NHC)copper(I) fluorides,[27-29] and closely related bifluoride complexes [(NHC)Cu(FHF)],[30,31] serve as effective precatalysts for challenging silylation reactions. A recently reported (phosphine)copper(I) fluoride dimer is a key intermediate in copper-catalyzed Suzuki-Miyaura couplings.[32] Trivalent [(NHC)Au(R)F_2] complexes, formed through oxidative fluorination of suitable (NHC)gold(I) alkyls, readily form fluoride-bridged dications $\{[(NHC)Au(R)(\mu\text{-}F)]_2\}^{2+}$.[33] The gold(III) (methyl)difluoro complex [(IDipp)Au(CH_3)F_2] (IDipp = 1,3-bis(2,6-diisopropylphenyl)imidazol-2-ylidene) undergoes facile transmetalation with arylboronates, followed by reductive C–C bond formation. Unlike its diiodo analogue[34] it does not form a methyl–halogen bond through reductive elimination, but related difluoro complexes with more sterically demanding R groups do form C–F bonds,[35] implicating the dissociation of a labile fluoride. The relevance of dinuclear Au(II) complexes to catalysis inspired the synthesis of a formamidinate-bridged digold(II) difluoride, in which terminal fluorides lie trans to a gold–gold bond.[36]

This thesis chapter describes the synthesis of a series of dinuclear μ-fluoro cations of copper(I), silver(I) and gold(I), supported by the NHC ligand SIDipp (1,3-bis(2,6-diisopropylphenyl)-4,5-dihydroimidazol-2-ylidene).[23] In these complexes, a single

fluoride acts as the sole bridging ligand between two group 11 metal centers. Such an arrangement has been characterized in a bis[(bisphosphino)silver(I)] μ-fluoro cation[37] and in a few copper(II) complexes,[38-40] but not in copper(I) or gold complexes. Close analogues, however, include salts of $\{[(IDipp)Cu]_2(OH)\}^+$[41] and $\{[(IDipp)Au]_2(OH)\}^+$.[42] In addition, a 2-phenanthrolinyl-substuted NHC precursor reacts with copper metal to form a $[Cu_2(\mu\text{-}X)]^+$ core (X = Cl, Br, I), bridged by both the halide and the terdentate ligands.[43] Cations of the form $[(LM)_2(\mu\text{-}F)]^+$ are isolobal with the fluoronium ion $[H_2F]^+$,[44] and their structures show the expected bending at fluoride. The metal–fluoride bonds in these complexes are more labile than in their terminal analogues, and the gold(I) complex is reactive both toward carbon–chlorine bonds and toward activated C=C bonds.

4.2. Results and Discussion

4.2.1. Improved preparation of terminal group 11 metal fluorides

Before synthesizing the desired μ-fluoro complexes, we revisited the synthesis of the neutral precursor complexes (SIDipp)MF (M = Cu, Ag, Au). These complexes were originally prepared by treatment of (SIDipp)M(O*t*Bu) in benzene solution with one-third of an equivalent of triethylamine trihydrofluoride (TREAT-HF or Et_3N•3HF, actually Et_3NH^+ $H_2F_3^-$) (Scheme 4.1a). This route is convenient in many respects, as Et_3N•3HF is a relatively benign HF equivalent, and was previously used in the synthesis of other late transition metal fluorides.[45,46] Although reactions of Et_3N•3HF may be run in glass vessels, the reagent is best stored in plastic containers. We found that the use of Et_3N•3HF that had been exposed to humid air, or stored too long under a rubber septum,

gave variable results. Using ^{1}H NMR spectroscopy, we observed the presence of $[(SIDipp)Au(NEt_3)]^+$[26] as a byproduct in some cases.

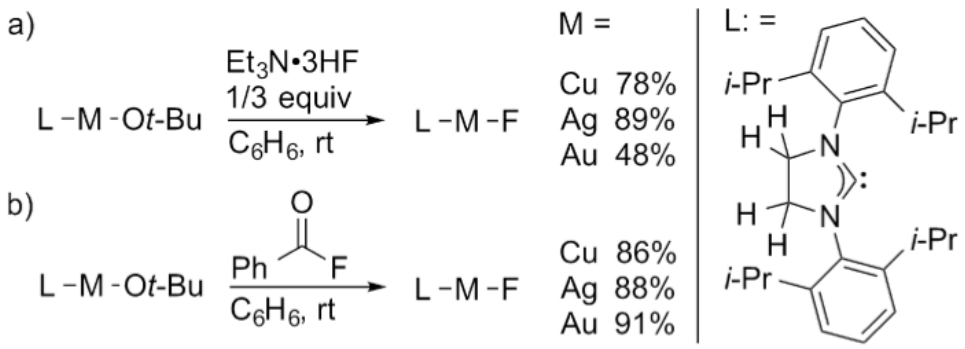

Scheme 4.1. Original (a; Refs.[24.25]) and improved (b) synthesis of group 11 metal fluorides.

Alternatively, the aprotic benzoyl fluoride reacts smoothly with all three complexes (SIDipp)M(O*t*Bu) to form the terminal fluorides (Scheme 4.1b) plus *tert*-butyl benzoate. As observed in the original method, the fluorides are only sparingly soluble in benzene or toluene, and can be isolated readily by simple filtration. The advantage of this method is that benzoyl fluoride may be stored in resealable glass vessels, and protected from moisture in storage and handling. The *tert*-butyl benzoate byproduct, unlike the triethylamine formed from Et_3N•3HF, shows no tendency to interact adversely with the desired products. Yields and purities of the resulting fluoride complexes are consistently high.

4.2.2. Synthesis of dinuclear μ-fluoro cations

In previous work, it was found that the treatment of terminal copper(I) and silver(I) alkoxides with one-half equivalent of triphenylcarbenium tetrafluoroborate resulted in clean alkoxide abstraction to form dinuclear μ-(alkoxo) cations.[47,48] This

method works well for fluoride abstraction from the terminal group 11 metal fluoride complexes (Equation 1). The byproduct fluorotriphenylmethane remains in solution as the product complex is crystallized or precipitated, and is easily removed by washing. Salts of the fluoride-bridged cations are obtained as colorless solids after drying, and may be recrystallized from mixtures of tetrahydrofuran and aliphatic or aromatic hydrocarbons. All three cations are highly sensitive to adventitious moisture, readily forming the hydroxy-bridged dinuclear cations as judged by ^{1}H NMR spectroscopy. Of the three, the salt of $\{(SIDipp)Au]_2(\mu\text{-}F)\}^+$ required the most careful drying of glassware and solvents to avoid hydrolysis, consistent with its marked hard/soft acid-base mismatch.[4]

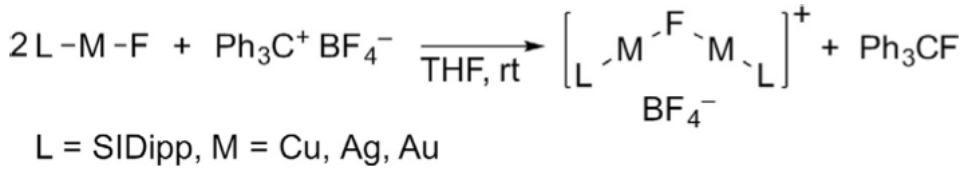

(1)

4.2.3. ^{19}F NMR spectroscopy of terminal fluorides and μ-fluoro cations

In the ^{19}F NMR spectra, the chemical shifts measured for the bridging fluorides are far more negative than those of the terminal fluorides (Table 4.1). Whereas the terminal fluoride resonances appear between δ –238.5 and –247.2 ppm, the resonances for the fluoride-bridged complexes in dichloromethane solution are observed between δ –308.5 and –318.5 ppm. Consistent with the hydrolytic instability of these complexes, observation of the resonance for the bridging fluoride requires rigorous exclusion of

protic impurities; even for a sample that appears pure by ^{1}H NMR spectroscopy, the resonance for the bridging fluoride is easily broadened into the baseline of the ^{19}F NMR spectrum.

Table 4.1. ^{19}F NMR chemical shifts of terminal and bridging fluorides. For all complexes, L = SIDipp; for cations, anion = BF_4^-. Chemical shifts reported in ppm relative to $CFCl_3$.

Metal	LMF (CD_2Cl_2)	$[(LM)_2(\mu\text{-}F)]^+$ (CD_2Cl_2)	$[(LM)_2(\mu\text{-}F)]^+$ (THF-d_8)
Cu	–238.5	–311.1	–291.1
Ag	–243.1	–308.5	–302.9
Au	–247.2	–318.5	–272.6

Because naturally occurring copper (^{63}Cu and ^{65}Cu) and gold (^{197}Au) nuclei are quadrupolar, coupling between ^{19}F and these metal centers is not observed. Naturally occurring silver, however, comprises two spin ½ nuclei: ^{107}Ag (52%) and ^{109}Ag (48%).[49] In the terminal fluoride (SIDipp)AgF, the fluorine resonance is observed as an apparent doublet with a large coupling constant ($J_{Ag–F}$ = 163 Hz), although the coupling of ^{19}F to ^{107}Ag versus ^{109}Ag could not be resolved. In the fluoride-bridged dinuclear cation, a triplet resonance might be expected to arise from coupling to two silver centers, with undifferentiated couplings to ^{107}Ag and ^{109}Ag, but only a single broad resonance was observed in dichloromethane solution.

The chemical shifts of the bridging fluoride resonances are highly solvent-dependent, with less negative shifts for samples in tetrahydrofuran solution rather than in dichloromethane solution. The difference is substantial for $\{[(SIDipp)Ag]_2(\mu\text{-}F)\}^+$, at 5.6 ppm, and dramatic for the fluoride-bridged dicopper (20 ppm) and digold (~46 ppm) complexes. We propose that dissolution of the fluoride-bridged cations in tetrahydrofuran

results in partial displacement to form the terminal fluoride plus a solvated $[(SIDipp)M]^+$ cation (Equation 2), and that interconversion of these species is rapid on the NMR timescale. Consistent with this premise, a single set of (SIDipp) resonances is observed in the ^1H NMR spectrum of each fluoride-bridged dinuclear complex in THF-d_8 solution. The ^{19}F NMR resonance for each complex in THF-d_8 solution would thus represent a weighted average of the bridging and terminal fluoride resonances in that system. Each complex may be recovered solvent-free from tetrahydrofuran solution.

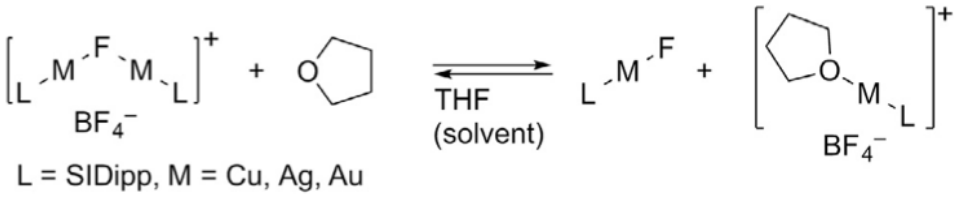

(2)

4.2.4. Structural aspects

All three $\{[(SIDipp)M]_2(\mu\text{-}F)\}^+ BF_4^-$ complexes crystallize with linear or nearly linear geometry about each metal center and a bent arrangement about the fluoride; the BF_4^- anions remain well outside the metal coordination spheres. In the case of the copper complex, two crystallographically distinct molecules are present in the asymmetric unit. The structure of $\{[(SIDipp)Au]_2(\mu\text{-}F)\}^+ BF_4^-$ is shown in Figure 4.1; key interatomic distances and M–F–M angles for the three congeners are summarized in Table 4.2. Whereas certain phosphine-supported $[LAu–X–AuL]^+$ cations aggregate to form $[(LAu)_4(\mu_2\text{-}X)_2]^{2+}$ dimers,[50] we have observed no tendency for the $\{[(SIDipp)M]_2(\mu\text{-}F)\}^+ BF_4^-$ complexes to form higher-order aggregates. The contrast between these

complexes may reflect the large steric demand of the SIDipp ligand and its strong donor ability.[51,52]

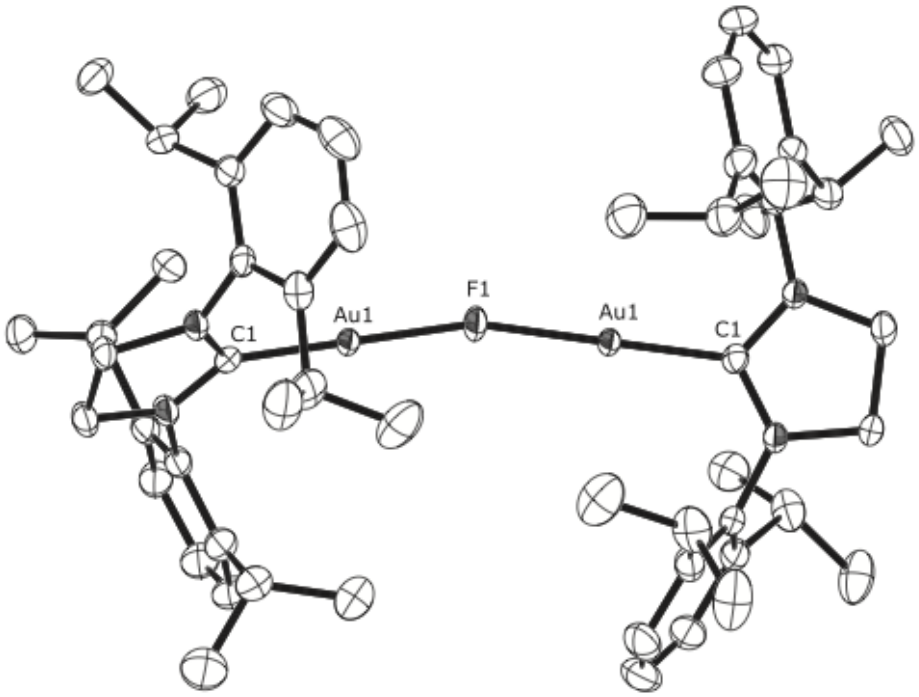

Figure 4.1. Solid-state structure of $\{[(SIDipp)Au]_2(\mu\text{-}F)\}^+ BF_4^-$. Hydrogen atoms and BF_4^- anion omitted for clarity.

Table 4.2. Selected bond lengths (Å) and angles (°) in $[(LM)_2(\mu\text{-}F)]^+ BF_4^-$ complexes. Note: Two entries for Cu describe crystallographically distinct molecules of $[(LCu)_2(\mu\text{-}F)]^+ BF_4^-$.

M	M–C	M–F	M···M	C–M–F	M–F–M
Cu	1.868(3)	1.843(2)	3.5130(7)	176.5(1)	142.99(17)
	1.876(3)	1.862(2)		172.5(1)	
Cu	1.850(3)	1.836(2)	3.4522(7)	174.5(1)	140.96(16)
	1.863(3)	1.827(3)		178.4(1)	
Ag	2.053(3)	2.0672(7)	4.0589(4)	176.60(11)	158.09(17)
		2.0671(7)			
Au	1.944(3)	2.060(1)	3.9495(5)	179.64(11)	146.93(10)

Despite the difference in charge, the metal–fluorine and metal–carbon distances in the $\{[(SIDipp)M]_2(\mu\text{-}F)\}^+$ complexes are quite similar to those determined for the corresponding neutral (SIDipp)MF complexes.[24,25] In the case of gold, the Au–F distance is slightly longer in the μ-fluoro cation than in the terminal fluoride: 2.060(1) Å versus 2.0281(17) Å. Despite the difference in gold oxidation state, these Au–F distances are quite similar to those of 2.034(3) Å and 2.124(3) Å in the $\{[(SIDipp)Au^{III}(Me)(\mu\text{-}F)]_2\}^{2+}$ cation.[33] The difference between Ag–F distances in the bridging and terminal binding modes is insignificant: 2.0672(7) and 2.0671(7) Å for the μ-fluoro cation versus 2.0682(13) Å for $(SIDipp)AgF\bullet 2CH_2Cl_2$. The four Cu–F distances in $\{[(SIDipp)Cu]_2(\mu\text{-}F)\}^+$, ranging from 1.827(3) Å to 1.862(2) Å, bracket the distance of 1.8426(10) Å measured for (SIDipp)CuF.

Crystals of the $\{[(SIDipp)Ag]_2(\mu\text{-}F)\}^+$ and $\{[(SIDipp)Au]_2(\mu\text{-}F)\}^+$ salts are isomorphous, with a slightly larger unit cell volume for the silver complex (Table 4.3). The difference in metal–fluorine distances is very small, but the metal–carbon distance is notably shorter in the gold complex: 1.944(3) Å, compared to 2.053(3) Å in the silver complex. Likewise, an earlier comparison of crystal structures for $[(Mes_3P)Ag(PMes_3)]^+$ and $[(Mes_3P)Au(PMes_3)]^+$ (Mes = 2,4,6-trimethylphenyl) revealed that the metal–phosphorus distances were significantly shorter in the gold complex, supporting the thought-provoking contention that gold is smaller in radius than its lighter congener.[53]

Although its shorter metal–ligand distances offer the potential for greater steric interaction between its large SIDipp ligands, the $\{[(SIDipp)Cu]_2(\mu\text{-}F)\}^+$ complex displays the smallest metal–fluorine–metal angles in the series, 140.96(16)° and 142.9(17)°. The Au–F–Au angle in $\{[(SIDipp)Au]_2(\mu\text{-}F)\}^+$ is similar at 146.93(10)°. For comparison,

Nolan and coworkers have published the structures of $\{[(IDipp)Au]_2(\mu\text{-}OH)\}^+$ complexes (IDipp = 1,3-bis(2,6-diisopropylphenyl)imidazole-2-ylidene, the fully unsaturated analogue of SIDipp), and the Au–O–Au angle is considerably smaller at 127.6(4)° for the SbF_6^- salt.[42]

The angle about fluoride in $\{[(SIDipp)Ag]_2(\mu\text{-}F)\}^+$ is 158.09(17)°, very close to that of 158.6(5)° found in a bisphosphine-supported analogue[37] and distinctly larger than that of its copper and gold congeners. Although we cannot rule out a shallow potential energy surface for bending about the fluorides, which could allow crystal packing effects to predominate, this difference may reflect a larger ionic contribution to the Ag–F interactions than to the Cu–F or Au–F interactions. The filled d-orbitals of silver(I) are more stabilized, and the empty s-orbital higher in energy, than those of copper(I) or gold(I);[54] thus AgF, unlike CuF and AuF, exists as a stable ionic solid under ordinary conditions. In a purely electrostatic bonding interaction, the $L–M^+\ F^-\ {}^+M–L$ arrangement should be linear. In the limit of covalency, a pronounced bending about the fluoride should be observed. For the parent fluoronium ion, calculations based on gas-phase FT-IR measurements give an H–F–H angle of 112.2°,[55] very similar to the 113.9° predicted by ab initio calculations.[56]

For each μ-fluoro cation, the intermetallic distance is far larger than twice the van der Waals radius. In the corresponding μ-hydrido complexes, the intermetallic distances are short enough to suggest an attractive interaction, likely resulting from three-center, two-electron bonding.[57] Because the bridging fluoride can use separate orbitals in bonding to each metal center, no metal–metal interaction need be invoked. Yet certain μ-chlorodigold(I) cations display notably short Au–Au distances, ascribed to the well-

established aurophilic interaction.[58] In $\{[(Ph_3P)Au]_2(\mu\text{-}Cl)\}^+$, for example, the Au–Au distances are 3.0843 Å and 3.0346 Å, with Au–Cl–Au angles of 82.72° and 80.70°.[59] The absence of a close intermetallic approach in a μ-fluoro cation, and the wider Au–X–Au angle, may again reflect a large ionic component to the gold–fluoride bonding.

4.2.5. Reactivity

Despite their overall positive charge, all three $\{[(SIDipp)M]_2(\mu\text{-}F)\}^+$ complexes display considerable basicity at fluoride. Their facile hydrolysis to form the corresponding (μ-OH) complexes has been described. We could not account for the fate of the fluoride using ^{19}F NMR spectroscopy, but the HF liberated according to the reaction stoichiometry may have reacted with the surface of the borosilicate reaction vessels.

To minimize solvent-mediated dissociation of the μ-fluoride complexes, we initially obtained all NMR spectra in CD_2Cl_2 solution, in which the complexes appeared to be inert during the time required to prepare samples and acquire data. Indeed, $\{[(SIDipp)Ag]_2(\mu\text{-}F)\}^+ BF_4^-$ is not observed to react with CD_2Cl_2 over periods up to 24 hours at ambient temperature, although trace decomposition to form the known $[(SIDipp)_2Ag]^+$ was apparent in the resulting ^1H NMR spectrum, and a faint silver mirror was observed. The copper complex $\{[(SIDipp)Cu]_2(\mu\text{-}F)\}^+ BF_4^-$ appears to be stable at least overnight in CD_2Cl_2 solution. In contrast, $\{[(SIDipp)Au]_2(\mu\text{-}F)\}^+ BF_4^-$ is completely consumed on standing in CD_2Cl_2 for 24 hours at ambient temperature. The ^1H NMR spectrum of the resulting product displays a single set of SIDipp resonances, consistent with the clean formation of $\{[(SIDipp)Au]_2(\mu\text{-}Cl)\}^+$; the ^{19}F NMR spectrum shows

characteristic quintet resonances at δ –170.85 ppm for FCD_2Cl, and at –144.10 ppm for CD_2F_2 (Equations 3 and 4). Grushin and coworkers observed this displacement reaction, including the competitive formation of difluoromethane along with fluorochloromethane, while studying the generation of fluoride ion from arylpalladium(II) fluoride complexes.[2]

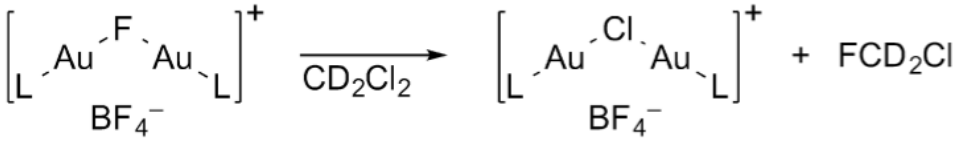

(3)

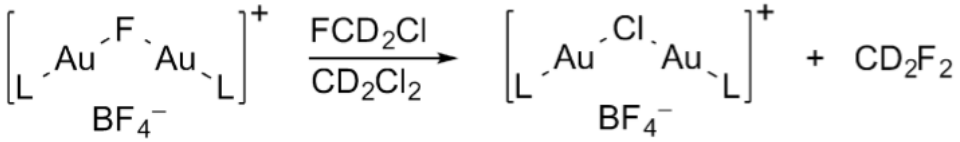

(4)

The addition of gold–heteroatom bonds add across reactive C=C bonds is a key step in a number of catalytic reactions.[60] Because allenes are important substrates for such reactions, we examined the reaction of 3-methyl-1,2-butadiene with $\{[(SIDipp)Au]_2(\mu\text{-}F)\}^+$ BF_4^- in THF-d_8 solution. This reaction proceeds rapidly at ambient temperature, with complete consumption of the starting gold complex within five minutes as judged by ^1H NMR spectroscopy, and the formation of a new complex with a single set of SIDipp resonances, consistent with the equivalence of the (SIDipp)Au fragments on the NMR timescale. The salient feature of the new spectrum was a doublet integrating to six protons at δ 0.31 ppm, with a coupling constant of 20 Hz. Reasoning that this pattern could arise from a $–C(F)(CH_3)_2$ moiety, with an unusually high-field signal resulting from its attachment to a bridging carbanion and its enforced proximity to

the SIDipp aryl groups, we acquired the ^{19}F NMR spectrum, and were delighted to observe a septet with a matching coupling constant at δ –128.40 ppm.

Under similar conditions, the reaction of $\{[(SIDipp)Cu]_2(\mu\text{-}F)\}^+ BF_4^-$ with 3-methyl-1,2-butadiene rapidly gives rise to a small doublet resonance in the ^1H NMR spectrum at δ 0.10 ppm, but after 30 minutes this resonance and the associated SIDipp signals integrate to less than 10% of the total of SIDipp complexes present, and no further conversion was observed after several hours. These observations may reflect an unfavorable equilibrium between the starting fluoro complex and the addition product, as has been observed between (SIDipp)AuF and 1-phenylpropyne.[26] No reaction was observed between $\{[(SIDipp)Ag]_2(\mu\text{-}F)\}^+ BF_4^-$ and the allene.

The μ-fluorodigold addition product was assigned as a diaurated allylic fluoride. Geminally diaurated vinyl species have been identified as intermediates in gold-catalyzed C–C bond-forming processes.[61] Crystals of this product proved highly disordered, but the solid-state structure serves to confirm the regiochemistry of the fluoride addition (Figure 4.2). Interestingly, this structure indicates an asymmetric binding of the fluoroallyl moiety, with the vinyl anion acting as a σ-donor to one gold center, and the C=C π-bond donating to the other. The symmetric binding suggested by ^1H NMR spectroscopy is consistent with rapid equilibration between equivalent structures in solution at ambient temperature, possibly via a symmetric bridging mode (Scheme 4.2). A similar binding mode has been examined in alkynyl-bridged digold cations,[62] but vinyl-bridged dicopper complexes exhibit the σ-bridging mode instead.[48,63] The formation of the diaurated allylic fluoride represents a rare addition of metal fluoride across a C–C multiple bond.

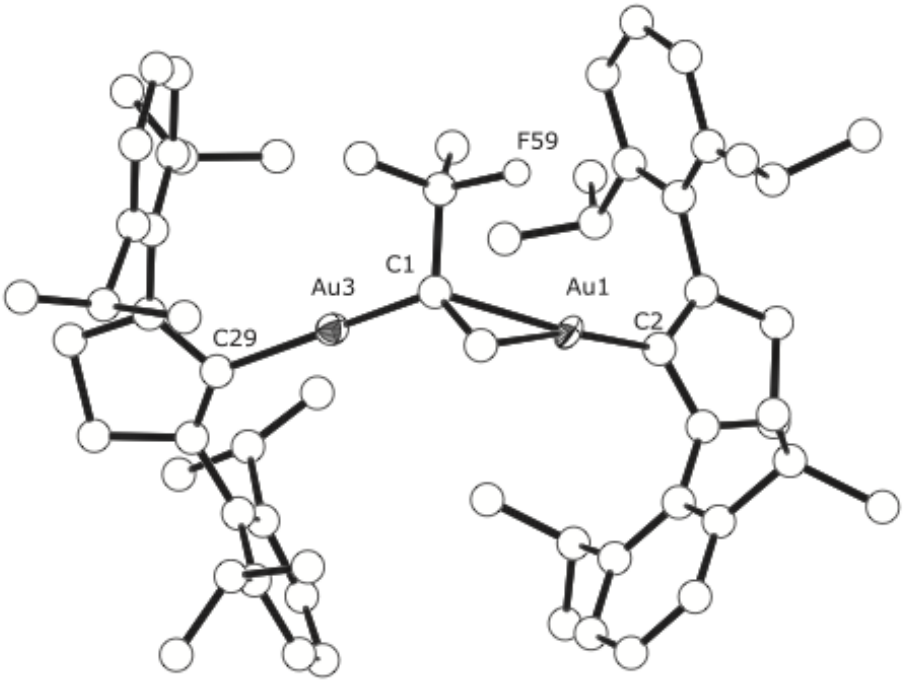

Figure 4.2. Solid-state structure of $\{[(SIDipp)Au]_2(\mu\text{-}C(=CH_2)CF(CH_3)_2)\}^+$ BF_4^-. Hydrogen atoms, BF_4^- anion and co-crystallized solvent are omitted for clarity.

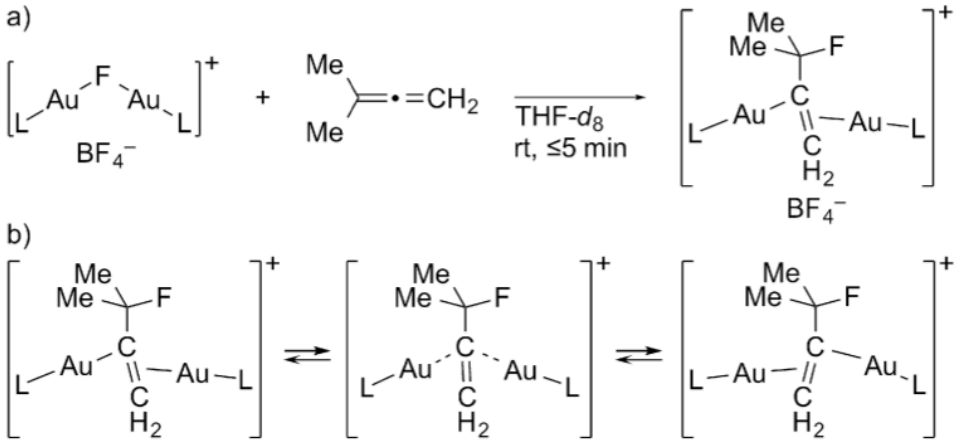

Scheme 4.2. (a) Addition of $[(LAu)_2(\mu\text{-}F)]^+$ BF_4^- to an allene C=C bond (L = SIDipp); (b) proposed equilibration between equivalent asymmetric binding modes.

4.3. Conclusion

The N-heterocyclic carbene ligand supports an isoleptic series of dinuclear μ-fluoro cations, formally isolobal to $[H_2F]^+$, with the group 11 metals. The μ-fluoro

cations are obtained through the partial abstraction of fluoride from the corresponding terminal fluoride complexes, for which an improved preparation has been devised using a Lewis acidic rather than a protic fluoride source. Conversion of a metal-bound fluoride from a terminal to a bridging ligand results in a pronounced shift to high field for the ^{19}F NMR resonance. The solid-state structures exhibit bent arrangements about the bridging fluorides, with a distinctly wider angle in the silver complex than in the copper or gold complexes; no metallophilic interactions are apparent. The gold complex is the most reactive in the series, activating the C–Cl bonds of CD_2Cl_2 and adding rapidly across an allene C=C bond to form an allylic C–F bond and a vinyl anion bound asymmetrically to the two gold(I) centers.

4.4. Experimental

4.4.1. General considerations

Unless otherwise indicated, manipulations were performed in an MBraun glovebox under an inert atmosphere of nitrogen, or in resealable glassware on a Schlenk line under an atmosphere of argon. Glassware and magnetic stir bars were dried in a ventilated oven at 160 °C and were allowed to cool under vacuum. Compounds of silver were stored in the dark as a precaution against photodegradation, and glassware was covered with aluminum foil during manipulations to minimize exposure to light.

^{1}H, ^{13}C, ^{19}F, NMR spectra were obtained using a Bruker DSX 400 MHz spectrometer, a Varian Vx 400 MHz spectrometer, and a Varian Mercury 300 spectrometer (300.323 MHz for ^{1}H). ^{1}H and ^{13}C NMR chemical shifts are referenced with respect to solvent signals and are reported relative to tetramethylsilane. ^{19}F NMR chemical shifts were referenced to external neat hexafluorobenzene (Alfa-Aesar, δ –

164.90 ppm) and are reported with respect to fluorotrichloromethane. Samples for infrared spectroscopy were prepared as pellets in potassium bromide, using a pellet die which was dried in a ventilated oven at 160 °C and cooled under vacuum prior to use. The pellets were prepared in the glovebox under an atmosphere of dry nitrogen, and were exposed to air as briefly as possible prior to data collection. Spectra were recorded using a Perkin Elmer Spectrum 1000 or a Bruker Alpha-P infrared spectrometer. Elemental analyses were performed by Atlantic Microlab, Inc. in Norcross, GA.

4.4.2. Materials and methods

Hexanes (EMD Millipore Omnisolv), tetrahydrofuran (THF, EMD Millipore Omnisolv), and toluene (EMD Millipore Omnisolv) were sparged with ultra high purity argon (NexAir) for 30 minutes prior to first use, and dried using an MBraun solvent purification system. These solvents were further dried over sodium benzophenone ketyl, transferred under vacuum to an oven-dried sealable flask, and degassed by successive freeze-pump-thaw cycles. Anhydrous benzene (EMD Millipore Drisolv) was stored over 3Å molecular sieves (Alfa-Aesar) in a glovebox.

Dichloromethane-d_2 (Cambridge Isotope Laboratories) was dried by stirring overnight over calcium hydride. It was then vacuum-transferred to an oven-dried resealable Schlenk flask, and degassed by successive freeze-pump-thaw cycles. Tetrahydrofuran-d_8 (Cambridge Isotope Laboratories) was dried over sodium benzophenone ketyl, transferred under vacuum to an oven-dried resealable flask, and degassed by successive freeze-pump- thaw cycles.

Sodium tert-butoxide (TCI America), copper(I) chloride (Alfa-Aesar), triphenylcarbenium tetrafluoroborate (Alfa-Aesar), 2,6-diisopropylaniline (Sigma-

Aldrich), acetic acid (Alfa-Aesar), glyoxal 40% w/w aqueous solution (Alfa-Aesar), methanol (BDH), acetone (BDH), dichloromethane (BDH) hydrochloric acid (EMD), sodium borohydride (Alfa-Aesar), benzoyl fluoride (Alfa-Aesar), triethyl orthoformate (Alfa-Aesar), formic acid (Alfa-Aesar), potassium carbonate (Alfa-Aesar), 3-methyl-1,2-butadiene (Sigma-Aldrich), silver(I) oxide (Sigma-Aldrich), dimethyl sulfide (Alfa-Aesar), tetrachloroauric acid (Strem), sodium metal (Alfa-Aesar), benzophenone (Alfa-Aesar), calcium hydride (Alfa-Aesar), potassium bromide (Sigma-Aldrich), nitrogen (NexAir), and argon (both industrial and ultra high purity grades, NexAir) were used as received. SIDipp·HCl,[23] (SIDipp)CuCl,[25] (SIDipp)Cu(O*t*Bu),[25] (SIDipp)AgCl,[24] (SIDipp)Ag(O*t*Bu),[47] (SIDipp)AuCl,[64] and (SIDipp)Au(O*t*Bu),[24] were prepared as described previously, and characterized by ^{1}H NMR spectroscopy.

Preparation of (SIDipp)CuF

Benzoyl fluoride (0.089 mL, 0.102 g, 0.818 mmol) was added to a solution of (SIDipp)Cu(O*t*Bu)[25] (0.287 g, 0.544 mmol) in toluene (4 mL) with stirring. After 3 hours, a white precipitate had formed. The precipitate was collected on a fritted glass filter and washed with two portions of toluene (6 mL each) and two portions of hexanes (5 mL each). Residual solvents were removed under vacuum at 40 °C over 18 hours, affording the product as a white powder (0.221 g, 0.467 mmol, 86%). ^{1}H NMR (400 MHz, CD_2Cl_2): δ (ppm) 7.45 (t, *J* = 7.8 Hz, 2 H, *para*-C*H*), 7.30 (d, *J* = 7.8 Hz, 4 H, *meta*-C*H*), 4.01 (s, 4 H, NCH_2), 3.07 (sept, *J* = 6.9 Hz, 4 H, C*H*$(CH_3)_2$), 1.36 (d, *J* = 6.8 Hz, 12 H, CH(CH_3)$_2$), 1.35 (d, *J* = 6.8 Hz, 12 H, CH(CH_3)$_2$). ^{13}C{^{1}H} NMR (100 MHz, CD_2Cl_2): δ (ppm) 203.7 (br. N*C*Cu), 147.2 (*ortho*-*C*), 135.1 (*ipso*-*C*), 130.0 (*para*-*C*), 124.9 (*meta*-*C*), 54.1 (NCH_2), 29.2 (*C*H$(CH_3)_2$), 25.5 (CH(*C*H_3)$_2$), 24.0 (CH(*C*H_3)$_2$). ^{19}F

NMR (375 MHz, CD_2Cl_2): δ (ppm) –238.5. IR: ν (cm^{-1}) 3075 (w), 2962 (s), 2924, 2867, 1591 (w), 1482 (s), 1458 (s), 1421, 1384, 1361, 1327, 1300, 1269 (s), 1180 (w), 1164 (w), 1099 (w), 1061, 1017 (w), 993 (w), 936, 925, 807 (s), 766, 708 (w), 619 (w), 560, 543, 504 (w), 477 (w), 449, 425 (w), 398 (w). Anal. Calcd. for $C_{27}H_{38}N_2CuF$: C, 68.54; H, 8.10; N, 5.92; F, 4.02. Found: C, 68.21; H, 7.98; N, 5.79; F, 3.96.

Preparation of $\{[(SIDipp)Cu]_2(\mu\text{-}F)\}^+ BF_4^-$

Triphenylcarbenium tetrafluoroborate (0.025 g, 0.076 mmol) was added to a solution of (SIDipp)CuF (0.072 g, 0.152 mmol) in THF (3 mL) with stirring. After 1 hour, hexanes (15 mL) were added to the reaction mixture, resulting in the formation of a white precipitate. The mother liquor was decanted, and the residual solvents were removed under vacuum at 35 °C over 18 hours, affording the product as a white powder (0.059 g, 0.058 mmol, 77%). ^{1}H NMR (400 MHz, CD_2Cl_2): δ (ppm) 7.42 (t, J = 7.8 Hz, 4 H, *para*-C*H*), 7.20 (d, J = 7.8 Hz, 8 H, *meta*-C*H*), 3.99 (s, 8 H, NCH_2), 2.90 (sept, J = 6.9 Hz, 8 H, C*H*(CH_3)$_2$), 1.30 (d, J = 6.8 Hz, 24 H, CH(CH_3)$_2$), 1.06 (d, J = 6.8 Hz, 24 H, CH(CH_3)$_2$). ^{13}C{^{1}H} NMR (100 MHz, CD_2Cl_2): δ (ppm) 200.7 (br. N*C*Cu), 147.1 (*ortho*-*C*), 134.6 (*ipso*-*C*), 130.3 (*para*-*C*), 125.0 (*meta*-*C*), 54.5 (N*C*H_2), 29.1 (*C*H(CH_3)$_2$), 25.6 (CH(*C*H_3)$_2$), 24.0 (CH(*C*H_3)$_2$). ^{19}F NMR (375 MHz, CD_2Cl_2): δ (ppm) −153.26 (s, $^{10}BF_4^-$), −153.31 (s, $^{11}BF_4^-$), –311.11 (br. s, Cu*F*Cu). IR: ν (cm^{-1}) 3074 (w), 2963 (s), 2924, 2867, 1490 (s), 1459 (s), 1384, 1363, 1329, 1273 (s), 1176 (w), 1057 (s), 931 (w), 806, 761, 620 (w), 448 (w). Anal. Calcd. for $C_{54}H_{76}N_4Cu_2BF_5$: C, 63.96; H, 7.55; N, 5.52; F, 9.37. Found: C, 63.62; H, 7.60; N, 5.37; F, 9.04.

^{1}H NMR (400 MHz, THF-d_8): δ (ppm) 7.35 (t, J = 7.6 Hz, 4 H, *para*-C*H*), 7.21 (d, J = 8.0 Hz, 8 H, *meta*-C*H*), 4.09 (s, 8 H, NCH_2), 3.08 (sept, J = 6.8 Hz, 8 H, C*H*(CH3)$_2$), 1.28 (d, J = 6.8 Hz, 24 H, CH(CH_3)$_2$), 1.12 (d, J = 6.8 Hz, 24 H, CH(CH_3)$_2$). ^{19}F NMR (375 MHz, THF-d_8): δ (ppm) −152.79 (s, $^{10}BF_4^-$), −152.84 (s, $^{11}BF_4^-$), –291.14 (br. s, Cu*F*Cu).

Diffraction-quality crystals were grown by layering toluene onto a THF solution of $\{[(SIDipp)Cu]_2(\mu\text{-}F)\}^+ BF_4^-$.

Preparation of (SIDipp)AgF

Benzoyl fluoride (0.374 mL, 0.426 g, 3.43 mmol) was added to a solution of (SIDipp)Ag(O*t*Bu) (1.308 g, 2.288 mmol) in benzene (4 mL). The reaction flask was covered with foil to exclude light, and the mixture was stirred for 3 hours. The resulting white precipitate was collected on a fritted glass filter and washed with three portions of benzene (2 mL each). Residual solvents were removed in the dark under vacuum at 40 °C for 16 hours, affording the product as a white powder (1.045 g, 2.019 mmol, 88%). ^{1}H NMR (400 MHz, CD_2Cl_2): δ (ppm) 7.45 (t, J = 7.8 Hz, 2 H, *para*-C*H*), 7.29 (d, J = 7.8 Hz, 4 H, *meta*-C*H*), 4.07 (s, 4 H, NCH_2), 3.06 (sept, J = 6.9 Hz, 4 H, C*H*(CH_3)$_2$), 1.34 (d, J = 6.9 Hz, 12 H, CH(CH_3)$_2$), 1.33 (d, J = 6.9 Hz, 12 H, CH(CH_3)$_2$). ^{13}C{^{1}H} NMR (100 MHz, CD_2Cl_2): δ (ppm) 206.3 (app. dd, J(^{13}C-^{109}Ag) = 271 Hz, J(^{13}C-^{107}Ag) = 240 Hz N*C*Ag), 147.1 (*ortho*-*C*), 135.2 (*ipso*-*C*), 130.2 (*para*-*C*), 125.0 (*meta*-*C*), 54.3 (d, J(^{13}C-Ag) = 9 Hz N*C*H$_2$), 29.1 (*C*H(CH$_3$)$_2$), 25.5 (CH(*C*H$_3$)$_2$), 24.1 (CH(*C*H$_3$)$_2$). ^{19}F NMR (375 MHz, CD_2Cl_2): δ (ppm) –243.13 (d, $J_{Ag\text{-}F}$ = 163 Hz). IR: ν (cm^{-1}) 3073 (w) 3036 (w), 2963 (s), 2943, 2868, 1965 (w), 1820 (w), 1718 (w), 1591 (w), 1486 (s), 1477 (s), 1384,

1364, 1326, 1269, 1180, 1103, 1058, 936, 914, 807, 763, 683, 619, 548, 448. Anal. Calcd. for $C_{27}H_{38}N_2AgF$: C, 62.67; H, 7.40; N, 5.41; F, 3.67. Found: C, 62.48; H, 7.31; N, 5.32; F, 3.40.

Preparation of $\{[(SIDipp)Ag]_2(\mu\text{-}F)\}^+ BF_4^-$

Triphenylcarbenium tetrafluoroborate (0.064 g, 0.19 mmol) was added to a solution of (SIDipp)AgF (0.200 g, 0.386 mmol) in THF (4 mL). The reaction flask was covered with foil to exclude light, and the mixture was stirred for 2 hours. A layer of hexanes (12 mL) was carefully added over the THF solution, and the layers were allowed to mix by diffusion at −35 °C for 16 hours, resulting in the formation of colorless crystals. The mother liquor was decanted, and the crystals were washed with two portions of hexanes (2 mL each). Residual solvents were removed in the dark under vacuum at 40 °C for 16 hours, affording the product as a white powder (0.177 g, 0.160 mmol, 83%). ^{1}H NMR (400 MHz, CD_2Cl_2): δ (ppm) 7.43 (t, *J* = 7.8 Hz, 2H, *para*-C*H*), 7.24 (d, *J* = 7.8 Hz, 4H, *meta*-C*H*), 4.07 (s, 4H, NCH_2), 2.98 (sept, *J* = 6.9 Hz, 4H, C*H*$(CH_3)_2$), 1.32 (d, *J* = 6.9 Hz, 12H, CH(CH_3)$_2$), 1.17 (d, *J* = 6.9 Hz, 12H, CH(CH_3)$_2$). ^{13}C{^{1}H} NMR (100 MHz, CD_2Cl_2): δ (ppm) 204.9 (app. dd, *J*(^{13}C-^{109}Ag), = 300 Hz, *J*(^{13}C-^{107}Ag) = 261 Hz, N*C*Ag), 147.0 (*ortho*-*C*), 134.9 (*ipso*-*C*), 130.3 (*para*-*C*), 125.0 (*meta*-*C*), 54.4 (d, *J*(^{13}C-Ag), = 10 Hz, N*C*H_2), 29.1 (*C*H$(CH_3)_2$), 25.5 (CH(*C*H_3)$_2$), 24.0 (CH(*C*H_3)$_2$). ^{19}F NMR (375 MHz, CD_2Cl_2): δ (ppm) −153.60 (s, $^{10}BF_4^-$), −153.65 (s, $^{11}BF_4^-$), −308.5 (br. s, Ag*F*Ag). IR: ν (cm^{-1}) 3073 (w), 2966 (s), 2945, 2871, 1590 (w), 1489 (s), 1462 (s), 1385, 1365, 1327, 1275 (s), 1183, 1103, 1062 (s), 936, 932, 807, 759, 711, 620, 548, 520, 449. Anal. Calcd. for $C_{54}H_{76}N_4Ag_2BF_5$: C, 58.81; H, 6.95; N, 5.08; F, 8.61. Found: C, 59.07; H, 7.13; N, 5.07; F, 8.38.

^{1}H NMR (400 MHz, THF-d_8): δ (ppm) 7.38 (mult, J = 7.8 Hz, 2H, *para*-C*H*), 7.25 (mult, J = 7.8 Hz, 4H, *meta*-C*H*), 4.18 (s, 4H, NCH_2), 3.13 (sept, J = 6.9 Hz, 4H, CH(CH_3)$_2$), 1.32 (d, J = 6.9 Hz, 12H, CH(CH_3)$_2$), 1.19 (d, J = 6.9 Hz, 12H, CH(CH_3)$_2$). ^{19}F NMR (375 MHz, THF): δ (ppm) −154.23 (s, $^{10}BF_4^-$), −154.28 (s, $^{11}BF_4^-$), −302.9 (br. s, Ag*F*Ag).

Diffraction-quality crystals were grown by cautious layering of toluene onto a THF solution of {[(SIDipp)Ag]$_2$(μ-F)}$^+$ BF_4^- followed by diffusion in the dark at –35 °C.

Preparation of (SIDipp)AuF

Benzoyl fluoride (0.065 mL, 0.074 g, 0.597 mmol) was added to a solution of (SIDipp)Au(O*t*Bu) (0.265 g, 0.401 mmol) in toluene (4 mL) with stirring. After 3 hours, a white precipitate had formed. The precipitate was collected on a fritted glass filter and washed with two portions of toluene (6 mL each) and two portions of hexanes (5 mL each). Residual solvents were removed under vacuum at 35 °C over 18 hours, affording the product as a white powder (0.216 g, 0.356 mmol, 91%). ^{1}H NMR (400 MHz, CD_2Cl_2): δ (ppm) 7.47 (t, J = 7.8 Hz, 2 H, para-C*H*), 7.29 (d, J = 7.6 Hz, 4 H, *meta*-C*H*), 4.05 (s, 4 H, NCH_2), 3.04 (sept, J = 6.9 Hz, 4 H, CH(CH_3)$_2$), 1.41 (d, J = 6.8 Hz, 12 H, CH(CH_3)$_2$), 1.34 (d, J = 6.8 Hz, 12 H, CH(CH_3)$_2$). ^{19}F NMR (375 MHz, CD_2Cl_2): δ (ppm) –247.16. The ^{1}H and ^{19}F NMR spectra for this sample match those of (SIDipp)AuF prepared according to the previously published method.[24]

Preparation of {[(SIDipp)Au]$_2$(μ-F)}$^+$ BF_4^-

Triphenylcarbenium tetrafluoroborate (0.019 g, 0.058 mmol) was added to a solution of (SIDipp)AuF (0.070 g, 0.115 mmol) in THF (4 mL) in a flame-dried resealable flask with stirring. The flask was sealed, removed from the glovebox and brought out to the Schlenk line. After 1 hour, the solution was concentrated to a volume of about 1 mL. Hexanes (*ca.* 20 mL) were transferred under vacuum from a solution of sodium benzophenone ketyl into the reaction mixture, resulting in the formation of a white precipitate. The mother liquor was decanted via cannula, and the residual solvents were removed over 18 hours under vacuum at 35 °C, affording the product as a white powder (0.063 g, 0.049 mmol, 84%). ^{1}H NMR (400 MHz, THF-d_8): δ (ppm) 7.39 (t, J = 7.8 Hz, 4 H, *para*-C*H*), 7.24 (d, J = 8.0 Hz, 8 H, *meta*-C*H*), 4.21 (s, 8 H, NCH_2), 3.13 (sept, J = 6.8 Hz, 8 H, CH(CH_3)$_2$), 1.30 (d, J = 6.8 Hz, 48 H, CH(CH_3)$_2$). ^{13}C{^{1}H} NMR (75 MHz, THF-d_8): δ (ppm) 182.2 (br. N*C*Au), 147.7 (*ortho*-*C*), 135.1 (*ipso*-*C*), 130.5 (*para*-*C*), 125.1 (*meta*-*C*), 54.6 (N*C*H$_2$), 29.3 (CH(CH$_3$)$_2$), 25.5 (*C*H(CH$_3$)$_2$), 24.1 (CH(*C*H$_3$)$_2$). ^{19}F NMR (375 MHz, THF-d_8): δ (ppm) −154.44 (s, $^{10}BF_4^-$), −154.49 (s, $^{11}BF_4^-$), –272.60 (br. s, Au*F*Au). IR: ν (cm^{-1}) 3072 (w), 3026 (w), 2967 (s), 2931, 2868, 1595, 1500 (s), 1467 (s), 1391, 1365, 1345, 1329, 1309 (w), 1280 (s), 1234 (w), 1181, 1102, 1063 (s), 1020, 941, 809 (s), 760 (s), 704 (w), 664 (w), 625, 588, 549, 526 (w), 451. Anal. Calcd. for $C_{54}H_{76}N_4Au_2BF_5$: C, 50.63; H, 5.98; N, 4.37; F, 7.42. Found: C, 50.35; H, 5.83; N, 4.18; F, 7.13.

^{1}H NMR (400 MHz, CD_2Cl_2): δ (ppm) 7.45 (t, J = 7.8 Hz, 4 H, *para*-C*H*), 7.23 (d, J = 8.0 Hz, 8 H, *meta*-C*H*), 4.10 (s, 8 H, NCH_2), 2.90 (sept, J = 6.8 Hz, 8 H, CH(CH_3)$_2$), 1.31

(d, J = 6.8 Hz, 24 H, CH(CH_3)$_2$), 1.21 (d, J = 6.8 Hz, 24 H, CH(CH_3)$_2$). ^{19}F NMR (375 MHz, CD_2Cl_2): δ (ppm) −153.50 (s, $^{10}BF_4^-$), −153.55 (s, $^{11}BF_4^-$), –318.45 (br. s, Au*F*Au).

Diffraction-quality crystals were grown by cautious layering of toluene onto a THF solution of {[(SIDipp)Au]$_2$(μ-F)}$^+$ BF_4^-.

Halide exchange between {[(SIDipp)Au]$_2$(μ-F)}$^+$ BF_4^- and CD_2Cl_2

A solution of {[(SIDipp)Au]$_2$(μ-F)}$^+$ BF_4^- (0.060 g, 0.047 mmol) in CD_2Cl_2 (0.7 mL) was transferred to an NMR tube equipped with a J. Young valve. After 24 hours, the solution had turned yellow in color, and the starting complex had been completely consumed as judged by ^{1}H NMR and ^{19}F NMR spectroscopy. New resonances in the ^{1}H and ^{19}F spectra were assigned to {[(SIDipp)Au]$_2$(μ-Cl)}$^+$ BF_4^-, CD_2ClF and CD_2F_2. ^{1}H NMR (300 MHz, CD_2Cl_2): δ (ppm) 7.44 (t, J = 7.8 Hz, 4 H, *para*-C*H*), 7.22 (d, J = 7.8 Hz, 8 H, *meta*-C*H*), 4.10 (s, 8 H, NCH_2), 2.92 (sept, J = 6.7 Hz, 8 H, C*H*(CH_3)$_2$), 1.31 (d, J = 6.9 Hz, 24 H, CH(CH_3)$_2$), 1.17 (d, J = 6.9 Hz, 24 H, CH(CH_3)$_2$). ^{19}F NMR (375 MHz, CD_2Cl_2): δ (ppm) −144.10 (quint, CD_2F_2), −153.44 (s, $^{10}BF_4^-$), −153.50 (s, $^{11}BF_4^-$), –170.85 (quint, CD_2ClF).

Reaction of {[(SIDipp)Au]$_2$(μ-F)}$^+$ BF_4^- with 3-methyl-1,2-butadiene

A solution of {[(SIDipp)Au]$_2$(μ-F)}$^+$ BF_4^- (0.063 g, 0.049 mmol) in THF-d_8 (0.7 mL) was transferred to an NMR tube equipped with a J. Young valve. The tube was then opened, and 3-methyl-1,2-butadiene (4.8 μL, 0.049 mmol) was added. After 5 minutes, the starting complex had been completely consumed as judged by ^{1}H NMR and ^{19}F NMR

spectroscopy. New resonances in the ^{1}H and ^{19}F spectra were assigned to $\{[(SIDipp)Au]_2[\mu\text{-}C(=CH_2)CF(CH_3)_2]\}^+ BF_4^-$. ^{1}H NMR (400 MHz, THF-d_8): δ (ppm) 7.37 (t, J = 7.8 Hz, 4 H, *para*-C*H*), 7.20 (mult., 8 H, *meta*-C*H*), 4.89 (d, J = 4.8 Hz, 1 H, CCH_2), 4.22 (mult., 1 H, CCH_2), 4.15 (s, 8 H, NCH_2), 3.06 (sept, J = 6.8 Hz, 8 H, CH(CH$_3$)$_2$), 1.26 (mult., 24 H, CH(CH_3)$_2$), 1.18 (d, J = 6.8 Hz, 12 H, CH(CH_3)$_2$), 1.11 (d, J = 6.8 Hz, 12 H, CH(CH_3)$_2$), 0.31 (d, J = 20.4 Hz, 6 H, CF(CH_3)$_2$). $^{13}C\{^{1}H\}$ NMR (75 MHz, THF-d_8): δ (ppm) 205.8 (br. N*C*Au), 184.5 (br. Au*C*Au), 147.6 (*ortho*-*C*), 140.7 (C*C*H$_2$), 135.3 (*ipso*-*C*), 130.6 (*C*(CH$_3$)$_2$F), 130.3 (*para*-*C*), 125.2 (*meta*-*C*), 125.0 (*meta*-*C*), 54.9(N*C*H$_2$), 35.3 (C(*C*H$_3$)$_2$F), 28.8 (C(*C*H$_3$)$_2$F, 29.4 (*C*H(CH$_3$)$_2$), 29.2 (*C*H(CH$_3$)$_2$), 25.5 (CH(*C*H$_3$)$_2$), 25.4 (CH(*C*H$_3$)$_2$), 23.9 (CH(*C*H$_3$)$_2$). ^{19}F NMR (375 MHz, THF-d_8): δ (ppm) −128.40 (sept, J = 20.6 Hz, C(CH$_3$)$_2$F), −152.73 (s, $^{10}BF_4^-$), –152.78 (s, $^{11}BF_4^-$).

Crystals were grown by vapor diffusion of hexanes into a THF solution of $\{[(SIDipp)Au]_2(\mu\text{-}C(=CH_2)CF(CH_3)_2)\}^+ BF_4^-$.

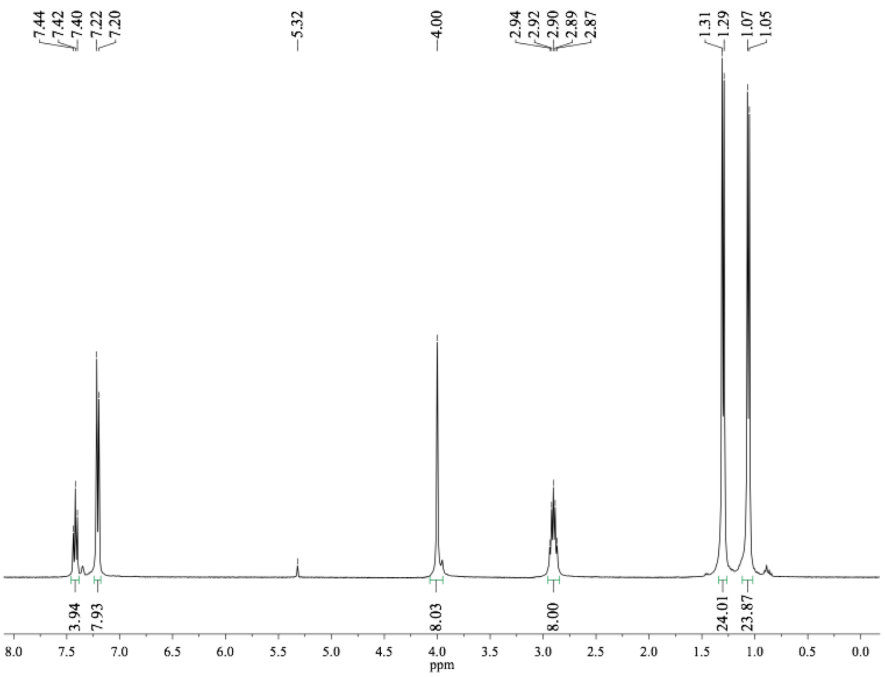

Figure 4.3. ^{1}H NMR spectrum (400 MHz, CD_2Cl_2) of $\{[(SIDipp)Cu]_2(\mu\text{-}F)\}^+ BF_4^-$.

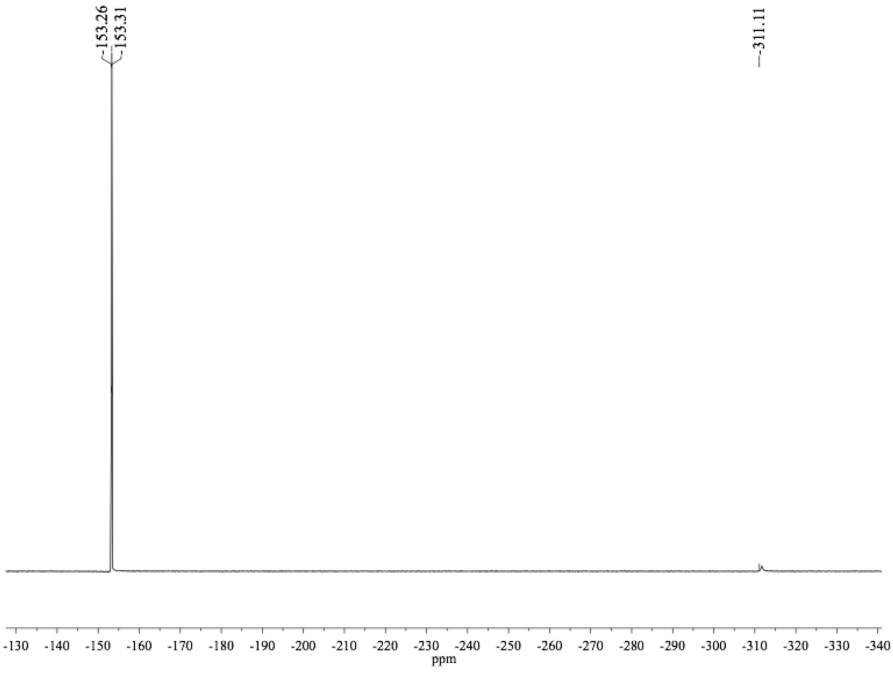

Figure 4.4. ^{19}F NMR spectrum (375 MHz, CD_2Cl_2) of $\{[(SIDipp)Cu]_2(\mu\text{-}F)\}^+ BF_4^-$.

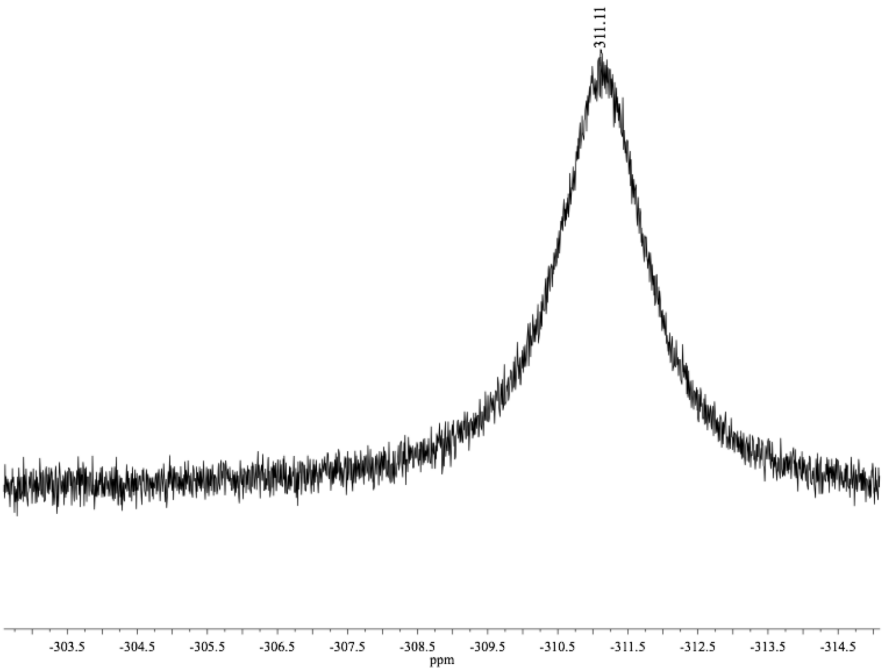

Figure 4.5. ^{19}F NMR spectrum (375 MHz, CD_2Cl_2) of $\{[(SIDipp)Cu]_2(\mu\text{-}F)\}^+ BF_4^-$.

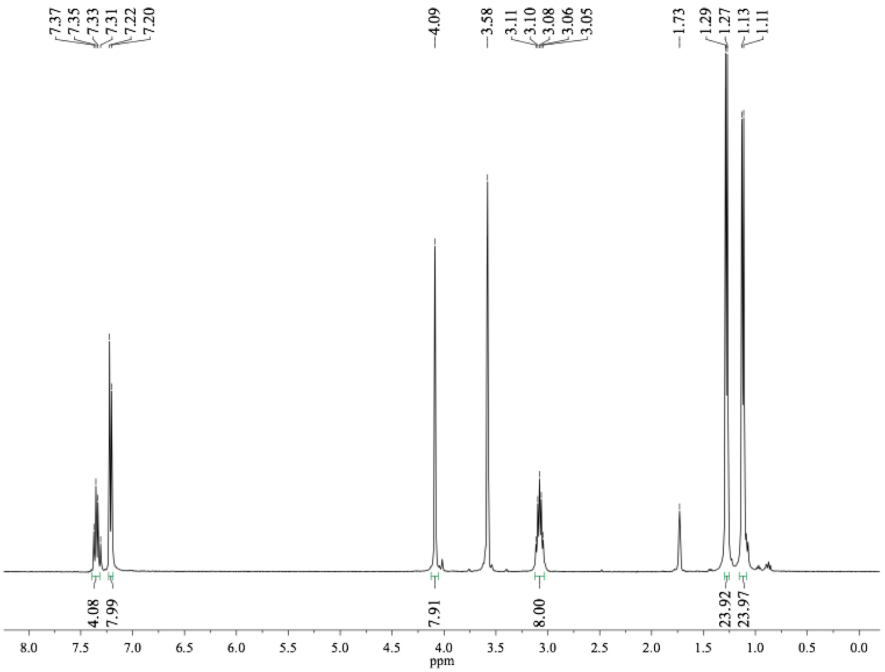

Figure 4.6. ^1H NMR spectrum (400 MHz, THF-d_8) of $\{[(SIDipp)Cu]_2(\mu\text{-}F)\}^+ BF_4^-$. A trace of benzene (δ 7.31 ppm) is present as the result of benzophenone ketyl decomposition.

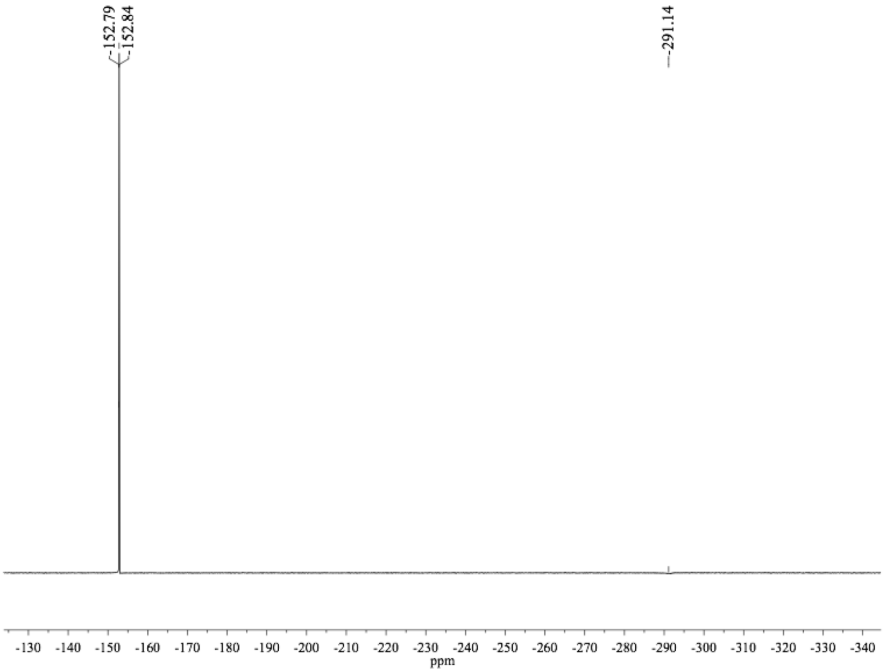

Figure 4.7. ^{19}F NMR spectrum (375 MHz, THF-d_8) of $\{[(SIDipp)Cu]_2(\mu\text{-}F)\}^+ BF_4^-$.

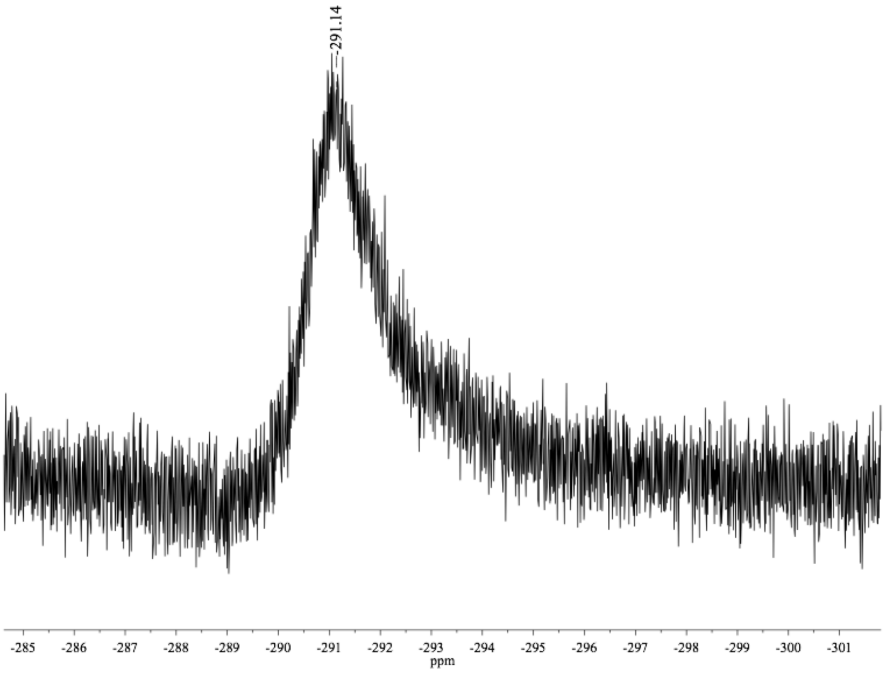

Figure 4.8. ^{19}F NMR spectrum (375 MHz, THF-d_8) of $\{[(SIDipp)Cu]_2(\mu\text{-}F)\}^+ BF_4^-$.

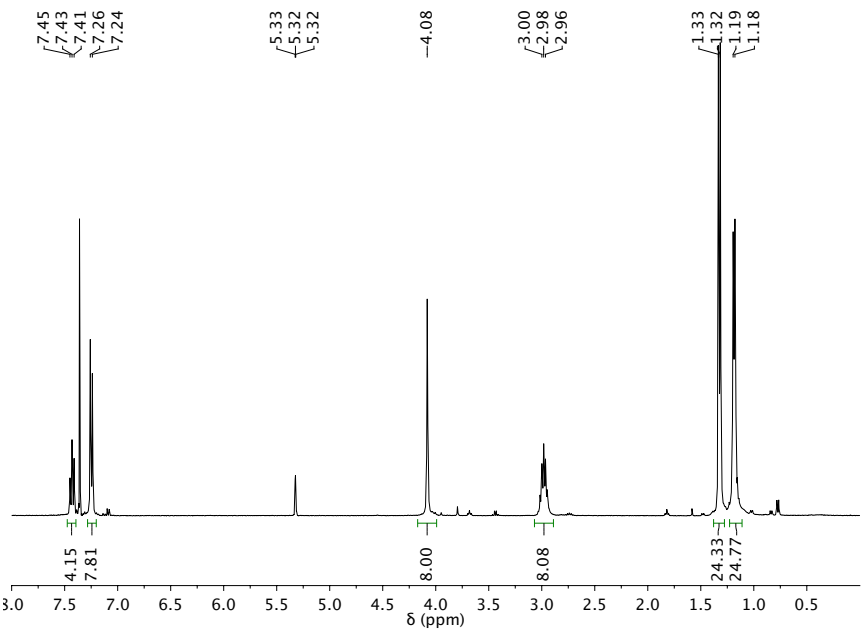

Figure 4.9. ^{1}H NMR spectrum (400 MHz, CD_2Cl_2) of $\{[(SIDipp)Ag]_2(\mu\text{-}F)\}^+ BF_4^-$. Adventitious benzene (δ 7.31 ppm) and a trace of the known complex $[(SIDipp)_2Ag]^+$ are present.

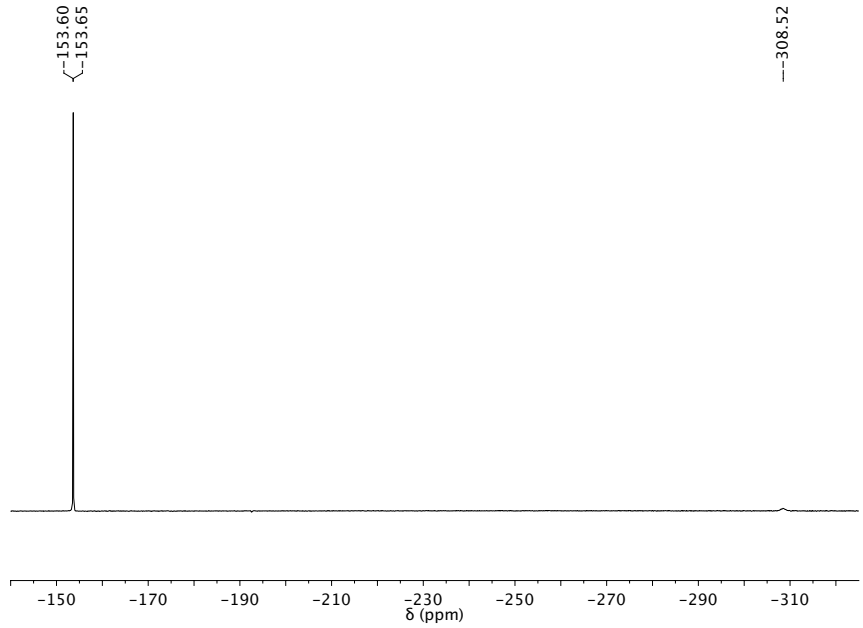

Figure 4.10. ^{19}F NMR spectrum (375 MHz, CD_2Cl_2) of $\{[(SIDipp)Ag]_2(\mu\text{-}F)\}^+ BF_4^-$.

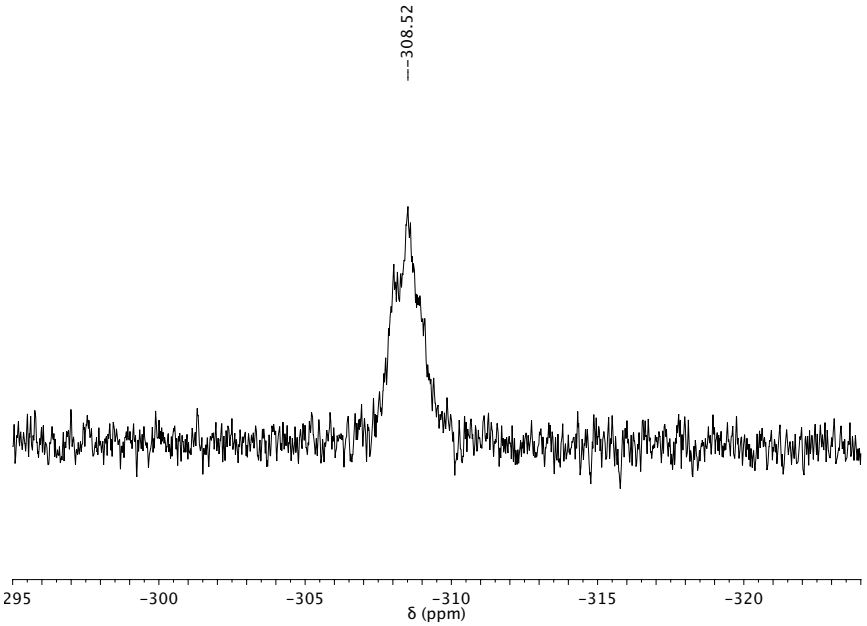

Figure 4.11. ^{19}F NMR spectrum (375 MHz, CD_2Cl_2) of $\{[(SIDipp)Ag]_2(\mu\text{-}F)\}^+ BF_4^-$.

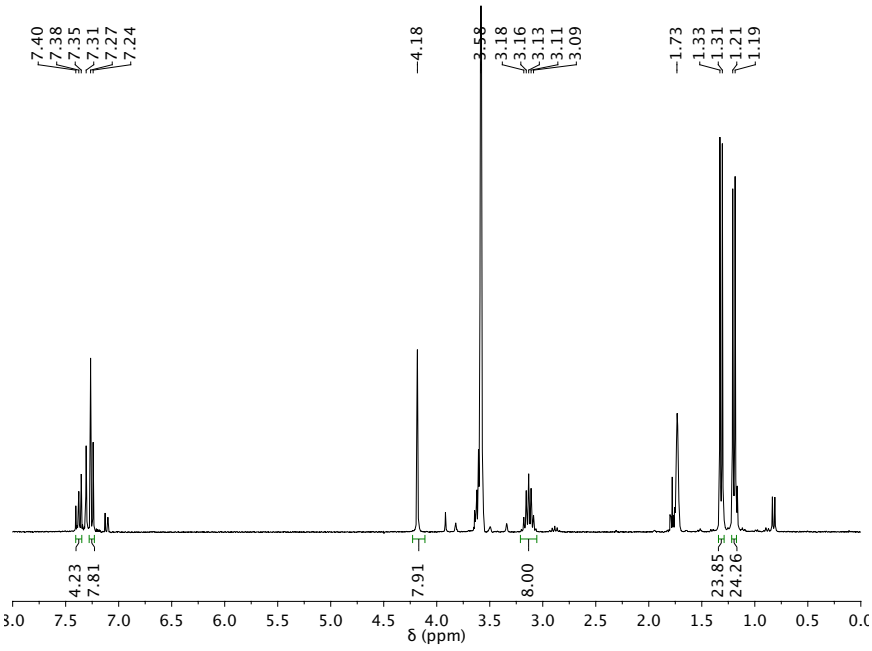

Figure 4.12. ^1H NMR spectrum (400 MHz, THF-d_8) of $\{[(SIDipp)Ag]_2(\mu\text{-}F)\}^+ BF_4^-$. Benzene (δ 7.31 ppm) from benzophenone ketyl decomposition, residual THF, and a trace of the known complex $[(SIDipp)_2Ag]^+$ are present.

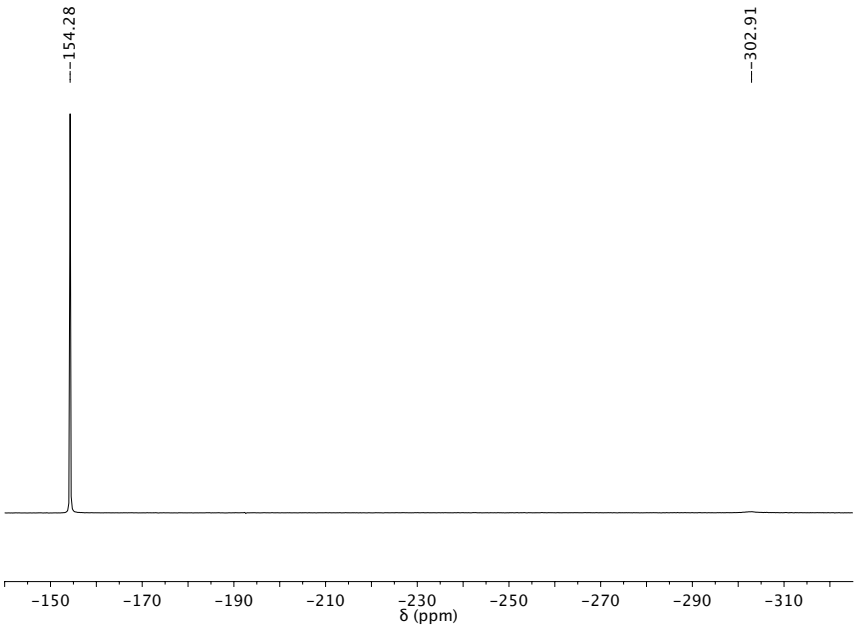

Figure 4.13. ^{19}F NMR spectrum (375 MHz, THF-d_8) of $\{[(SIDipp)Ag]_2(\mu\text{-}F)\}^+ BF_4^-$.

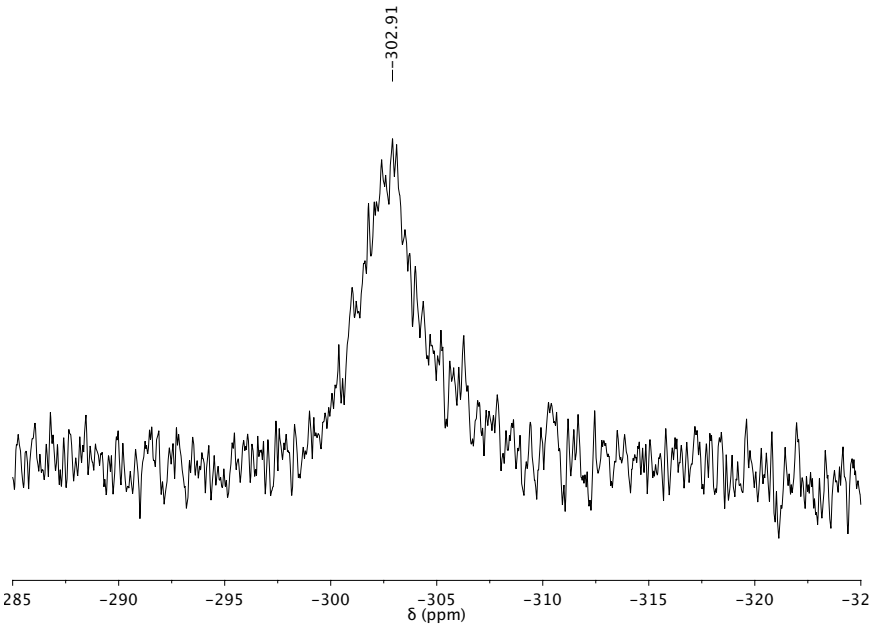

Figure 4.14. ^{19}F NMR spectrum (375 MHz, THF-d_8) of $\{[(SIDipp)Ag]_2(\mu\text{-}F)\}^+ BF_4^-$.

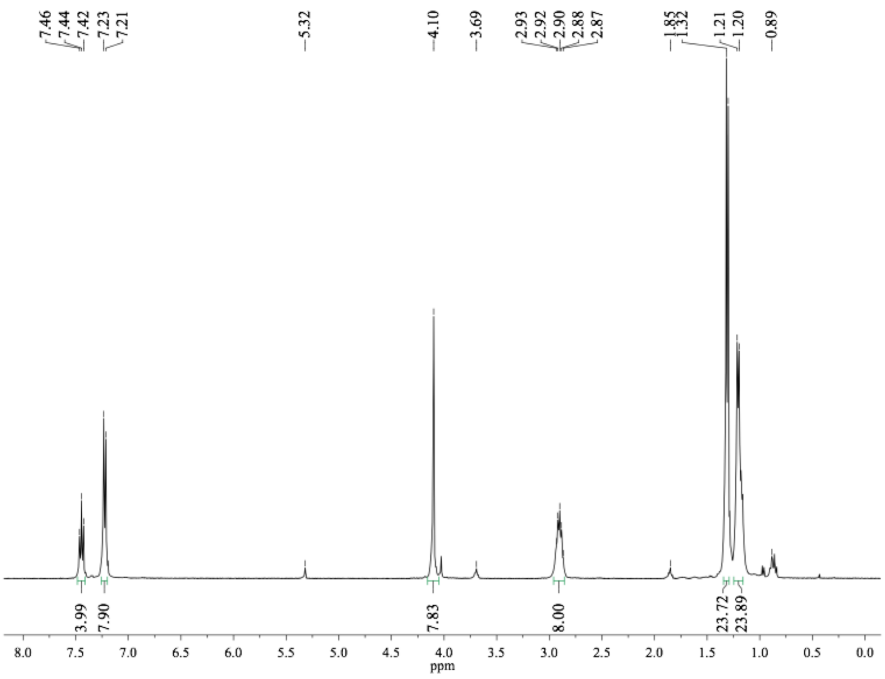

Figure 4.15. ^{1}H NMR spectrum (400 MHz, CD_2Cl_2) of $\{[(SIDipp)Au]_2(\mu\text{-}F)\}^+ BF_4^-$. A trace of residual solvent, THF (δ 3.69 and 1.85 ppm) and hexane (δ 0.89), is present.

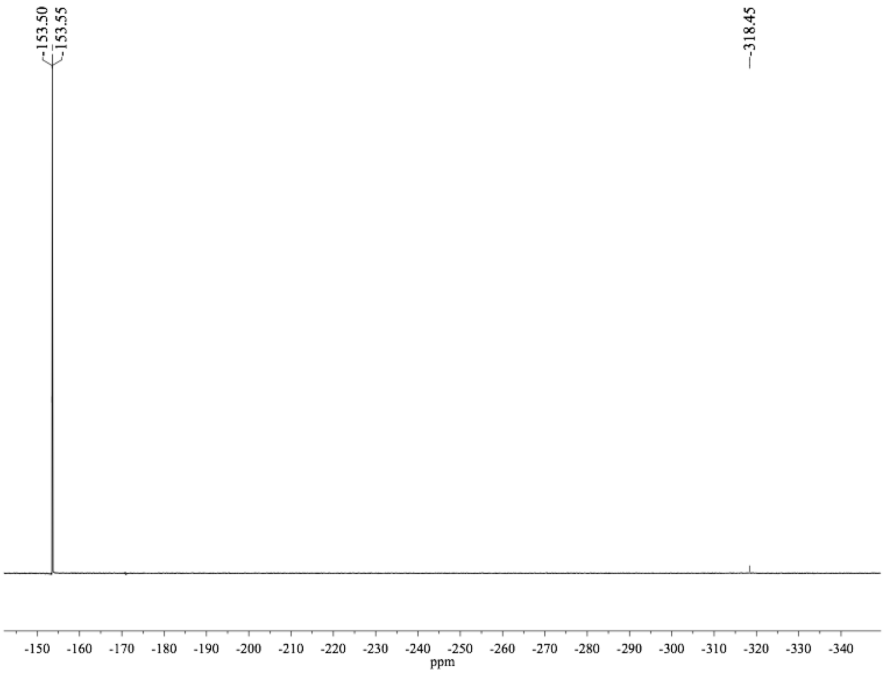

Figure 4.16. ^{19}F NMR spectrum (375 MHz, CD_2Cl_2) of $\{[(SIDipp)Au]_2(\mu\text{-}F)\}^+ BF_4^-$.

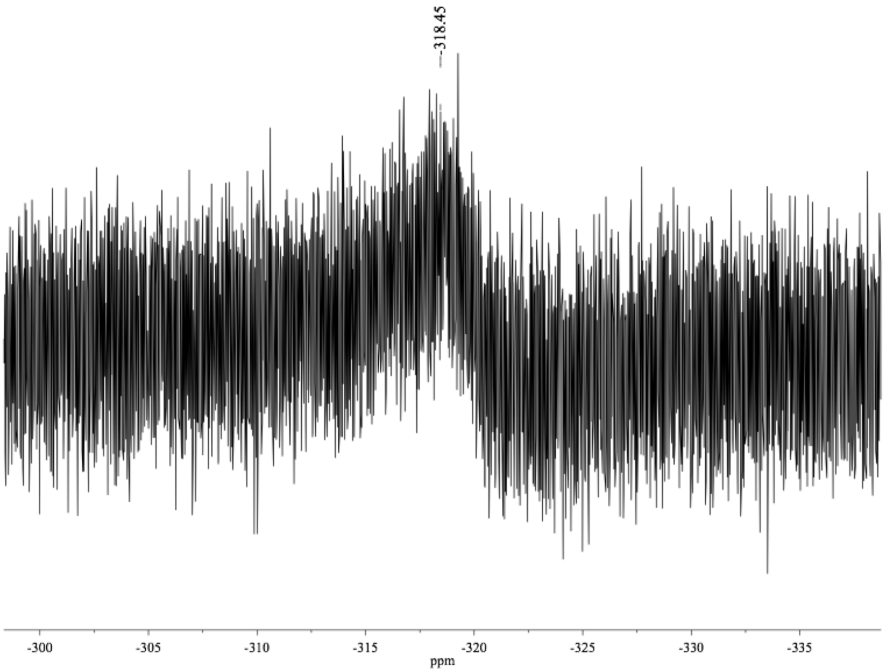

Figure 4.17. ^{19}F NMR spectrum (375 MHz, CD_2Cl_2) of $\{[(SIDipp)Au]_2(\mu\text{-}F)\}^+ BF_4^-$.

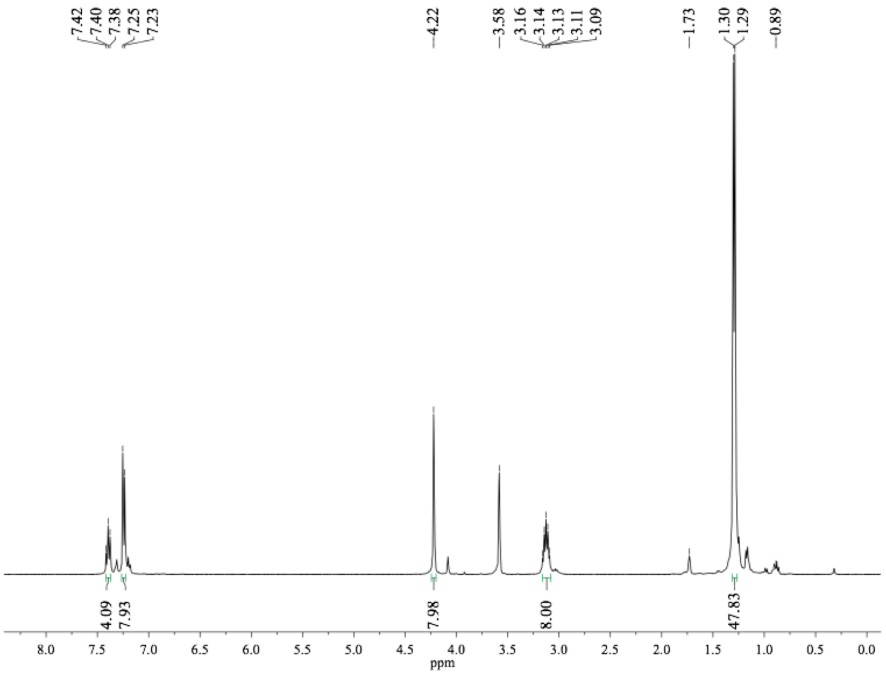

Figure 4.18. ^1H NMR spectrum (400 MHz, THF-d_8) of $\{[(SIDipp)Au]_2(\mu\text{-}F)\}^+ BF_4^-$. A trace of residual solvent, hexane (δ 0.89), is present.

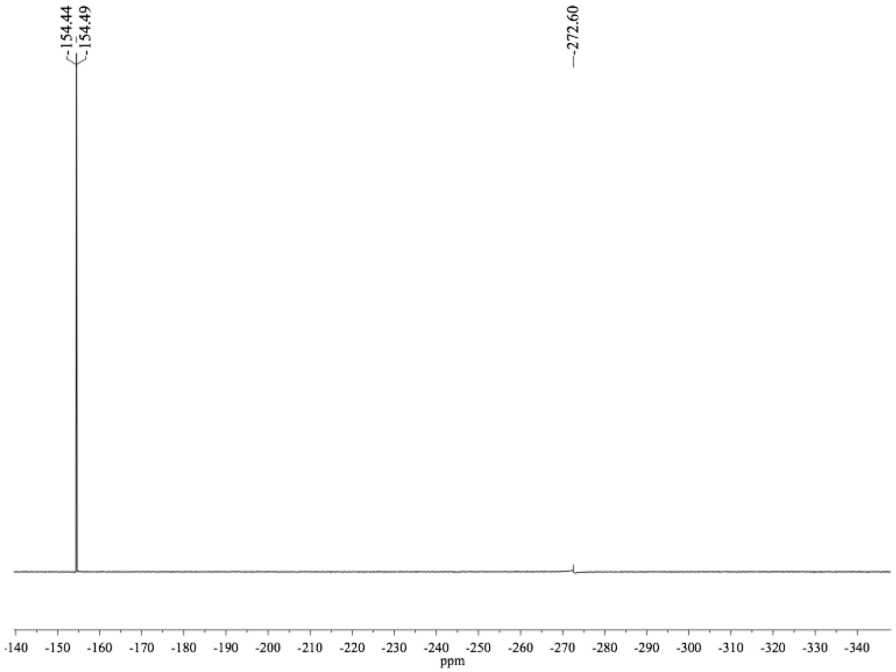

Figure 4.19. ^{19}F NMR spectrum (375 MHz, THF-d_8) of $\{[(SIDipp)Au]_2(\mu\text{-}F)\}^+ BF_4^-$.

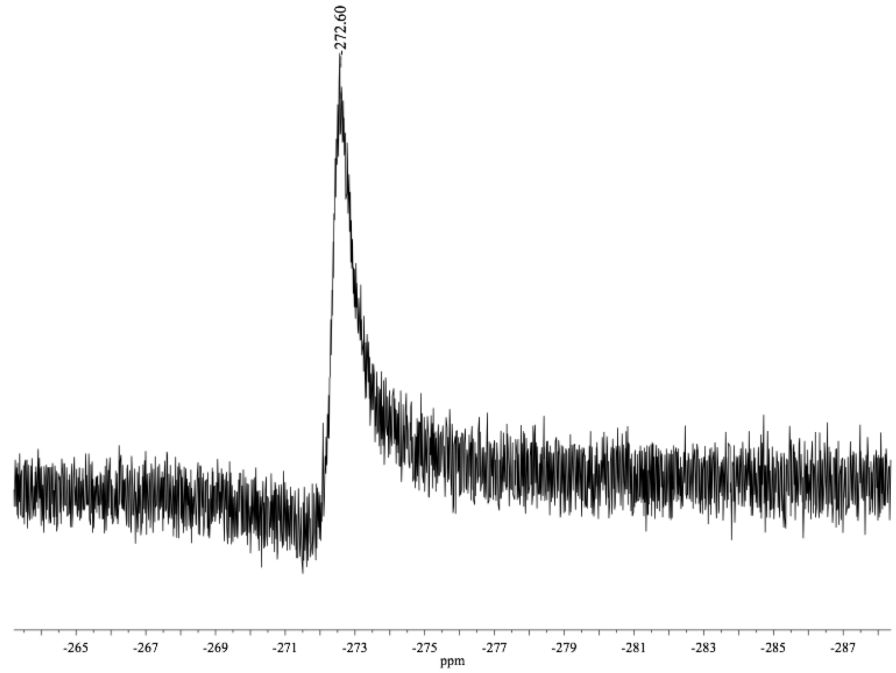

Figure 4.20. ^{19}F NMR spectrum (375 MHz, THF-d_8) of $\{[(SIDipp)Au]_2(\mu\text{-}F)\}^+ BF_4^-$.

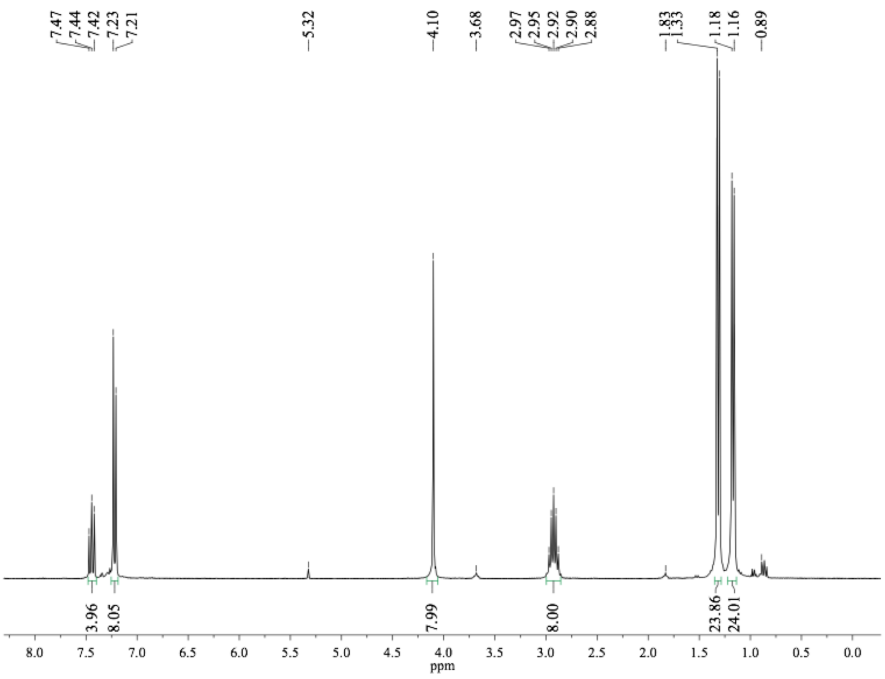

Figure 4.21. ^{1}H NMR spectrum (300 MHz, CD_2Cl_2) of halide exchange between $\{[(SIDipp)Au]_2(\mu\text{-}F)\}^+ BF_4^-$ and CD_2Cl_2. A trace of residual solvent, THF (δ 3.68 and 1.83 ppm) and hexane (δ 0.89), is present.

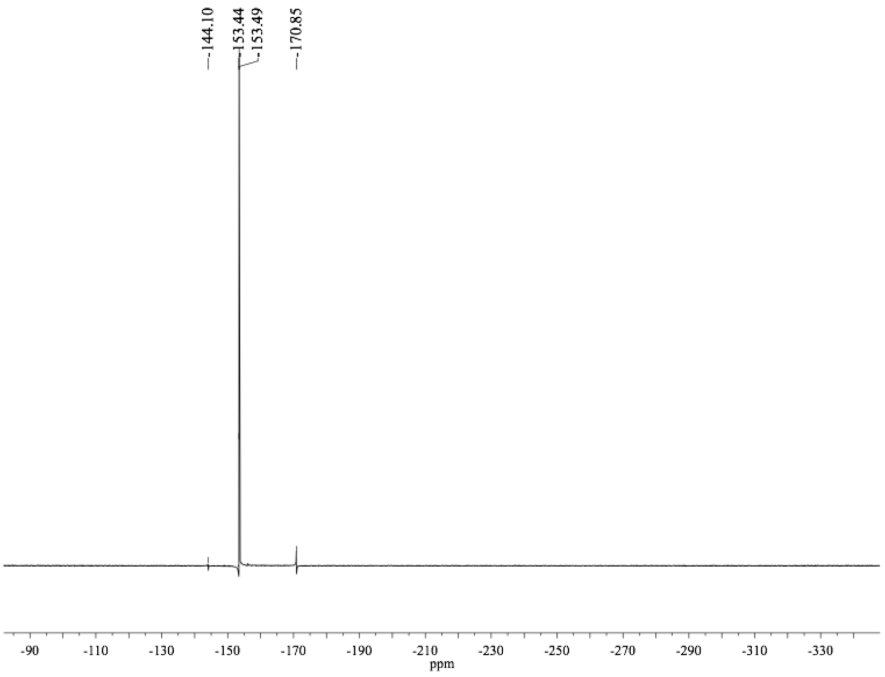

Figure 4.22. ^{19}F NMR spectrum (375 MHz, CD_2Cl_2) of halide exchange between $\{[(SIDipp)Au]_2(\mu\text{-}F)\}^+ BF_4^-$ and CD_2Cl_2.

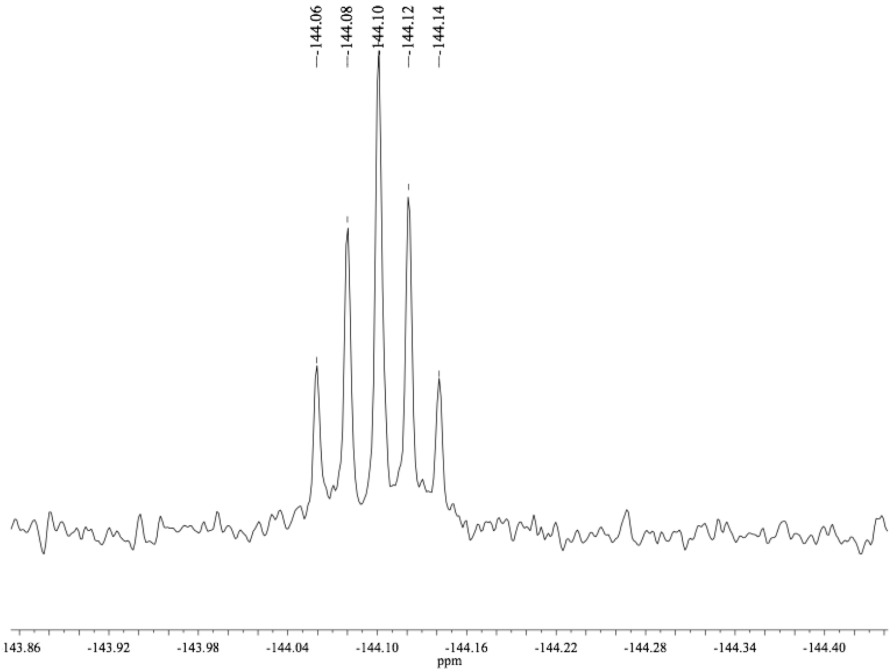

Figure 4.23. ^{19}F NMR spectrum (375 MHz, CD_2Cl_2) of CD_2F_2 from halide exchange between $\{[(SIDipp)Au]_2(\mu\text{-}F)\}^+ BF_4^-$ and CD_2Cl_2.

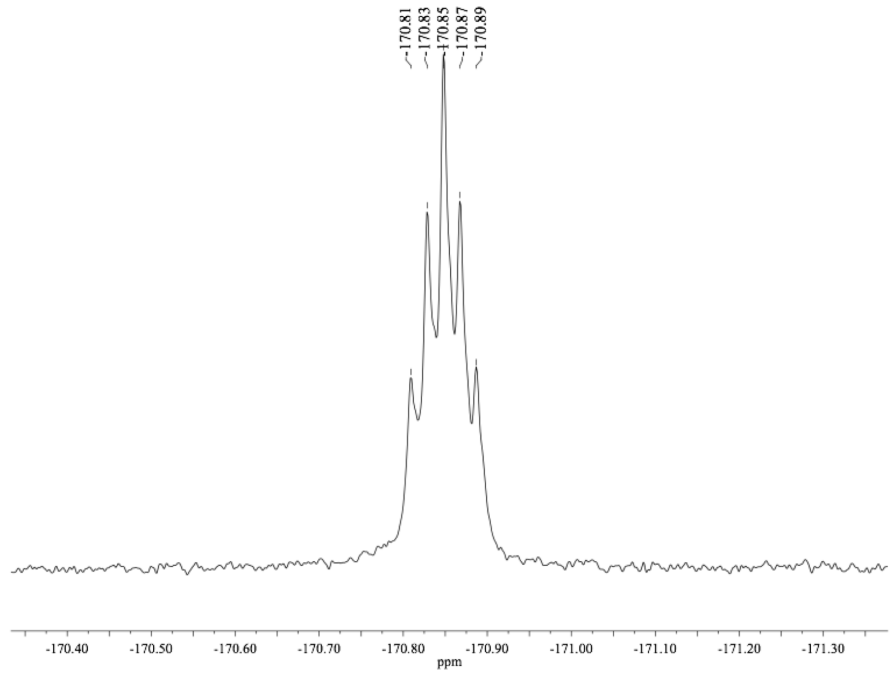

Figure 4.24. ^{19}F NMR spectrum (375 MHz, CD_2Cl_2) of CD_2ClF from halide exchange between $\{[(SIDipp)Au]_2(\mu\text{-}F)\}^+ BF_4^-$ and CD_2Cl_2.

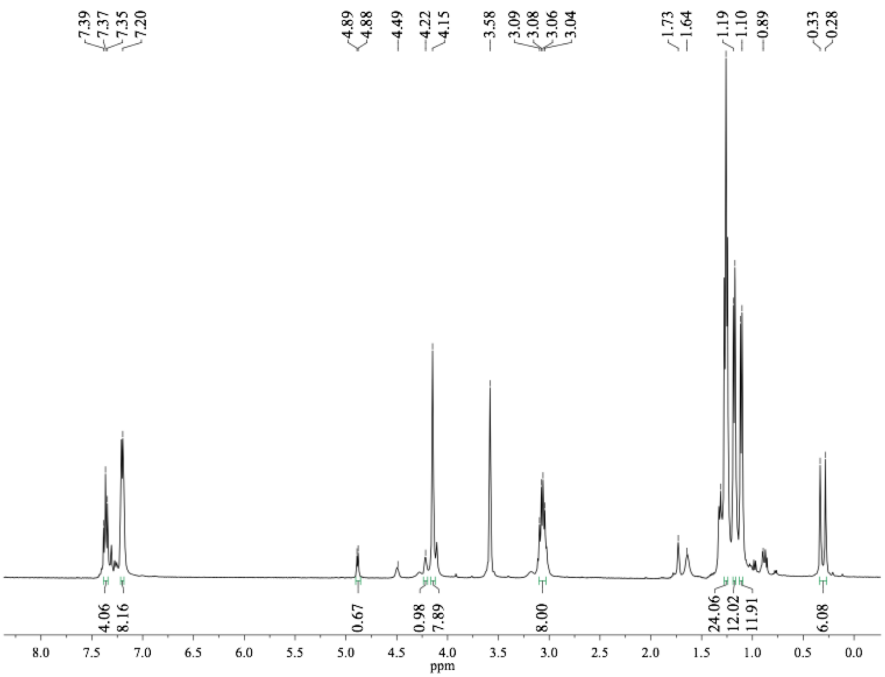

Figure 4.25. ^{1}H NMR spectrum (400 MHz, THF-d_8) of the reaction of $\{[(SIDipp)Au]_2(\mu\text{-}F)\}^+ BF_4^-$ with 3-methyl-1,2-butadiene. A trace of residual solvent, hexane (δ 1.31 and 0.89), and small excess of 3-methyl-1,2-butadiene (δ 4.49 and 1.64) is present.

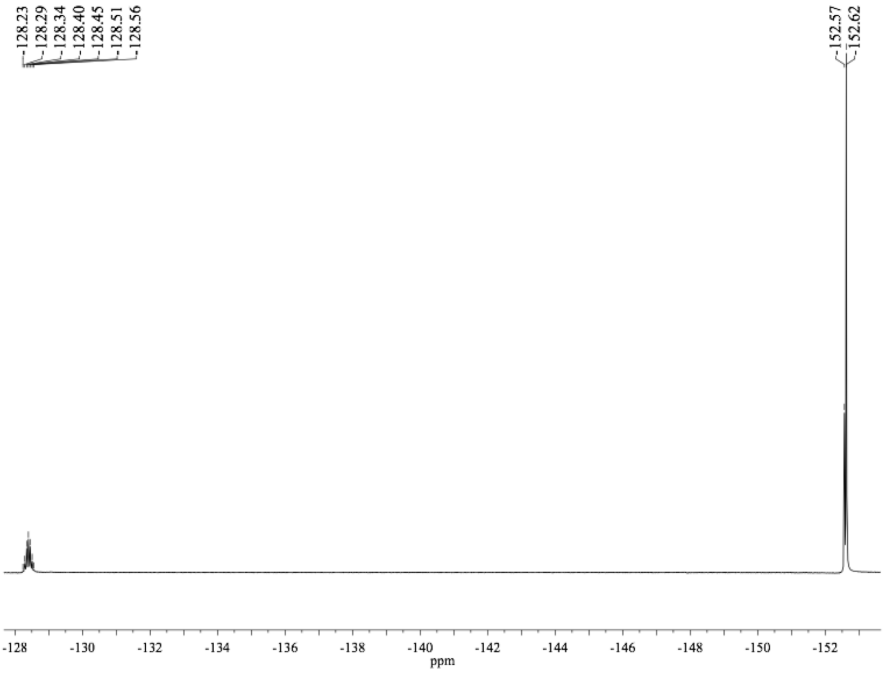

Figure 4.26. ^{19}F NMR spectrum (375 MHz, THF-d_8) of the reaction of $\{[(SIDipp)Au]_2(\mu\text{-}F)\}^+ BF_4^-$ with 3-methyl-1,2-butadiene.

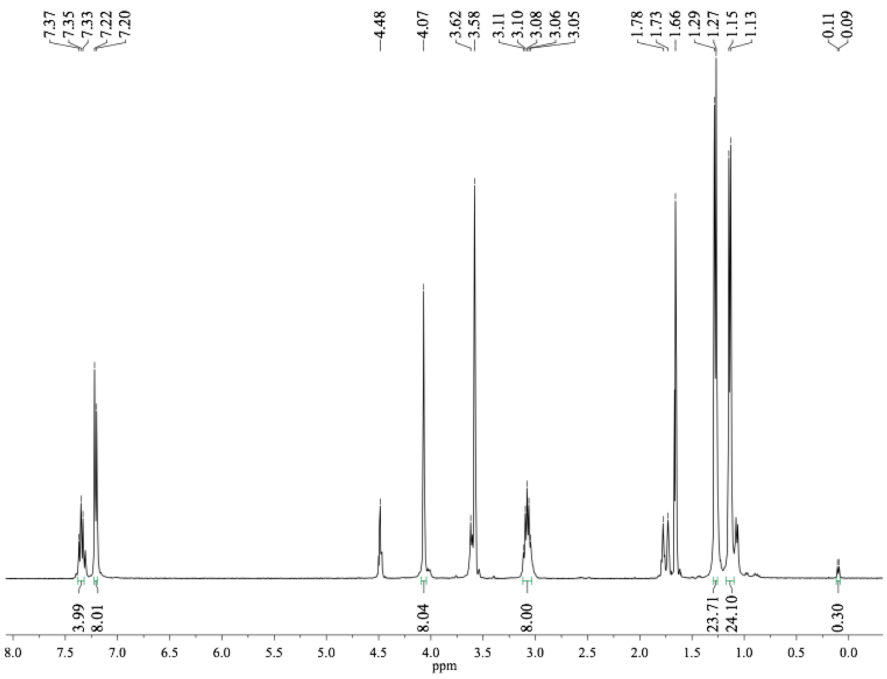

Figure 4.27. ^{1}H NMR spectrum (400 MHz, THF-d_8) of the reaction of $\{[(SIDipp)Cu]_2(\mu\text{-}F)\}^+$ BF_4^- with 3-methyl-1,2-butadiene. A trace of residual solvent, THF (δ 3.62 and 1.78), and 3-methyl-1,2-butadiene (δ 4.48 and 1.66) is present.

X-ray crystallography

For each complex, a suitable crystal was selected and mounted on a loop with Paratone oil on an ApexII Mo diffractometer (Mo Kα radiation, λ = 0.71073 Å). The crystal was maintained at low temperature (see Table 4.3) during data collection. Using Olex2,[65] the structure was solved with the Superflip[66] structure solution program, using the Charge Flipping solution method. The model was refined with the ShelXL[66] refinement package using Least Squares minimization.

Table 4.3. X-ray crystallographic parameters and refinement data.

Complex	$\{[(SIDipp)Cu]_2(\mu\text{-}F)\}^+ BF_4^-$	$\{[(SIDipp)Ag]_2(\mu\text{-}F)\}^+ BF_4^-$	$\{[(SIDipp)Au]_2(\mu\text{-}F)\}^+ BF_4^-$	$\{[(SIDipp)Au]_2[\mu\text{-}C(=CH_2)CF(CH_3)_2]\}^+ BF_4^-$
Empirical formula	$C_{245}H_{344}B_4Cu_8F_{20}N_{16}O_2$	$C_{54}H_{76}Ag_2BF_5N_4$	$C_{54}H_{76}Au_2BF_3N_4$	$C_{118}H_{166}Au_4BF_6N_6$
Formula weight	4476.90	1102.77	1242.93	2609.25
Crystal system	Triclinic	monoclinic	Monoclinic	triclinic
Space group	*P*-1	*C*2/*c*	*C*2/*c*	*P*-1
Crystal size (mm)	0.951 x 0.397 x 0.174	0.792 x 0.212 x 0.06	0.589 x 0.276 x 0.118	0.509 x 0.227 x 0.164
a (Å)	17.182(2)	15.8655(13)	15.7389(11)	12.6672(16)
b (Å)	18.104(2)	26.516(2)	26.8181(19)	16.445(2)
c (Å)	22.066(3)	16.179(2)	16.0218(17)	33.120(4)
α (°)	75.996(2)	90	90	94.890(3)
β (°)	69.967(2)	107.4930(10)	108.6460(10)	92.006(4)
γ (°)	73.915(2)	90	90	98.452(3)
V (Å³)	6113.4(13)	6491.6(11)	6407.6(9)	6791.6(14)
Z	1	4	4	2
Absorption coefficient (mm^{-1})	0.75	0.652	4.614	4.348
D_{calc} (g/cm^3)	1.196	1.128	1.288	1.207
T (K)	173(2)	173(2)	110(2)	110(2)
θ (°)	2.38-57.12	3.072-59.228	1.562-31.136	2.472-56.55
Reflections collected	75207	32060	40960	41257
Independent reflections (R_{int})	31125 (0.0515)	9116 (0.0527)	10296 (0.0385)	30711 (0.0419)
Data/restraints/parameter	31125/10/1316	9116/30/320	10296/18/310	30711/1081/1216
Final R_1 indices [I > 2σ(I)]	$R_1 = 0.0665$, $wR_2 = 0.1656$	$R_1 = 0.0470$, $wR_2 = 0.1134$	$R_1 = 0.0363$, $wR_2 = 0.0953$	$R_1 = 0.1004$, $wR_2 = 0.2700$
R indices (all data)	$R_1 = 0.1137$, $wR_2 = 0.1916$	$R_1 = 0.0845$, $wR_2 = 0.1354$	$R_1 = 0.0547$, $wR_2 = 0.1059$	$R_1 = 0.1609$, $wR_2 = 0.2930$
Largest difference peak/hole (e $Å^{-3}$)	0.85/–0.65	1.44/–0.57	3.694/–1.188	5.03/–2.13
Goodness of fit (GOF) on F^2	1.027	1.005	1.034	1.015

Refinement of the crystal data for $\{[(SIDipp)Au]_2(\mu\text{-}F)\}^+ BF_4^-$ gave rise to large difference peaks, ascribed to ghost peaks from the gold atoms. The largest peak lies along the Au–Au vector, and the distance from this peak to the crystallographic unique Au atom (3.95 Å) coincides with the Au–Au distance. These peaks probably arise from undetected twinning and translational disorder. This contribution, however, is small and difficult to detect: A search for twinning and/or supersymmetry yielded no results.

The crystal structure of $\{[(SIDipp)Au]_2[\mu\text{-}C(=CH_2)CF(CH_3)_2]\}^+ BF_4^-$ exhibits substantial disorder. In addition to the normal degree of translational order, the crystal is made of molecules with small differences in orientations. This disorder affects all the Au atoms, which were refined as split atoms with two different positions for each atom. The distance between split Au atoms was about 0.7 Å. The large peaks close to the Au atoms

are due to unresolved disorder. No further modeling of this disorder was attempted. The structure was modeled after removal of the BF_4^- anion, co-crystallized solvent and part of the disorder of the main molecules, and after the masking of reflections resulting from this disorder. This analysis does not support a detailed discussion of metrics in this complex, but it allows confirmation of the assigned connectivity, and affords insight into the binding mode of the vinyl anion.

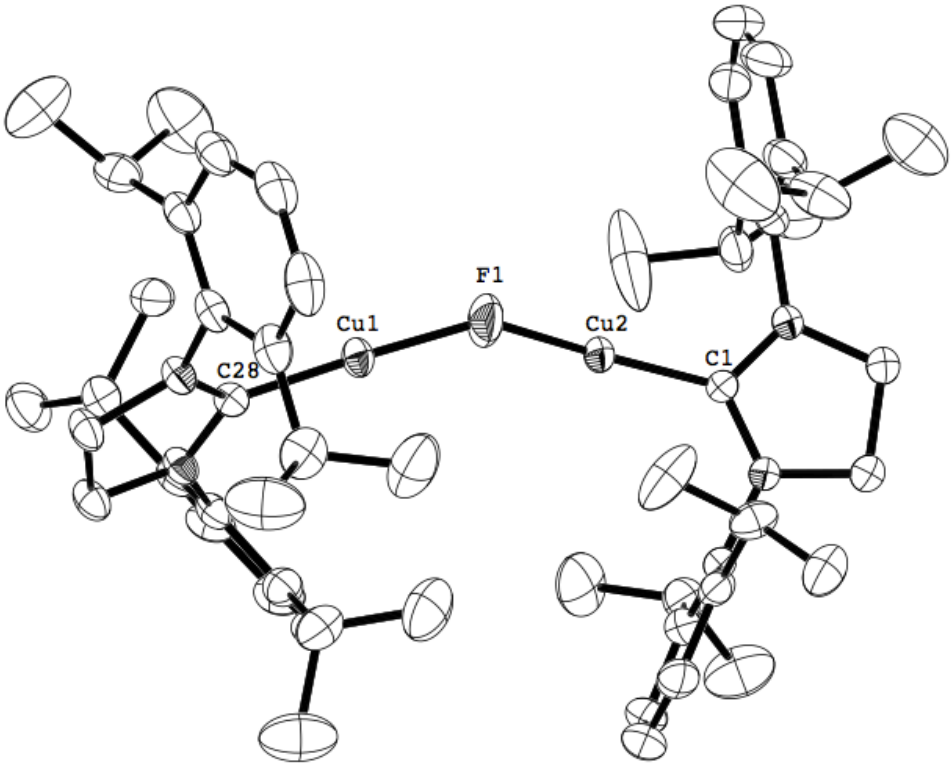

Figure 4.28. Solid-state structure of $\{[(SIDipp)Cu]_2(\mu\text{-}F)\}^+ BF_4^-$. Note: One of two crystallographically distinct molecules is shown; key metrics for both are given in Table 4.2. BF_4^- anion and co-crystallized solvent have been omitted for clarity.

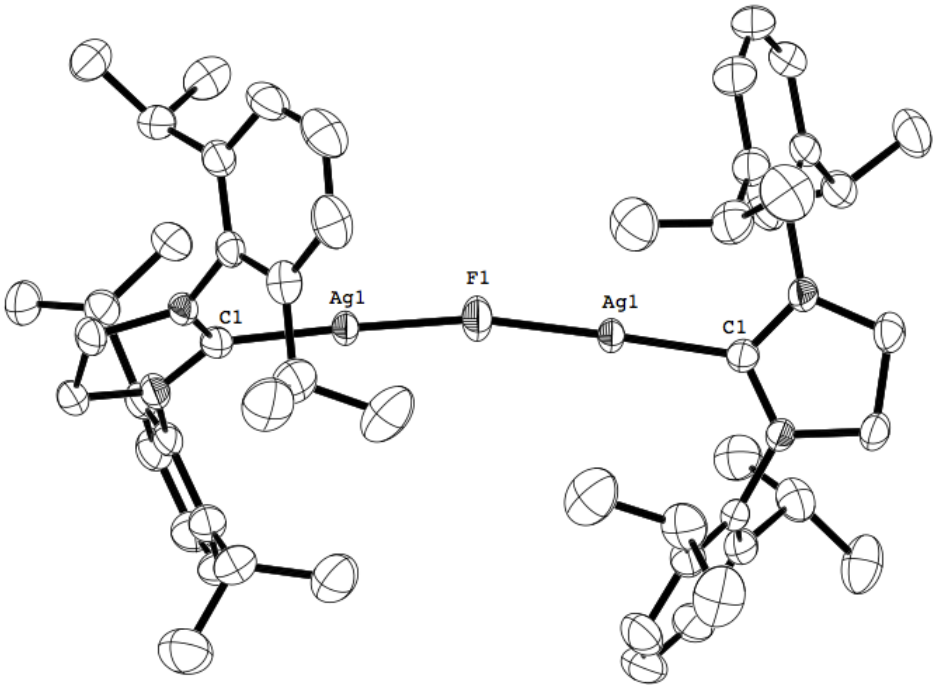

Figure 4.29. Solid-state structure of $\{[(SIDipp)Ag]_2(\mu\text{-}F)\}^+ BF_4^-$. BF_4^- anion and co-crystallized solvent have been omitted for clarity.

4.5. References

1. Calculated Pd–X bond enthalpies are larger in PdF_2 than in $PdCl_2$: P.E.M. Siegbahn, Theor. Chim. Acta 87 (1994) 441.

2. Halide affinities of $[(Ph_3P)_2Pd(Ph)]^+$: J.P. Flemming, M.C. Pilon, O.Ya. Borbulevitch, M.Yu. Antipin, V.V. Grushin, Inorg. Chim. Acta 280 (1998) 87.

3. Halide affinities of $[(Ph_3P)_2Rh(CO)]^+$ and $[(Ph_3As)_2Rh(CO)]^+$: F. Araghizadeh, D.M. Branan, N.W. Hoffman, J.H. Jones, E.A. McElroy, N.C. Miller, D.L. Ramage, A.B. Salazar, S.H. Young, Inorg. Chem. 27 (1988) 3752.

4. R.G. Pearson, J. Am. Chem. Soc. 85 (1963) 3533.

5. A. Walsh, C.R.A. Catlow, R. Galvelis, D.O. Scanlon, F. Schiffmann, A.A. Sokol, S.M. Woodley, Chem. Sci. 3 (2012) 2565.

6. P.R. Gibbs, P.R. Graves, D.J. Gulliver, W. Levason, Inorg. Chim. Acta 45 (1980) L207.

7. S. Sirol, J. Coumarcel, N. Mostefai, O. Riant, Org. Lett. 3 (2011) 4111.

8. M. Omote, M. Tanaka, M. Tanaka, A. Ikeda, A. Tarui, K. Sato, A. Ando, J. Org. Chem. 78 (2013) 6196.

9. D.J. Gulliver, W. Levason, M. Webster, Inorg. Chim. Acta. 52 (1981) 153.

10. P.C. Healy, J.V. Hanna, J.D. Kildea, B.W. Skelton, A.H. White, Aust. J. Chem. 44 (1991) 427.

11. M.K. Chaudhuri, S.S. Dhar , N. Vijayashree, Trans. Met. Chem. 25 (2000) 559.

12. B.F. Straub, F. Rominger, P. Hofmann, P. Inorg. Chem. 39 (2000) 2113.

13. E.L. Muetterties, C.W. Alegranti, J. Am. Chem. Soc. 94 (1972) 6386.

14. Q.-M. Wang, T.C.W. Mak, J. Am. Chem. Soc. 122 (2000), 7608.

15. P.J. Steel, C.J. Sumby, Chem. Commun. (2002) 322.

16. D. Rais, D.M.P. Mingos, R. Vilar, A.J.P. White, D.J. Williams, J. Organomet. Chem. 652 (2002) 87.

17. Q.-M. Wang, G.-C. Guo, T.C.W. Mak, Polyhedron 22 (2003), 217.

18. A. Yanagisawa, T. Touge, T. Arai, Angew. Chem. Int. Ed. 44 (2005) 1546.

19. F.W.B. Einstein, R.P. Rao, J. Trotter, N. Bartlett, J. Chem. Soc. A: Inorg. Phys. Theor. (1967) 478.

20. I.-C. Hwang, K. Seppelt, Angew. Chem. Int. Ed. 40 (2001) 3690.

21. T. Mathieson, A. Schier, H. Schmidbaur, Z. Naturforsch, B 55 (2000) 1000.

22. A.J. Arduengo III, R.L. Harlow, M. Kline, J. Am. Chem. Soc. 113 (1991) 361.

23. A.J. Arduengo III, R. Krafczyk, R. Schmutzler, H.A. Craig, J.R. Goerlich, W.J. Marshall, M. Unverzagt, Tetrahedron 55 (1999) 14523.

24. D.S. Laitar, P. Müller, T.G. Gray, J.P. Sadighi, Organometallics 24 (2005) 4503.

25. D.S. Laitar, *Synthetic and Catalytic Studies of Group 11 N-Heterocyclic Carbene Complexes*. Dissertation, Massachusetts Institute of Technology. Cambridge Massachusetts, 2006.

26. J.A. Akana, K.X. Bhattacharyya, P. Müller, J.P. Sadighi, J. Am. Chem. Soc. 129 (2007) 7736.

27. J.R. Herron, Z.T. Ball, J. Am. Chem. Soc. 130 (2008) 16486.

28. J.R. Herron, V. Russo, E.J. Valente, Z.T. Ball, Chem. Eur. J. 15 (2009) 8713.

29. T. Fujihara, T. Xu, K. Semba, J. Terao, Y. Tsuji, Angew. Chem. Int. Ed. 50 (2011) 523.

30. T. Vergote, F. Nahra, A. Welle, M. Luhmer, J. Wouters, N. Mager, O. Riant, T. Leyssens, Chem. Eur. J. 18 (2012) 793.

31. T. Vergote, F. Nahra, D. Peeters, O. Riant, T. Leyssens, J. Organomet. Chem. 730 (2013) 95.

32. S.K. Gurung, S. Thapa. A. Kafle, D.A. Dickie, R. Giri, Org. Lett. 16 (2014) 1264.

33. N.P. Mankad, F.D. Toste, J. Am. Chem. Soc. 132 (2010) 12859.

34. V.J. Scott, J.A. Labinger, J.E. Bercaw, Organometallics 29 (2010) 4090.

35. N.P. Mankad, F.D. Toste, Chem. Sci. 3 (2012) 72.

36. D.Y. Melgarejo, G.M. Chiarella, J.P. Fackler Jr., L.M. Perez, A. Rodrigue-Witchel, C. Reber, Inorg. Chem. 50 (2011) 4238.

37. M. Camalli, F. Caruso, L. Zambonelli, Inorg. Chim. Acta 61 (1982) 195.

38. S. Noro, T. Akutagawa, T. Nakamura, Chem. Commun. 46 (2010) 4619.

39. D.L. Reger, A.E. Pascui, M.D. Smith, J. Jezierska, A. Ozarowski, Inorg. Chem. 51 (2012) 11820.

40. M. Royzen, J.J. Wilson, S.J. Lippard, J. Inorg. Biochem. 118 (2013) 162.

41. H. Ibrahim, R. Guillot, F. Cisnetti, A. Gautier, Chem. Commun. 50 (2014) 7154.

42. R.S. Ramón, S. Gaillard, A. Poater, L. Cavallo, A.M.Z. Slawin, S.P. Nolan, Chem. Eur. J. 17 (2011) 1238.

43. B. Liu, C. Chen, Y. Zhang, X. Liu, W. Chen, Organometallics 32 (2013) 5451.

44. H.G. Raubenheimer, H. Schmidbaur, Organometallics 31 (2012) 2507.

45. S.L. Fraser, M. Yu. Antipin, V.N. Khroustalyov, V.V. Grushin, J. Am. Chem. Soc. 119 (1997) 4769.

46. M.K. Whittlesey, R.N. Perutz, B. Greener, M.H. Moore, Chem. Commun. (1997) 187.

47. B.K. Tate, C.M. Wyss, J. Bacsa, K. Kluge, L. Gelbaum, J.P. Sadighi, Chem. Sci. 4 (2013) 3068.

48. C.M. Wyss, B.K. Tate, J. Bacsa, T.G. Gray, J.P. Sadighi, Angew. Chem. Int. Ed. 52 (2013) 12920.

49. G.H. Penner, X. Liu, Prog. Nucl. Magn. Reson. Spectrosc. 49 (2006) 151.

50. H. Schmidbaur, A. Hamel, N.W. Mitzel, A. Schier, S. Nogal, Proc. Nat. Acad. Sci. U.S.A. 99 (2002) 4916.

51. A sterically demanding dialkylphosphinobiphenyl ligand supports $[(LAu)_2(\mu\text{-}Cl)]^+$ complexes: A. Homs, I. Escofet, A.M. Echavarren, Org. Lett. 15 (2013) 5782. No dimerization was reported even for complexes with bulky anions (cf. Ref. 49).

52. The cation $\{[(OC)Au]_2(\mu\text{-}Cl)\}^+$ has been structurally characterized: J. Schaefer, A. Kraft, S. Reininger, G. Santiso-Quinones, D. Himmel, N. Trapp, U. Gellrich, B. Breit, I. Krossing, Chem. Eur. J. 19 (2013) 12468. No dimerization was reported.

53. A. Bayler, A. Schier, G.A. Bowmaker, H. Schmidbaur, J. Am. Chem. Soc. 118 (1996) 7006.

54. J.A. Tossell, D.J. Vaughan, Inorg. Chem. 20 (1981) 3333.

55. R. Fujimori, Y. Hirata, I. Morino, K. Kawaguchi, J. Phys. Chem. A 117 (2013) 9882.

56. Y. Li, X. Wang, F. Jensen, K.N. Houk, G.A. Olah, J. Am. Chem. Soc. 112 (1990) 3922.

57. For a review, see: J.C. Green, M.L.H. Green, G. Parkin, Chem. Commun. 48 (2012) 11481.

58. H. Schmidbaur, A. Schier, Chem. Soc. Rev. 41 (2012) 370.

59. P.G. Jones, G.M. Sheldrick, R. Uson, A. Laguna, Acta Crystallogr., Sect. B 36 (1980) 1486.

60. A. Corma, A. Leyva-Pérez, M.J. Sabater, Chem. Rev. 111 (2011) 1657.

61. See for example: T.J. Brown, D. Weber, M.R. Gagné, R.A. Widenhoefer, J. Am. Chem. Soc. 134 (2012) 9134, and references cited therein.

62. See for example: T.J. Brown, R.A. Widenhoefer, Organometallics 30 (2011) 6003.

63. P. Schulte, U. Behrens, F. Olbrich, *Z.* Anorg. Allg. Chem. 626 (2000) 1692.

64. A. Collado, A. Gómez-Suárez, A.R. Martin, A.M.Z. Slawin, S.P. Nolan, Chem. Commun. 49 (2013) 5541.

65. O.V. Dolomanov, L.J. Bourhis, R.J. Gildea, J.A.K. Howard and H. Puschmann, J. Appl. Crystallogr. 42 (2009) 339.

66. SHELXS-97 (Sheldrick, 2008).

CHAPTER 5

Conclusion

This thesis describes the synthesis, structure and reactivity of singly bridged dinuclear Group 11 complexes supported by N-heterocyclic carbene (NHC) ligands. These anion-bridged dicopper(I) cations all display bent arrangements around the bridging ligands, but only some feature short copper–copper interactions. The shortest intermetallic distance is 2.4082(2) Å for the boryl-bridged dicopper cation $\{[(SIDipp)Cu]_2(\mu\text{-}BO_2C_6H_4)\}^+ BF_4^-$, the first complex of its type to be isolated. The boryl bridge gives rise to a shorter Cu–Cu distance than a hydride-bridged dicopper cation. We found intermetallic distances of 2.5331(15) and 2.5354(15) Å for $\{[(IDipp)Cu]_2(\mu\text{-}H)\}^+ BF_4^-$, and Lalic and coworkers recently found 2.541(2) Å for $\{[(SIDipp)Cu]_2(\mu\text{-}H)\}^+ OTf^-$.[1] A carbanion bridge, as in the vinyl-bridged $\{[(IDipp)Cu]_2(\mu\text{-}trans\text{-}CHCHPh)\}^+ BF_4^-$, gives rise to a larger intermetallic separation of 2.6303(4) Å. The NHC ligand also stabilizes a dicopper μ-fluoro cation, for which a short copper–copper interaction is not observed. We rationalize the large copper–copper separation, well outside possible bonding distance, in terms of three-center, four-electron bonding.

These findings are in agreement with previously reported computational studies on model dimers, which found that the Cu–Cu interaction increases with increasing σ-donor bridging ligands.[2-5] Simple σ-donors donate electron density into empty σ– and π–bonding Cu–Cu bonding orbitals, increasing the Cu–Cu interaction. Halide bridges,

however, π-donate into the empty σ* and π* combinations in addition to σ-donating into σ and π Cu–Cu bonding orbitals, causing the M–M bond to vanish (Figure 5.1).

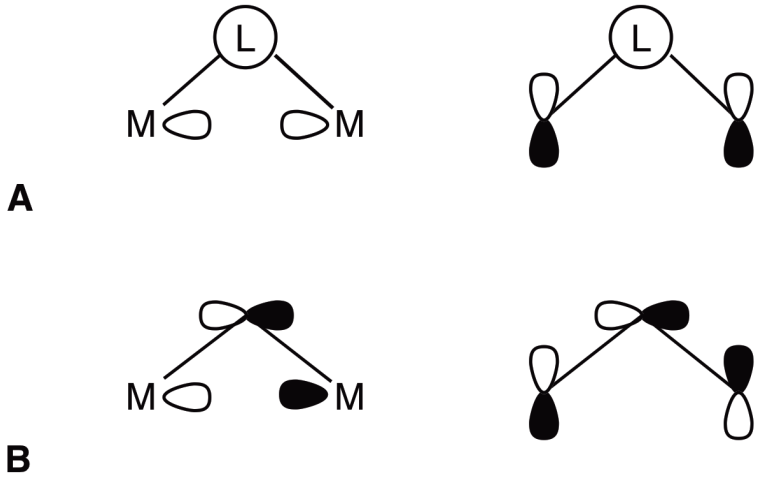

Figure 5.1. (**A**) L σ-donates into empty σ– and π–bonding Cu–Cu bonding orbitals; (**B**) L π-donates into empty σ* and π* combinations.

Investigating the reactivity of these complexes, we found that $\{[(SIDipp)Cu]_2(\mu\text{-}BO_2C_6H_4)\}^+$ BF_4^- deprotonates phenylacetylene to form a phenylacetylide dicopper complex instead of inserting the alkyne, as has been inferred and even observed for other Cu-based boryl systems.[6] The $[(LCu)_2H]^+$ cation, however, inserts phenylacetylene to afford a *gem*-dicopper vinyl cation, which in turn reacts with a borane to regenerate the $[(LCu)_2H]^+$ cation and form a new C–B bond. We cannot explain for the difference in reactivity toward a terminal alkyne. The dicopper(I) μ-fluoro cation was shown to be highly sensitive to adventitious moisture, readily forming the hydroxide-bridged dicopper cation. However, it is not as reactive as the gold(I) analogue, which has a larger hard/soft acid-base mismatch. The gold(I) analogue activates the C–Cl bonds of CD_2Cl_2 and adds rapidly across an allene C=C bond.

Lalic and coworkers recently proposed $\{[(IDipp)Cu]_2(\mu\text{-}H)\}^+$, $\{[(IDipp)Cu]_2(\mu\text{-}F)\}^+$, and $\{[(IDipp)Cu]_2(\mu\text{-alkenyl})\}^+$ to be key catalytic intermediates in the copper-catalyzed hydroalkylation of terminal alkynes using alkyl triflates as electrophiles.[1] A previously proposed mechanism, now disproven, had attributed the catalytic activity to terminal analogues of each complex.[7] They also provide evidence that the dinuclear complexes are responsible for the anti-Markovnikov regioselectivity that provides exclusively (*E*)-alkenes without the reduction or fluorination of the alkyl triflates.[1] This proposed mechanism suggests that the anion-bridged catalytic intermediates have profoundly different reactivities than their terminal analogues. The hydride-bridged and fluoride-bridged dicopper complexes demonstrate finely tuned reactivities that are essential for the hydroalkylation reaction. This new mechanistic hypothesis provides opportunities for the development of new transformations such as the hydrofunctionalization of alkynes with other strong electrophiles.

5.1. References

1. A.M. Suess, M.R. Uehling, W. Kaminsky, G. Lalic, J. Am. Chem. Soc. 137 (2015) 7747.

2. H.L. Hermann, G. Boche, P. Schwerdtfeger, Chem. Eur. J. 7 (2001) 5333.

3. C. Kölmel, R. Ahlrichs, J. Phys. Chem. 94 (1990) 5536.

4. C. Mealli, S.S.M.C. Godinho, M.J. Calhorda, Organometallics 20 (2001) 1734.

5. P. Alemany, S. Alvarez, Inorg. Chem. 31 (1992) 4266.

6. a) L. Zhang, J. Cheng, B. Carry, Z. Hou, J. Am. Chem. Soc. 134 (2012) 14314; b) H. Jang, A.R. Zhugralin, Y. Lee, A.H. Hoveyda, J. Am. Chem. Soc. 133 (2011) 7859;

c) J.H. Moon, H.-Y. Jung, Y.J. Lee, S.W. Lee, J. Yun, J.Y. Lee, Organometallics 34 (2015) 2151.

7. M.R. Uehling, A.M. Suess, G. Lalic, J. Am. Chem Soc. 137 (2015) 1424.

APPENDIX A

Collaborator Contributions

Much of this research presented in this thesis was a result of collaborative efforts. This appendix serves to credit collaborators and their respective contributions.

A.1. Bonding and Reactivity of μ-Hydrido Dicopper Cation

Dr. Thomas Gray performed all of the DFT calculations within this chapter. Dr. John Bacsa performed all of the X-ray diffraction studies and solved all solid-state structures within this chapter. Mr. Brandon Tate provided insightful discussions and suggestions on related reactivity of late transition metal hydride complexes.

A.2. Bonding and Reactivity of μ-Boryl Dicopper Cation

In the methodology part of this chapter, many of the initial reactions and optimizations to isolate $\{[(SIDipp)Cu]_2(\mu\text{-}BO_2C_6H_4)\}^+$ BF_4^- were performed by Ms. Jamie Bitting. All DFT calculations within this chapter were performed by Dr. Thomas Gray. Dr. John Bacsa performed all of the X-ray crystallography studies and solved the solid-state structure within this chapter.

A.3. Dinuclear μ-Fluoro Cations of Copper, Silver, and Gold

Mr. Brandon Tate did all of the research pertaining to $\{[(SIDipp)Ag]_2(\mu\text{-}F)\}^+$ BF_4^-. Dr. John Bacsa and Ms. Marika Wieliczko performed the X-ray crystallography studies and solved the solid-state structures within this chapter.

VITA

Chelsea M. Wyss

Chelsea M. Wyss was born in Fort Wayne, Indiana. She attended Bishop Luers High School. Chelsea received a B.S. in Chemistry from The University of the South, Sewanee, Tennessee in 2010. She obtained her Ph.D. in chemistry from Georgia Institute of Technology in 2015.